DISCOVERY, CHARACTERIZATION, AND DEVELOPMENT OF SMALL MOLECULE INHIBITORS OF GLYCOGEN SYNTHASE

Buyun Tang

Submitted to the faculty of the University Graduate School
in partial fulfillment of the requirements
for the degree
Doctor of Philosophy
in the Department of Biochemistry and Molecular Biology,
Indiana University

June 2020

Accepted by the Graduate Faculty of Indiana University, in partial fulfillment of the requirements for the degree of Doctor of Philosophy.

Doctoral Committee

_____
Thomas D. Hurley, Ph.D., Chair

_____
Peter J. Roach, Ph.D.

April 30, 2020

_____
Millie M. Georgiadis, Ph.D.

_____
Steven M. Johnson, Ph.D.

_____
Jeffrey S. Elmendorf, Ph.D.

Dedication

I dedicate this work to my beloved family, my grandparents, my parents, and my brother.

Acknowledgement

First and foremost, I would like to express my deepest gratitude to my thesis advisor, Dr. Thomas D. Hurley. I am grateful to have him as my research mentor over the past four years. He has continuously guided, supported, and inspired me during my study at IUSM. His passion for science and devotion of mentorship offered me the best training experience I could ever receive in graduate school. His easygoing personality reminded me of all the wonderful times inside and outside of the lab. I remember him instructing me handling crystal instrument hand by hand, flying with me to San Diego for a conference, and driving me to a farm restaurant at Illinois. Dr. Hurley is not only an outstanding research mentor, but also a trustful friend. I deeply thank him for all his time, patience, and encouragement along my graduate training.

I would like to specially thank Drs. Peter J. Roach and Anna A. DePaoli-Roach for their mentorship. Their enduring enthusiasm for science, tremendous knowledge, and scientific innovation always inspire me. I deeply appreciate their expertise, dedication, and love of science. Besides, I also very much miss all the delicious Italian food Dr. DePaoli-Roach prepared at our laboratory group meetings.

I want to give many thanks to my doctoral committee members, Drs. Peter J. Roach, Millie M. Georgiadis, Steven M. Johnson, and Jeffrey S. Elmendorf for their insightful discussion and feedback on my annual progress meetings. I appreciate their critiques, comments, and suggestions, which have helped me tackle all sorts of experimental issues. I sincerely thank them for their service on my thesis committee.

There are many people in the Hurley and Roach laboratories that I would like to acknowledge. Dr. Krishna K. Mahalingan taught me all kinds of enzymatic and biophysical

assays when I firstly joined in the lab. Dr. Christopher J. Contreras showed me how to operate HPAEC instrument. Dr. Anna A. DePaoli-Roach and Dyann M. Segvich shadowed me with cellular assays. I sincerely thank them for all their generous instruction. Additionally, I want to thank my lab colleagues including Cyrus Takahashi, Mikhail Chtcherbinine, Dr. Cindy A. Morgan, Dr. Cameron D. Buchman, Dr. Alexandre V. Skurat, and Dr. Safnas F. Abdul Salam for their help and support. They all contribute to cultivate a pleasant, relaxing, and productive working environment.

I want to recognize many people in the Department of Biochemistry and Molecular Biology. I thank Dr. Mark G. Goebl for serving as my curriculum advisor, staff at the Chemical Genomic Core including Dr. Jingwei Meng, Dr. Lifan Zeng, and Erica L. Woodall for providing technical support, and the Biochemistry office staff for taking care of many paperwork during my graduate study. I also want to express my thankfulness to many good friends: Jeremy Liu, Peng Wu, Yefeng Ruan, Michelle Li, Guomin Shan, and Ben Shi. My life at Indianapolis would not have been this enjoyable without their company and encouragement.

Lastly, I would like to extend my most profound affection to my beloved family, my grandma, grandpa, mom, dad, and brother. Thank you all for your unconditional love, patience, and encouragement. I could not have reached thus far without your support.

Buyun Tang

DISCOVERY, CHARACTERIZATION, AND DEVELOPMENT OF SMALL MOLECULE INHIBITORS OF GLYCOGEN SYNTHASE

The over-accumulation of glycogen appears as a hallmark in various glycogen storage diseases (GSDs), including Pompe, Cori, Andersen, and Lafora disease. Glycogen synthase (GS) is the rate-limiting enzyme for glycogen synthesis. Recent evidence suggests that suppression of glycogen accumulation represents a potential therapeutic approach for treating these diseases. Herein, we describe the discovery, characterization, and development of small molecule inhibitors of GS through a multicomponent study including biochemical, biophysical, and cellular assays. Adopting an affinity-based fluorescence polarization assay, we identified a substituted imidazole molecule (**H23**), as a first-in-class inhibitor of yeast glycogen synthase 2 (yGsy2) from the 50,000 ChemBridge DIVERSet library. Structural data derived from X-ray crystallography at 2.85 Å, and enzyme kinetic data, revealed that **H23** bound within the uridine diphosphate glucose binding pocket of yGsy2. Medicinal chemistry efforts examining over 500 **H23** analogs produced structure-activity relationship (SAR) profiles that led to the identification of potent pyrazole and isoflavone compounds with low micromolar potency against human glycogen synthase 1 (hGYS1). Notably, several of the isoflavones demonstrated cellular efficacy toward suppressing glycogen accumulation. In an alternative effort to screen inhibitors directly against human GS, an activity-based assay was designed using a two-step colorimetric approach. This assay led to the identification of compounds with submicromolar potency to hGYS1 from a chemical library comprised of 10,000 compounds. One of the hit molecules, hexachlorophene, was crystallized bound to the active site of yGsy2. The

structure was determined to 3.15 Å. Additional kinetic, mutagenic, and SAR studies validated the binding of hexachlorophene in the catalytic pocket and its non-competitive mode of inhibition. In summary, these two novel assays provided feasible biochemical platforms for large-scale screening of small molecule modulators of GS. The newly-developed, potent analogs possess diverse promising scaffolds for drug development efforts targeting GS activity in GSDs associated with excess glycogen accumulation.

Thomas D. Hurley, Ph.D., Chair

Table of contents

List of tables

List of figures

List of schemes

List of abbreviations

CIAP	Calf intestinal alkaline phosphatase
CNS	Central nervous system
DIDS	4,4'-diisothiocyanato-2,2'-stilbenedisulfonic acid
EC	Epicatechin
EGC	Epigallocatechin
EGCG	Epigallocatechin-3-monogallate
FP	Fluorescence polarization
G1P	Glucose-1-phosphate
G6P	Glucose-6-phosphate
GBE	Glycogen-branching enzyme
GlcN6P	Glucosamine-6-phosphate
GLUT	Glucose transporter
GN	Glycogenin
GPCR	G-protein-coupled-receptor
GS	Glycogen synthase
GSD	Glycogen storage disease
GSK3	Glycogen synthase kinase-3
GT	Glycosyltransferases
HCLP	Hexachlorophene
hGYS1	Human glycogen synthase 1
hGYS2	Human glycogen synthase 2
HPAEC	High-performance anion exchange chromatography

HPLC	High-performance liquid chromatography
hSCAN-1	Human soluble calcium-activated nucleotidase-1
HTS	High-throughput screening
IR	Insulin receptor
LB	Lafora body
LD	Lafora disease
MS	Mass spectrometry
PAINS	Pan-assay interference compounds
PhK	Phosphorylase kinase
PI3K	Phosphoinositide 3-kinase
PKA	Protein kinase A
PKB	Protein kinase B
PP1	Type 1 protein phosphatase
PTG	Protein-targeting-to-glycogen
PYG	Glycogen phosphorylase
SAR	Structure-activity relationship
T1D	Type I diabetes
T2D	Type II diabetes
UDP	Uridine diphosphate
UDPG	Uridine diphosphate glucose
yGSY1	Yeast glycogen synthase 1
yGSY2	Yeast glycogen synthase 2

I. Introduction

A. Glycogen

1. Function and localization

Carbohydrate is one of the major energy sources for many forms of life. Glucose polymerization is a universal mechanism for carbohydrate storage in nature. Starch, a polymeric carbohydrate consisting of amylose and amylopectin, is produced by most green plants as an energy reserve[1]. Glycogen, on the other hand, is a multi-tiered branched polymer of glucose that serves as a major storage form for many prokaryotes and eukaryotes including archaea, bacterial, animals, and humans[2].

The two main tissues for glycogen deposition in mammals are liver and skeletal muscle. Other tissues are also capable of synthesizing and storing glycogen, albeit at much lower levels usually. These additional tissue deposits include brain, heart, kidney, and skin. However, the physiological role glycogen plays in different tissue types varies. Liver plays an essential role in glucose homeostasis by converting stored glycogen to glucose for release when needed to support glucose-centric metabolism in the brain and erythrocytes[3]. In muscle, glycogen acts as an intracellular glycolytic fuel when energy demand rises, such as during extended muscle contraction or in response to the fight-or-flight reaction. Within the brain, glycogen is primarily found in astrocytes, where it can be metabolized to lactate as an energy substrate for neighboring cells[4].

Glycogen is not homogenously distributed inside cells. Subcellular localization of glycogen appears organelle-specific where it supports different functions. In skeletal muscle, three pools of glycogen have been identified; subsarcolemmal glycogen, intermyofibrillar glycogen, and intramyofibrillar glycogen[5]. These compartmentalized

glycogen deposits show distinct effects on muscle fiber function[6]. During deposition and depletion, it is reported that glycogen particles are tightly associated with smooth endoplasmic reticulum, which contains various enzymes required for glycogen metabolism[7]. Although glycogen is mostly found in the cytoplasm, it can also be found in mitochondria[8,9] and in the nucleus[10]. Nuclear glycogen is believed to carry out various functions, such as providing a structural scaffold for nuclear assembly[11,12], sequestration of critical kinases and phosphatases[12], and as a carbon source for histone acetylation[13].

2. Structure

As a highly branched glucose polymer, glycogen structure is optimized to function as an efficient fuel reserve. The linear polymerization of glycogen is mediated through the formation of α-1,4-glycosidic bonds, and branch points are produced through the formation of α-1,6-glycosidic bonds (**Figure 1A**). According to Whelan's model, glycogen forms a fractal structure comprised of two categories of chain, the inner B-chains that possess two branches on each chain, and outer A-chains that are unbranched[14,15] (**Figure 1B**). Chemical analysis of mammalian glycogen revealed each chain has an average of 13 glucose units, whereas the precise location of branchpoints on each chain is not clearly defined[16]. In this model, glycogen grows with a spherical shape consisting of a series of concentric tiers (**Figure 1C**). Mathematical modeling suggested that a full glycogen molecule has a maximum of 12 tiers with ~55,000 glucose residues, a molecular mass of 10^7 Da, and a 44 nm average diameter[2]. Notably, the outermost tier of any molecule formed in this way contains 50% of total glucose residues that would be involved in regular synthesis-degradation cycle[15].

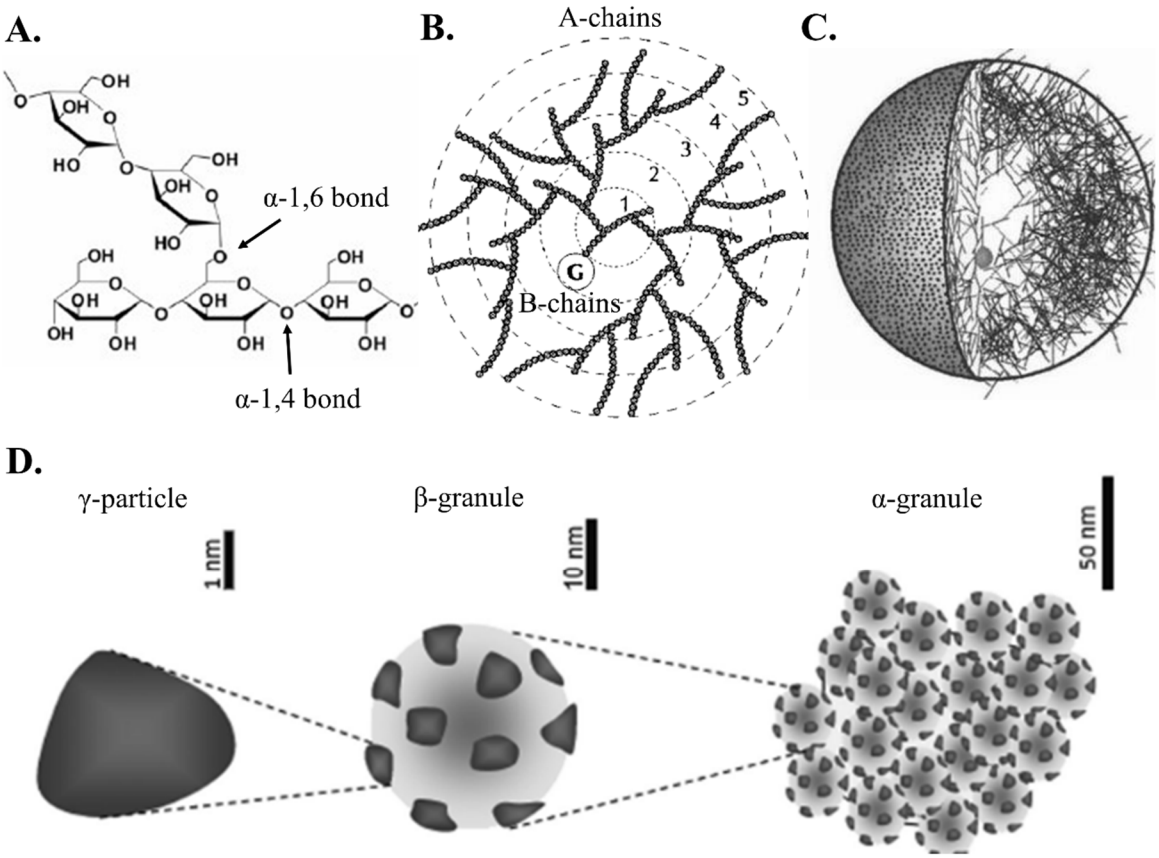

Figure 1. Glycogen structure. **(A)** Glycogen linear polymerization is achieved through the formation of α-1,4-glycosidic linkages, and branches are produced through the formation of α-1,6-glycosidic linkages. **(B)** The fractal structure of glycogen contains inner B-chains which possess two branches on each chain, and outer unbranched A-chains. The number shown represents different tiers. The circled "G" denotes glycogenin. **(C)** The spherical shape of a full-sized glycogen molecule. **(D)** The three types of glycogen structures (α- and β-granule and γ-particle) identified using transmission electron microscopy are shown. (Adapted from Roach *et al*.[2], Melendez *et al*.[15], and Prats *et al*.[17])

Each glycogen granule is associated with a number of regulatory proteins, and forms an organelle-like structure, which has been termed the glycosome. Analysis using transmission electron microscopy revealed there are three types of glycogen structures, namely α- and β-granule and γ-particle[17]. The γ-particle is an electro-dense 3 nm protein-rich structure that is bound to the β-granule, which is the carbohydrate polymer described above. The β-granule is 20-30 nm of size, has a molecular mass of 10^6-10^7 Da, and is

considered a rapid energy source. The α-granule, mostly present in liver, is composed of several β-granules in a broccoli-like fashion via a protein backbone rich in disulfide bonds. The α-granule can be as large as 300 nm in diameter, 10^8 Da in molecular weight, and is considered a slow energy source (**Figure 1D**)[17].

The way glycogen is constructed offers several metabolic advantages. First, its polymeric nature combined with hydrogen bond formation between its hydroxyl groups and water ensures glycogen solubility, while minimizing elevation of the osmotic pressure in cells by sequestering glucose in a polymeric form. Secondly, the tiered structure of glycogen allows rapid glucose incorporation and degradation, making glycogen a robust and renewable energy source. Thirdly, such a relatively simple, fractal structure provides an evolutionarily efficient approach for the regulation of glycogen metabolism.

3. Metabolism and regulation

Glycogen metabolism constitutes one of the key pathways in living cells regulating systemic carbon or energy allocation[18]. The synthesis and degradation of glycogen is a highly conserved, complex, and coordinated process. When glucose is transported into cells, it is first converted to glucose-6-phosphate (G6P) via hexokinase before it can enter one of several metabolic pathways; glycolysis, the pentose phosphate pathway, or glycogen synthesis. The synthetic pathway for glycogen begins with the reversible conversion of G6P to glucose-1-phosphate (G1P). Subsequent reaction of G1P with uridine-5'-triphosphate (UTP) forms uridine diphosphate glucose (UDPG), the immediate glucosyl donor for glycogen biosynthesis[19]. Typically, the initiation of glycogen synthesis is mediated by glycogenin (GN), which acts as a primer for glucose polymerization through the self-glycosylation at Tyr194 residue[20,21]. However, a primer protein may not be strictly

required for polysaccharide chain elongation, as $GN^{-/-}$ mice still accumulated normal levels of glycogen in liver and brain, while in skeletal and cardiac muscle elevated glycogen (four to seven times higher) was observed[22]. In any case, once the initial chain grows to 6-17 glucose residues, two key enzymes catalyze further chain elongation. Glycogen synthase (GS) lengthens linear chains through the progressive addition of α-1,4-linked glucose residues to the non-reducing end of the polymer, and glycogen-branching enzyme (GBE) catalyzes the intramolecular transfer of seven glucose residues to a C-6 hydroxyl group to produce α-1,6 branch points for further elongation[23]. The degradation of glycogen occurs in both the cytoplasm and lysosome. In the cytoplasm, glycogen breakdown is regulated by the coordinated action of glycogen phosphorylase (PYG) and debranching enzyme, resulting in the release of G1P and free glucose. In the lysosome, in contrast, α-glucosidase (GAA) catalyzes the complete hydrolysis of glycogen to free glucose (**Figure 2**)[17].

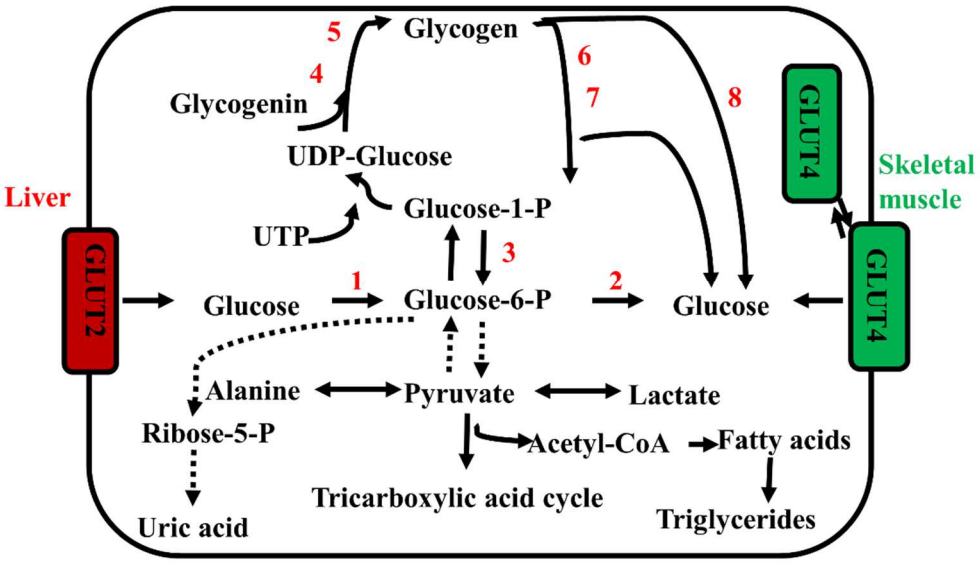

Figure 2. Glycogen metabolism. A simplified scheme of glycogen synthesis and degradation pathway. **1**. Hexokinase; **2**. Glucose-6-phosphatase; **3**. Phosphoglucomutase; **4**. Glycogen synthase (GS); **5**. Glycogen branching enzyme (GBE); **6**. Glycogen phosphorylase (PYG); **7**. Debranching enzyme; **8**. Lysosomal α-glucosidase (GAA).

The regulation of glycogen metabolism is primarily mediated through hormonal control, including the actions of insulin, glucagon, and epinephrine. When blood glucose levels rise, pancreatic β-cells secret insulin that binds to insulin receptors (IR) on target cells such as liver, muscle, and adipose tissue, resulting in the activation of protein kinase B (PKB) in a phosphoinositide 3-kinase (PI3K)-dependent manner. These actions lead to the subsequent phosphorylation and inactivation of glycogen synthase kinase-3 (GSK3). Lower GSK3 activity leads to lower phosphorylation levels at the C-terminal regulatory sites of GS and activation of GS, which promotes glycogen biosynthesis[24]. The dephosphorylation of GS is mediated by forms of type 1 protein phosphatase (PP1), the catalytic domain of which is held in close proximity to the glycogen granule and GS by a family of glycogen targeting subunits, including protein-targeting-to-glycogen (PTG), which is effectively an indirect activator of GS[25]. Activated PKB also plays an important role in the translocation of glucose transporters (GLUTs) to the plasma membrane, facilitating glucose delivery into cells[26,27]. In contrast, when blood glucose and insulin levels fall during fasting, the glucagon secreted by pancreatic α-cells binds to the glucagon receptor which is a member of the G-protein-coupled-receptor (GPCR) family. Glucagon binding to its receptor in the liver activates adenylate cyclase that converts adenosine triphosphate (ATP) to cyclic adenosine monophosphate (cAMP), which activates protein kinase A (PKA). PKA phosphorylates phosphorylase kinase (PhK), which in turn phosphorylates and activates glycogen phosphorylase, and leads to net glycogen degradation[28]. Similar to glucagon, epinephrine can also activate the breakdown of glycogen through the binding of β-adrenergic receptor, another class of GPCR[29]. Notably,

glucagon mostly works in liver, whereas epinephrine mainly acts on muscle, and to a lesser extent, in the liver (**Figure 3**).

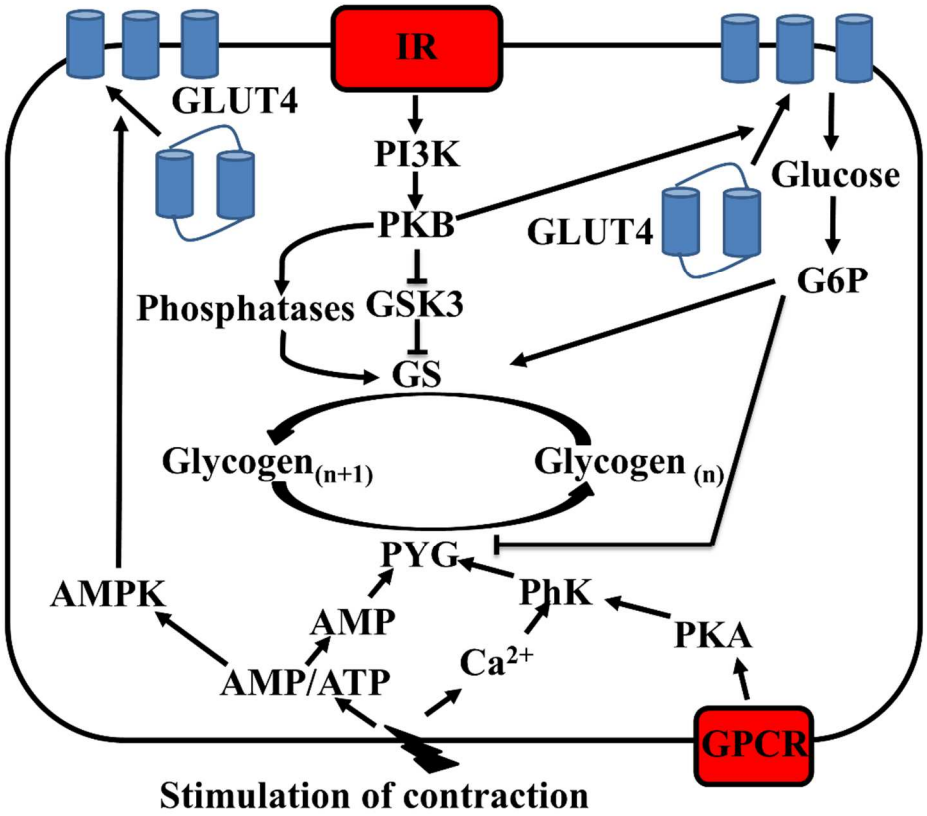

Figure 3. Regulation of glycogen metabolism. A simplified scheme of regulatory pathways for glycogen metabolism. Insulin receptor (IR); Phosphotidyl inositol 3-kinase (PI3K); Protein kinase B (PKB); Glycogen synthase kinase-3 (GSK3); Glucose transporter 4 (GLUT4); Glucose-6-phosphate (G6P); G-protein-coupled-receptor (GPCR); Phosphorylase kinase (PhK). (Adapted from Baskaran[30])

B. Glycogen synthase

1. Classification

GS is the rate-limiting enzyme in glycogen biosynthesis[31], and belongs to the super family of glycosyltransferases (GTs), a ubiquitous group of enzymes that catalyze the transfer of a sugar moiety from an activated sugar donor onto an acceptor. The enormous diversity of these enzymes arises from their exquisite specificity for both donors and acceptors. GTs are widely distributed in both prokaryotes and eukaryotes, where they

contribute to a broad range of biological functions including structural support, metabolic storage, and signal transduction. GTs have been classified into over 78 families based on amino acid sequence homology (denoted as GTX). However, based on available structural data (>100 crystal structures), only 3 distinct structural folds have been found. These three folds are 1) the GTA fold consisting of an α/β/α sandwich that resembles a Rossmann fold, 2) the GTB fold consisting of two Rossmann domains, and 3) a third unclassified fold that displays a different type of α/β/α sandwich. GS is further divided into two subfamilies within the GTB fold superfamily based on sequence identity and differences in regulatory responses. Specifically, bacterial and plant GS are categorized into the GT5 subfamily because they use adenosine diphosphate glucose (ADPG) as the donor, whereas animal and fungal GS are divided into GT3 subfamily since UDPG is the substrate and they are regulated by allosteric and post-translational mechanisms (**Figure 4**)[32,33].

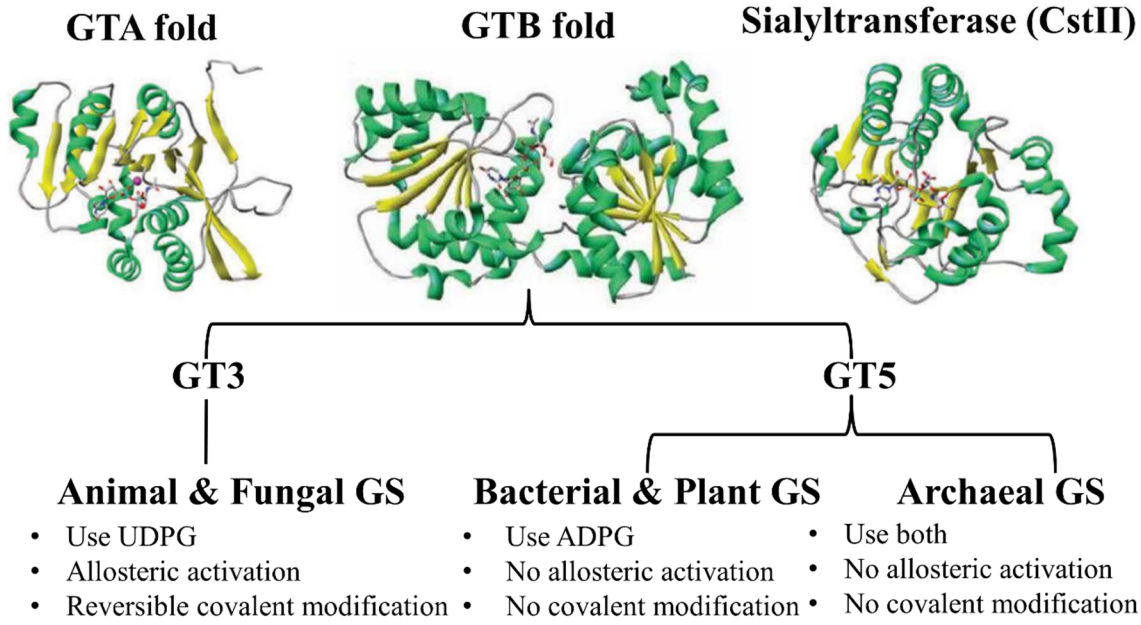

Figure 4. Classification of GTs based on structural folds and the subfamilies of GS. Three superfamily of GTs with representative crystal structure in each family are shown. GTs are represented with cartoon models in green (α-helix)/yellow (β-sheet). Bound nucleotide sugars are represented with stick models. (Adapted from Breton *et al*.[33])

For the research described in this thesis, I studied both human and yeast GS. In humans, there are two isoforms of GS, human glycogen synthase 1 (hGYS1) and human glycogen synthase 2 (hGYS2)[34,35]. These isoenzymes possess approximately 70% sequence identity at the protein level and display the greatest variation within the N- and C-terminal sequence extensions. The two GS isoenzymes are differentially expressed: expression of *hGYS2* occurs exclusively in liver, whereas expression of *hGYS1* occurs primarily in skeletal muscle but is also expressed in most other tissues. Similar to higher eukaryotes, *Saccharomyces cerevisiae* has two genes encoding GS, *yeast glycogen synthase 1* (*yGSY1*) and *yeast glycogen synthase 2* (*yGSY2*). The product of the *yGSY2* gene, yGsy2p, is the predominant isoform[36]. Additionally, the *yGSY1* gene is expressed constitutively throughout the growth cycle, whereas *yGSY2* gene is controlled by environmental signals such as nutrient deprivation and cell cycle regulation[36,37].

2. Structure

Although a structure for a mammalian GS remains elusive, crystal structures of two eukaryotic enzymes are known, including Gsy2 from *Saccharomyces cerevisiae*[38] and GS from *Caenorhabditis elegans*[39]. Subsequently, structures of GS in complex with different ligands such as G6P[38], maltooctaose[40], UDPG[41], or its associated protein GN[39] have been determined, providing more structural insight into GS and its interaction with substrates. The structures of GS obtained from these two systems demonstrated formation of a tetramer. The structure of one of the monomers with various bound ligands is shown in **Figure 5A**. The individual subunits contain two Rossmann-fold domains with an interdomain cleft that harbors the catalytic site. Within the C-terminal domain, a large

insertion of around 100 amino acids forms a two helical bundle that comprises much of the interface for tetramerization.

The allosteric activator of GS, G6P, binds to a pocket beneath a regulatory α-helix near the tetrameric interface in the C-terminal domain, and forms extensive interactions with surrounding residues on more than one subunit[38]. The pocket is composed of six residues, including His286, Lys290, His500, Arg580, Arg583, and Arg587, all of which form hydrogen bonding interactions with the phosphate group. The glucose binding site is formed upon the binding of G6P which rearranges a disordered loop (residues 277-285). The glucosyl moiety is stabilized through hydrogen bonds formed with Gln283, Asn284, and His280 in the intersubunit surface (**Figure 5B**). Binding of G6P induces large scale conformational changes and enzyme activation as shown in **Figure 6A** and is discussed further in the following section.

Multiple glycogen-binding sites were identified from crystal studies of yGsy2p in complex with maltooctaose, an 8-glucose polymer. These sites include one located in the N-terminus, two on the C-terminus, and an additional site in the interdomain cleft adjacent to the active site[40]. These sites distribute across the surface of the enzyme and are conserved across different eukaryotic species. Mutations of these surface sites decreased glycogen binding, enzyme catalytic efficiency, as well as glycogen accumulation in yeast cells[40]. Additionally, these glycogen-binding sites are proposed to serve distinct functions. For instance, site-1 and site-2 may provide a "toe-hold" mechanism to support tight association of GS with glycogen particle, whereas site-4 may be critical in positioning the non-reducing end of glycogen during catalysis.

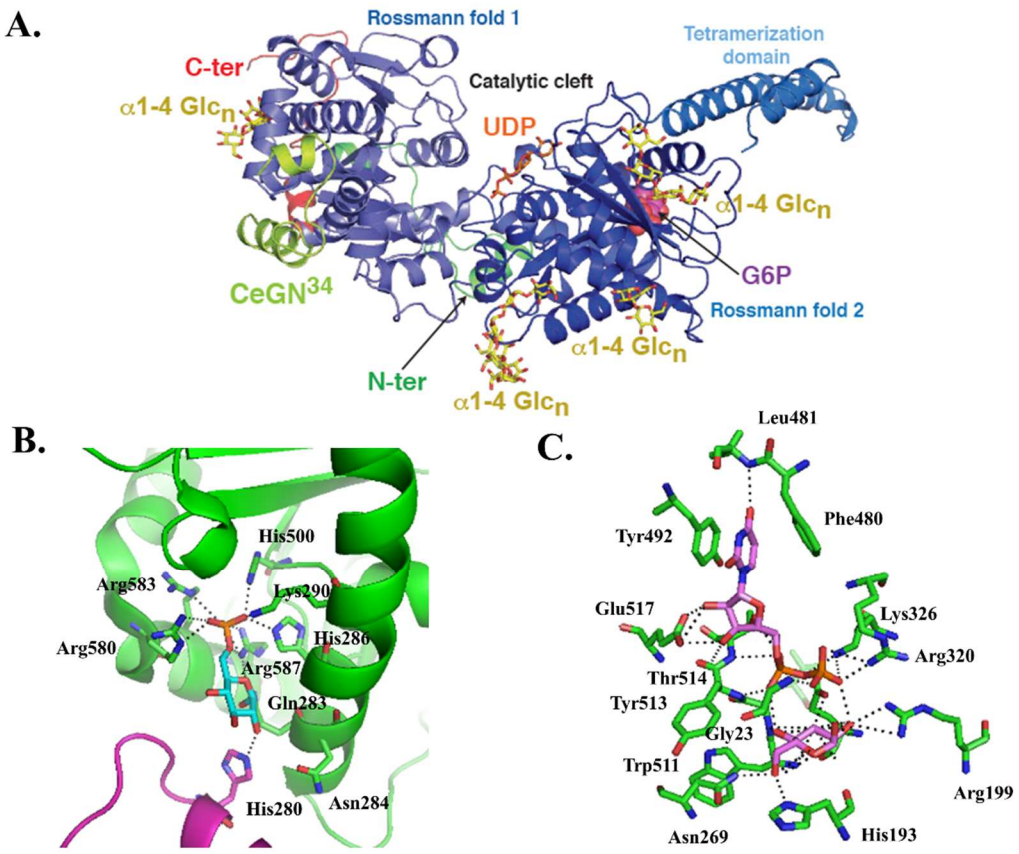

Figure 5. Crystal structures of GS. **(A)** An integrated structural model of GS based on crystal studies from *S. cerevisiae* and *C. elegans*. Each GS monomer contains two Rossmann fold domains with a linker region in between. The binding sites for UDP, G6P, glycogen (α1-4 Glc_n), and GN ($CeGN^{34}$) are shown. (Figure from Zeqiraj *et al*.[39]). **(B)** Cartoon representation of the G6P binding pocket (PDB: 3NB0). Individual subunits are colored either in green or magenta. G6P (cyan) and its interacting residues are represented with stick model. **(C)** Stick representation of the UDP•G (magenta) binding pocket (PDB: 4KQM). The dashed black lines represent hydrogen bond formation.

Crystal structures of yGsy2p in complex with UDP•G were obtained, revealing the binding of UDPG in the interdomain cleft. Noncovalent interactions dominate UDPG binding in the active site. Specifically, the uridine is sandwiched between Phe480 and Tyr492. The O4 group of the uracil moiety is within hydrogen bond distance to the backbone amide nitrogen of Leu481. The 2'- and 3'-OH groups on the ribosyl moiety form hydrogen bonds with Glu517 and Thr514. The α-phosphate of UDP interacts with the

peptide nitrogen of Tyr513 and the sidechain hydroxyl group of Thr514, whereas the β-phosphate forms hydrogen bonds with Arg320, Lys326, and Gly23. Additionally, both α- and β-phosphate form intramolecular hydrogen bonds with the sugar moiety. The glucosyl units form intensive interactions with surrounding residues, including His193, Asn269, Trp511, and Arg199 (**Figure 5C**).

The primer protein for glycogen synthesis, GN, was determined to bind to a conserved surface on the N-terminal domain of GS[42], an observation supported by the crystal structure of *C. elegans* GS in complex with a 33-residue region (301-333) of the C-terminal tail of human GN[39]. This study provides a structural basis for the recruitment of GS to the GN initiation complex. Furthermore, reciprocal mutagenic studies on the interaction motif demonstrated the GS-GN association is required for glycogen production *in vitro* and *in vivo*[39].

3. Relationship between structure and regulation

The available enzyme kinetic data supports a three-state activity model for GS[38,43,44]. These states include low activity phosphorylated state, the intermediate dephosphorylated (or basal) state, and G6P-activated state. A commonly used value that expresses the activity state of GS is the ratio of GS activity in the absence of as compared to the activity in the presence of G6P as an index of the phosphorylation level of the enzyme, where the value can vary between 0 (highly phosphorylated and inactive state) and 1 (fully activated state)[45]. Typical values for the mammalian enzymes are 0.02 for the highly phosphorylated form and 0.4 for the basal form[46].

The manner in which G6P and phosphorylation regulate GS activity is controlled by a cluster of six regulatory arginine. These residues are conserved across all eukaryotes.

In yGsy2p, simultaneous mutation of the first three arginine residues (R580A/R581A/R583A, or R580A3) produced an enzyme that can neither be activated by G6P nor inhibited by phosphorylation. Mutation of the last three arginine residues (R587A/R589A/R592A, or R587A3) created an enzyme that could be inhibited by phosphorylation but could not be activated by G6P[44]. Conformations of these three activity states of yGsy2p have all been determined (**Figure 6**), yielding structural mechanisms underlying the differences among GS activity states. It turned out that substrate accessibility to the active site is mainly responsible for the level of enzyme activation. In its inhibited state, the phosphorylated residue Thr668 plays a dominant role in suppressing GS activity[47]. This is achieved through the interaction between the first two arginine residues (R580/R581) and the phosphate moiety, leading to the closure of catalytic cleft. In the dephosphorylated state, the last two arginine residues (R589/R592) function to prevent the collapse of the regulatory helices toward the interface due to an electric repulsive effect, creating a basal state enzyme with an active site that is 5.9º more open than the inhibited state[43]. The distance between the regulatory helices between subunits in the basal state is 12 Å. The tetrameric interface is formed by a coiled-coil domain containing α15-α16 (residues 365-431), and a 12-mer disordered loop linking the two helices (residues 401-412). The distance between the equivalent α15 helices between subunits is 21 Å. Binding of G6P promotes a large conformational transition that drives the enzyme into an activated state, as reflected by the 13.3º degree of openness between the two Rossmann folds[38]. This change is induced by the interaction of G6P with two of the arginine residues (R583/R587) situated in the middle of the cluster, promoting a 16 Å translocation of the regulatory helices between subunits. Concomitantly, the interface α15

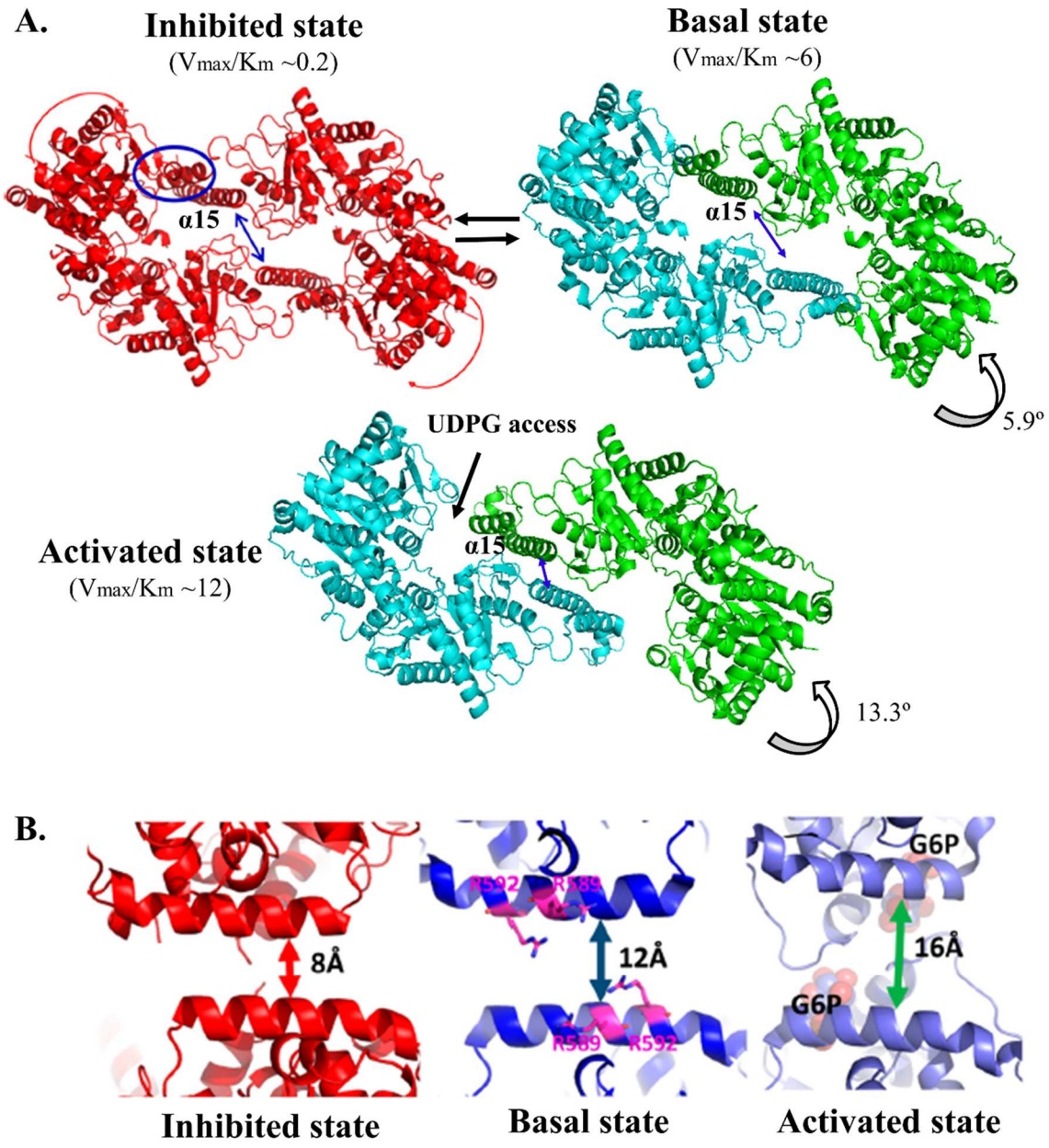

Figure 6. Comparison of the different activity-state structures of yGsy2p. **(A)** Cartoon representation of the inhibited state (R589A2) structure (PDB: 5SUL), the basal state (R580A3) structure (PDB: 3NAZ), and the G6P-activated state (PDB: 3NB0). The catalytic efficiency (denoted as V_{max}/K_m), and the degree of openness between the two Rossmann-fold, are shown for each activity-state. **(B)** Cartoon representation of the regulatory helices. The distance between the equivalent α15 helices between subunits for each state structure is shown. (Adapted from Mahalingan *et al*.[43,48])

helices are drawn toward each subunit to a distance of 5.5 Å, allowing the active site to be further opened. As a result, the enzyme catalytic efficiency, indicated by V_{max}/K_m, increased from 0.2 for the inhibited state, 6 for the basal state, to 12 for the G6P-activated state (**Figure 6A** and **6B**)[44].

4. Catalytic mechanism

The molecular mechanisms for both GN self-glycosylation and GS catalytic reaction have been under investigation over the past two decades, although a consensus regarding whether such reactions are S_Ni- or S_N2-based has not been reached. One view considers the glycosyl transfer event to be an S_N2-based reaction, which requires double nucleophilic enzyme substitution and the formation of a discrete enzyme-intermediate covalent complex. Enzyme studies on hGYS1 identified a consensus sequence (E-X_7-E) that is conserved across eukaryotic enzymes. Mutation of either of the glutamate residues led to almost complete reduction of enzyme activity. These conserved glutamate residues were proposed as the potential nucleophiles in GS enzymes[49]. However, kinetic and structural studies on many glucosyl transferases favor an S_Ni-based reaction in which one catalytic nucleophile on the donor molecule is capable of completing such reaction[41,50,51]. Briefly, in the S_Ni model, the donor sugar moiety is activated by the β-phosphate of UDP upon deprotonation of 1'-OH group, rendering the 4'-OH group of the acceptor molecule an attacking nucleophile. As a consequence, UDPG is hydrolyzed to UDP and glucose, with the latter being conjugated onto acceptors such as glycogen or the Tyr195 residue of GN (**Figure 7**). The S_N1 mechanism involves the formation of a carbocation intermediate, which allows two different avenues for nucleophile attack, both of which, would invert the stereochemistry of the anomeric carbon. As a consequence, the S_N1 process is not widely

accepted as the catalytic mechanism for glycosyl transferase enzymes that retain the configuration of the anomeric carbon.

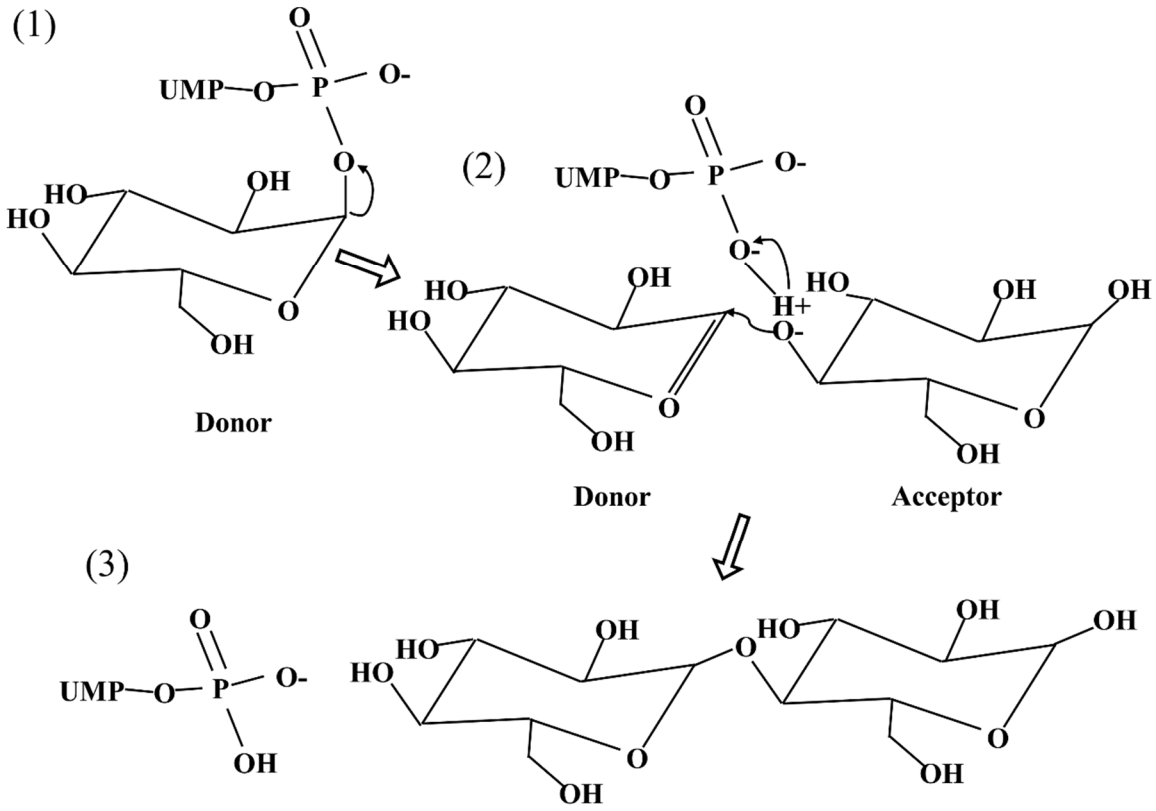

Figure 7. S_Ni-based catalytic mechanism for GS. Briefly, activation of the sugar moiety is initiated by the β-phosphate of UDP which deprotonates the 1'-OH group and forms an oxocarbenium-like intermediate. The 4'-OH group of the acceptor acts as an attacking nucleophile, resulting in UDPG hydrolysis to UDP and subsequent glucose transfer.

C. Glycogen and glycogen storage diseases

Abnormal glycogen metabolism is associated with a large family of diseases called glycogen storage diseases (GSDs) (**Table 1**)[19,52]. Typically, defects in enzymes directly involved either in glycogen synthesis or degradation are the major causes. For instance, proteins such as GS, GBE1, and glycogenin 1 (GYG1) are all glycogen biosynthetic enzymes, and their deficiencies lead to GSD0, GSD4, and GSD15, respectively. In addition, mutations of enzymes in glycogenolysis or glycolysis affect glycogen

degradation and glucose utilization, resulting in a wide variety of diseases ranging from GSD2-3 and GSD5-14. Nonetheless, mutations of indirect and/or regulatory proteins of glycogen metabolism also contribute to the pathogenesis of some types of GSD. Lafora disease (LD) is one representative in this category, since it is caused by mutations within either one of the two genes, *EPM2A* or *EPM2B*. Specifically, *EPM2A* encodes laforin, a dual specificity glycogen phosphatase; and *EPM2B* encodes malin, an E3-ubiquitin ligase. They function as a complex to modulate GS activity[53] and translocation of GLUTs[54] as an indirect means to monitor glycogen accumulation.

Various phenotypical symptoms and clinical courses are associated with GSDs depending on disease types and tissue specificity. Although liver and muscle are the major locations for glycogen storage, disease manifestation is present widely. In many GSD cases, the condition of hepatomegaly (an enlarged liver) is found in patients due to hepatic metabolic disorder. Such a defect is always accompanying with hypoglycemia. Exercise-induced intolerance, cramps, muscle weakness, and fatigue are typical symptoms in skeletal muscle. Cardiomyopathy and heart failure is associated with glycogen accumulation in cardiomyocytes. In addition, the peripheral and central nervous systems (CNS) and renal tubules also suffer from glycogen abnormalities. Besides, the defect of energy production and utilization exerts a deleterious effect to the whole body and leads to growth retardation. The fatal outcome, as demonstrated by death at early ages, is not uncommon in GSD patients.

One interesting fact is that glycogen over-accumulation is characteristic in most GSDs. In Pompe disease (GSD2), the deficiency of GAA leads to lysosomal glycogen accumulation in many tissues including skeletal, cardiac, and smooth muscle[55]. In Cori

disease (GSD3) and Andersen disease (GSD4), defects in the glycogen debranching enzyme (AGL) and GBE1, respectively, result in the deposition of glycogen with abnormal structure and in abnormal amounts[56,57]. LD is a fatal progressive myoclonus epilepsy accompanied by neurodegeneration for which the presence of abnormal glycogen inclusions known as Lafora bodies (LB)[58] are the hallmark. LBs are composed of poorly branched, hyperphosphorylated, and insoluble forms of glycogen that occur in neurons, muscle and other tissues[59,60,61]. A common finding with excess glycogen accumulation is an association with impaired autophagy and dysregulated mitochondrial metabolism. These derangements often lead to cell death and early-onset lethal, disease progression in GSD-affected patients[53,62,63].

Table 1. Human GSD types.

Type	Enzyme (gene) deficiency	Enzyme function	Symptoms
GSD0	Glycogen synthase (GYS1; GYS2)	Rate-limiting enzyme in glycogen biosynthesis, which catalyzes the transfer of glucose from UDPG to glycogen.	Occasional muscle cramping; Growth failure in some cases.
GSD1 (Von Gierke disease)	Glucose-6-phosphatase (G6PC/SLC37A4)	Completes the final step in gluconeogenesis, which hydrolyzes G6P, resulting in the creation of a phosphate group and free glucose.	Growth failure.
GSD2 (Pompe disease)	Lysosomal α-glucosidase (GAA)	Catalyzes the breakdown of glycogen in the lysosome.	Muscle weakness; Cardiomyopathy; Death by age ~2 years.
GSD3 (Cori disease)	Debranching enzyme (AGL)	Facilitates the breakdown of glycogen through glucosyltransferase and glucosidase activity.	Myopathy.
GSD4 (Andersen disease)	Branching enzyme 1 (GBE1)	Adds branches to the growing glycogen molecule during glycogen biosynthesis.	Myopathy and dilated cardiomyopathy; Death at age ~5 years.
GSD5 (McArdle disease)	Glycogen phosphorylase (PYGM)	The rate-limiting step in glycogenolysis, which catalyzes the release of G1P from the terminal α-1,4-glycosidic bond.	Exercise-induced cramps.

GSD6 (Hers disease)	Liver glycogen phosphorylase (PYGL)	Cleaves α-1,4-glycosidic bond to release G1P from liver glycogen stores.	Growth retardation.
GSD7 (Tarui disease)	Phosphofructokinase	Catalyzes a key step in glycolysis by converting fructose-6-phosphate to fructose 1,6-bisphosphate.	Exercise intolerance, with pain, cramps and, occasionally myoglobinuria.
GSD8	Hepatic Glycogen Phosphorylase Kinase (PYKL)	Phosphorylates and activates glycogen phosphorylase for glycogen degradation.	Hepatomegaly; Growth retardation; Hypertriglyceridemia, and fasting hyperketosis.
GSD9	Phosphorylase kinase	A key enzyme in triggering glycogen breakdown.	Hepatomegaly; Growth retardation; Exercise intolerance, with pain, cramps.
GSD10	Phosphoglycerate mutase (PGAM2)	Catalyzes a step in glycolysis by converting 3-phosphoglycerate to 2-phosphoglycerate (2PG).	Exercise-induced muscle cramps and weakness; Myoglobinuria.
GSD11	Muscle lactate dehydrogenase (LDHA)	Involved in glycolysis, which catalyzes the inter-conversion of pyruvate and L-lactate	Fatigue, muscle pain, and cramps during exercise.
GSD12	Aldolase A (ALDOA)	A glycolytic enzyme that catalyzes the reversible conversion of fructose-1,6-bisphosphate to glyceraldehyde 3-phosphate (G3P) and dihydroxyacetone phosphate (DHAP).	Exercise intolerance and cramps; Hemolytic anemia.

GSD13	β-enolase (ENO3)	Known as phosphopyruvate hydratase, catalyzes the penultimate step of glycolysis.	Muscle pain; Exercise intolerance.
GSD14	Phosphoglucomutase (PGM1)	Catalyzes the interconversion of G1P and G6P.	Hepatopathy; Growth retardation; Myopathy; Cardiomyopathy; Cardiac arrest.
GSD15	Glycogenin 1 (GYG1)	A key enzyme in glycogen biosynthesis.	Muscle atrophy; Slowly progressive weakness over decades.
LD (Lafora disease)	EPM2A or EMP2B	EPM2A encodes laforin, a phosphatase with polysaccharide-binding domain. EPM2B encodes an E3 ubiquitin ligase called malin. Both involve in glycogen production.	Myoclonic seizures; Neurodegeneration; Death at adolescent years.

D. Glycogen and diabetes

Diabetes is a group of metabolic diseases characterized by a high level of blood glucose. It is generally classified in one of two types, type I diabetes (T1D) which occurs when pancreatic β-cells undergo autoimmune destruction, and type II diabetes (T2D) caused by insulin insensitivity as well as insufficiency[64]. Altered glycogen metabolism is associated with both types of diabetes. T1D patients suffer from postprandial hyperglycemia and fasting hypoglycemia due to poor glycogen stores. Restoration of normal insulin and glucose levels rescued hepatic glycogen synthesis and glucose production[65,66]. In T2D cases, the defects in postprandial glycogen synthesis, impaired suppression of endogenous glucose production, and reduced glucose disposal are even more profoundly associated with the disease, such that even controlled hyperglycemic hyperinsulinemia cannot restore these functional deficits[67]. Such close association points to a complex interplay between abnormal glycogen metabolism and underlying diabetes.

Several clinical case studies support a direct link between abnormal glycogen storage and diabetes. In one GSD1 patient with an inborn defect of the gluconeogenic enzyme glucose 6-phosphatase, hepatomegaly and kidney disease was observed due to glycogen buildup. The patient gradually developed uncontrolled diabetic complications such as hyperglycemia and fasting hypoglycemia in adolescence[68]. In another study, a GSD3 patient diagnosed at age of 18 showed no signs of glucose intolerance, but developed diabetes with severe postprandial hyperglycemia[69]. Although the exact molecular mechanisms for the development of diabetes in GSD patients is not clear, in both cases treatment with a GAA inhibitor, which blocks lysosomal glycogen degradation, has demonstrated therapeutic efficacy for improved glycemic control. Through physiological,

immunochemical, and genetic analysis in diabetic animal models, one group has proposed that excess glycogen accumulation due to impaired glycogen metabolism, rather than hyperglycemia per se, is causative of β-cell dysfunction in T2D[62,70]. This is further supported by the fact that under hyperglycemic conditions, diabetic mice were restored with normal β-cell mass and function by treatment with the glucose-lowering drug metformin, whereas control mice did not recover β-cell function[62]. It is still under discussion whether abnormal glycogen metabolism is the cause of β-cell dysfunction, but it is conceivable that T2D could be grouped as one type of GSD.

E. Glycogen and cancer

Cancer cells accumulate glycogen to promote survival, proliferation, and metastasis[71,72,73,74]. Several studies identified oncogenic pathways that lead to glycogen biosynthesis in cancers. Hypoxia upregulates the expression of PP1, GS, and GLUTs in a hypoxia inducible factor (HIF)-dependent manner[75,76,77]. The oncogene Rab25 was identified as a positive regulator of glycogen synthesis partially through the modulation of PKB, which inhibits GSK3 activity and in turn leads to GS activation[78]. Interestingly, glycogen breakdown enzymes, in both cytosolic (PYG) and lysosomal (GAA) pathways, are upregulated in cancer cells[79]. Such an impact on glycogen metabolism is believed to support several important functions for cancer cell growth. The most obvious explanation is that glycogen functions as the primary energy source for cancer cells in response to nutrient deprivation in the tumor microenvironment. Additionally, glycogen-derived glucose can enter the pentose phosphate pathway, and provide building materials for macromolecule biosynthesis to support proliferation. Glucose metabolism also plays a key

role in scavenging reactive oxygen species (ROS) under stressed conditions and promotes cell survival.

The fact that defective glycogen metabolism is associated with cancer progression indicates that targeting glycogen metabolism could be a novel therapeutic approach for cancer treatment. Genetic or pharmacological intervention of glycogen metabolism was explored in a few cancer studies. For instance, as described earlier, Rab25 promotes glycogen synthesis whose expression is upregulated in many types of human cancers, whereas knockdown of Rab25 led to reduced glycogen accumulation and consequential cancer cell death[78]. AGL, a glycogen debranching enzyme, was found to be a novel tumor suppressor in bladder cancer, since loss of AGL leads to rapid growth of bladder cancer cells[80]. The rate-limiting enzyme in glycogen degradation, PYG, was believed to be an oncogene due to its ability to supply glucose and sustain proliferation, as well as preventing premature senescence in cancer cells[79]. Therefore, inhibiting PYG activity with small molecules has been exploited for cancer treatment, and showed promising outcomes such as reduced tumor growth and cell cycle arrest[81,82]. Notably, the negative regulator of GS, GSK3β, has gained extensive attention for its attractiveness as a viable cancer target. GSK3β is serine/threonine kinase involving in various aspects of cellular activity including proliferation, differentiation, motility, and survival[83]. However, its role in tumorigenesis is controversial because in certain types of cancer, GSK3β functions as a "tumor-suppressor", whereas in others as a "tumor-promoter". Therefore, GSK3β chemotherapies have to be explored and applied with precision with respect to the underlying drivers in each tumor type.

F. Rationale of the thesis study

1. Suppressing glycogen accumulation through inhibition of GS activity for the treatment of GSDs

Currently, there are no effective treatments for GSDs that ameliorate all cellular and organ dysfunction. For example, in Pompe disease, the administration of a genetically engineered enzyme (i.e., enzyme replacement therapy, ERT) that rescues the defective GAA in peripheral tissues failed to reverse the neurological defects. Accumulating evidence suggests that suppression of glycogen accumulation through inhibition of GS activity represents an alternative, potentially effective strategy for therapeutic approach for treating GSDs where ERT may not provide a complete solution. For instance, mouse models of LD that lack either of the causative genes, *EPM2A* or *EPM2B,* recapitulate aspects of the GSD patient phenotype, in that they accumulate polyglucosan bodies and misfolded proteins, display increased endoplasmic reticulum stress, and show signs of neurodegeneration[59, 63]. Such animal models provided a venue for disrupting either *PTG* or *GYS1* in these *EPM2A*$^{(-/-)}$ and *EPM2B*$^{(-/-)}$ knock-out mice as a mechanism for diminishing glycogen accumulation, LB formation, and the associated neurological and epileptic symptoms (**Figure 8**)[84,85,86]. Inhibition of GS activity via suppression of mTOR signaling also increases the effectiveness of treatments for Pompe disease in conjunction with ERT[87]. Moreover, a recent report has shown that GYS2 inhibition with RNAi prevents liver injury in mouse models of GSDs[88]. Although human clinical characteristics may vary from animal model phenotypes, the availability of these models and the appearance of promising therapeutic approaches suggest the feasibility of using small molecule interventions to treat GSDs.

The premise of this thesis study is that suppressing glycogen accumulation could alleviate the pathology of GSDs associated with excess glycogen accumulation. Our primary objective is to discover, characterize, and develop small molecule inhibitors of GS as a viable chemotherapeutic approach for treating GSDs. The molecules generated from this study can also be utilized as chemical probes for other disease applications, such as in diabetes and cancer, as described earlier.

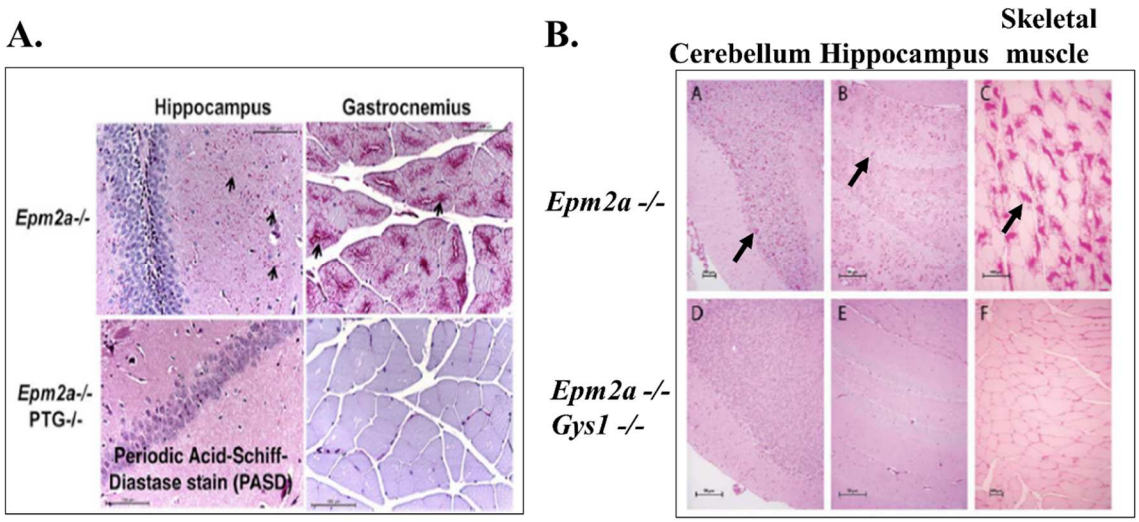

Figure 8. *PTG* or *GYS* knock-out mice alleviated LD pathology. **(A)** *PTG* deficiency suppresses LBs in brain (hippocampus) and muscle (gastrocnemius) of *Epm2a*$^{-/-}$ mice. **(B)** *Epm2a*$^{-/-}$ mice lacking *Gys1* have no LB in the cerebellum, hippocampus, and skeletal muscle. [Panel A (Anna A. DePaoli-Roach and Peter J. Roach, unpublished results), panel B adapted from Pederson *et al*.[85])

2. The necessity of developing high-throughput screening assays against GS

The traditional method to assess GS activity is through a radiochemical assay that measures ^{14}C-glucose incorporation from UDP-[U-^{14}C]glucose into glycogen[89]. Experimentally, this assay contains 5 major steps (**Figure 9**):

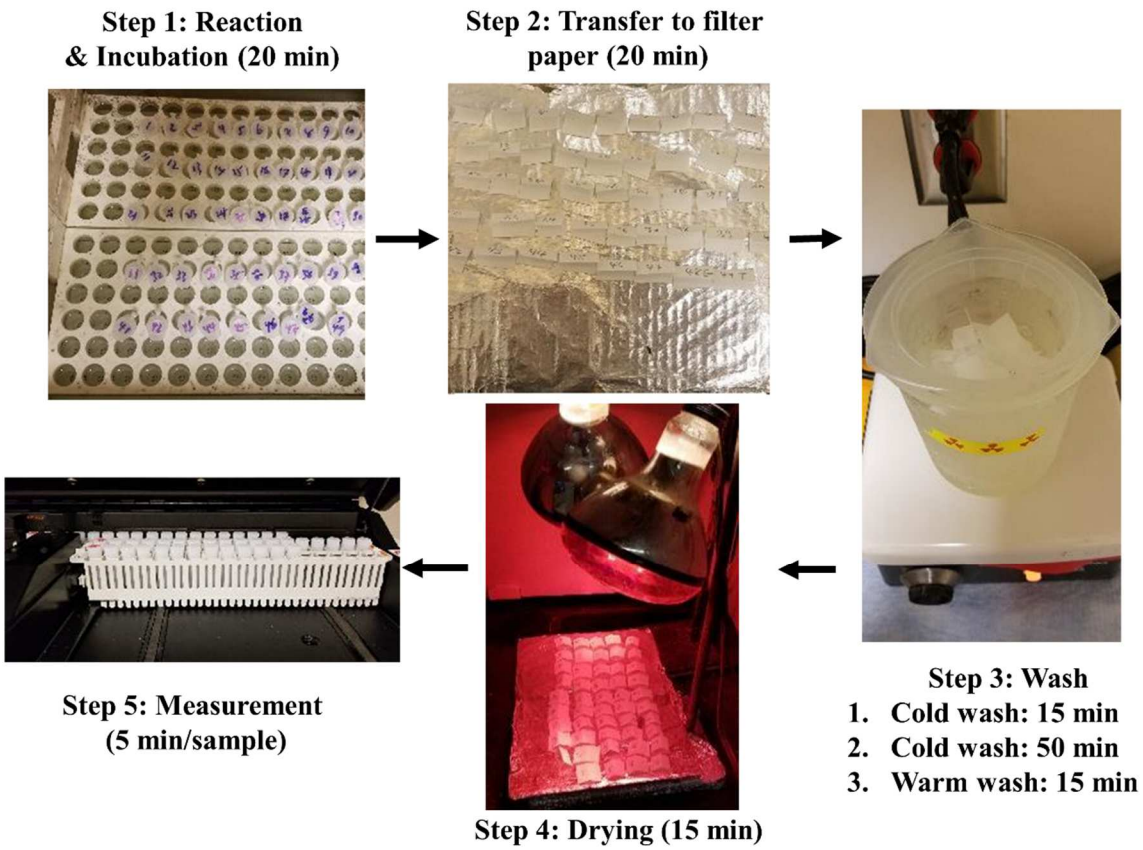

Figure 9. An outline of the ^{14}C-glucose incorporation assay protocol. This radiochemical assay features five main steps including incubation, transfer, washing, drying, and measurement. Experimental procedure and time consumption for each key step are shown.

1) Add GS to tube #1 containing assay mixtures including glycogen, UDPG, G6P, and UDP-[U-^{14}C]glucose, start timer. At 20 seconds interval, add GS to each remaining tube (#2-n). Total incubation time for enzyme reaction is 20 minutes.
2) After incubation, transfer assay mix from tube #1 to filter paper #1, and then from each remaining tube (#2-n) to corresponding filter paper, again at 20 seconds interval. Allow filter paper to absorb in assay solution briefly, and then place it into the wash beaker containing 66% ethanol.

3) Use ice cold ethanol in the first wash for 15 minutes, and another cold ethanol wash for 50 minutes, followed by a third wash at room temperature for an additional 15 minutes.
4) Place papers on aluminum foil and let them dry under heat lamp for 15 minutes.
5) Place each dried filter paper in separate vials, add scintillation fluid, and measure radioactivity with the scintillation counter. It typically takes a 5-minute measurement for each vial.

As the standard activity measurement for GS, this assay involves appropriate safety measures for handling radioisotopes as well as multiple transfer and washing steps to remove residual substrates. The combination of laboratory effort, cost, safety, and waste disposal makes this radiochemical assay unsuitable for high-throughput screening (HTS). As a result, the development of alternative rapid, robust, and nonradioactive screening assays becomes necessary to initiate the discovery of small molecule inhibitors of GS. Herein, I report our efforts to develop two novel HTS assays for the identification of small molecule inhibitors of GS. In one assay, we synthesized a G6P-coupled fluorescent probe, and screened compounds that can displace the G6P-conjugated fluorophore using a fluorescence polarization (FP) assay. In another assay, GS catalytic activity is linked to inorganic phosphate production which is then detected though the use of the malachite green reagent. Both assays have been proven to be suitable for HTS with excellent Z'-scores. We screened two chemical libraries using the FP assay as well as the coupled GS activity assay against 50,000 and 10,000 compounds, respectively. Primary hits were identified for subsequent characterization and development.

I used a number of biochemical and biophysical tools to characterize the hits, including enzyme kinetics, enzyme mutagenesis, and X-ray crystallography, through which I aimed to determine the mode of inhibition, binding affinity, and the structure of the ligand-enzyme complexes. Such information is utilized for structure-guided drug development and medicinal chemistry optimization through the development of structure-activity relationships (SAR). For lead compounds with promising *in vitro* properties, efficacy and toxicity were evaluated in our cell models for glycogen accumulation.

II. Experimental section

A. Material

1. Reagents

DI water was filtered with a MilliQ Ultra-Pure water system (EMD Millipore, Billerica, MA) prior to use. UDPG (Sigma U4625) concentration was determined via absorbance at 262 nm. Radioactive UDP-^{14}C-glucose was purchased from Perkin Elmer (NEC403000MC). G6P (Sigma G7879) was prepared in 50 mM Tris, pH 7.8. Rabbit liver glycogen (Sigma G8876) was prepared by mixing an 8 - 10% (w/v) solution over a TMD-8 ion exchange resin (Sigma M8157) for 1 hour and washed with water to elute glycogen, followed by at least two ice cold ethanol precipitations. Precipitated glycogen was collected by centrifugation at 5,000 rpm for 20 min at 4°C. Air-dried glycogen was diluted in water to a final concentration of 80 mg/ml and stored at -20°C. WST-1 cell proliferation reagent (ab155902) was purchased from Abcam. For the coupled malachite green HTS, a 2× assay master mix (800 μM G6P, 400 μM UDPG, 2 mg/mL glycogen, and 50 mM Tris, pH 7.8) was prepared in advance and stored in daily aliquots at -20°C. A second, 2× control assay mix was prepared identically to the 2× assay master mix but without G6P.

2. Commercial chemical libraries and compounds

Unless otherwise noted, most compounds were purchased from commercial chemical libraries. The 50K compound DIVERSet library, the primary hits **H1-H110** (**Figure 15A**), and analogs **IM1-4**, **PR7-9** were purchased from ChemBridge Corporation (San Diego, CA). Analogs **PR5**, **PR6** and **PR10** were purchased from Vitas-M Laboratory (Champaign, IL) (**Table 4**). The purity of these purchased compounds were >95% based

on the spectra (either LC/MS or NMR) provided by the vendors. All pyrazoles, which were synthesized in house, were validated by both LC/MS and NMR.

The 10K compound library was obtained from the Chemical Genomics Core Facility at Indiana University School of Medicine. The library consisted of drugs and natural products, including the LOPAC 1280 and Microsource Spectrum 2400, both consisting of drugs and bioactives, plus AnalytiCon's 1000 compound MEGx of natural products and the 5000 compound NATx of semi-synthetic natural compounds.

Compounds including hexachlorophene (45526), analogs **HC1** (SML1440), **HC2** (COM448626140), **HC3** (R579696), **HC5** (35992), **HC7** (93453), **HC8** (IDF00128), **HC10** (C44702), **HC12** (113700), **HC14** (B46808), **HC15** (S926744) were purchased from Sigma-Aldrich. Analog **HC6** (5222210) was purchased from ChemBridge corporation. Analogs **HC4** (0352-0636) and **HC13** (0089-0025) were purchased from ChemDiv Corporation. Analog **HC9** (MFCD01763607) was from Maybridge Ltd. Analog **HC11** (EN300-21338) was from ENAMINE Ltd (**Table 7**). According to the vendors, the purity of these compounds were >95%. All compounds were dissolved in 100% DMSO and stored at -20 °C.

3. Compounds synthesized in house

Synthesis of pyrazoles **PZ11-30** was performed in a 3-step procedure that included 1) synthesis of polyhydroxydeoxybenzoins; 2) ring-closure reaction for the synthesis of isoflavones with or without de-acetylation of phenolic groups; and 3) re-cyclization reaction of chromones in the presence of hydrazine[90] (**Scheme 1**). Initial Hoesch reaction of substituted polyphenols and arylacetonitriles in boron trifluoride etherate with passing of anhydrous HCl led to formation of the A-ring polyhydroxylated deoxybenzoins **I2-1** –

I2-5 and **I2-9** – **I2-12**[91]. Alternative condensation of pyrogallol or 4-flouroresorcinol with phenylacetic acids in boron trifluoride etherate at heating was performed for the synthesis of 4'-hydroxy- or 4'-cyano deoxybenzoins **I2-6** – **I2-8**[92]. Ring-closure reaction with Vilsmeier reagent or trifluoroacetic anhydride in pyridine after work-up with water afforded the 2-unsubstituted or 2-trifloromethyl isoflavones. Synthesis of 2-methyl isoflavones **I3-1**, **I3-2**, **I3-8**, and **I3-19** was performed by reaction of polyhydroxydeoxybenzoins with acetic anhydride in the presence of potassium acetate, with the subsequent deacylation in ethanol done without purification of the intermediate acetates. Target pyrazoles **PZ11-30** (**Table 4**) were synthesized by reacting the synthesized 2-(un)substituted isoflavones **I3-1** – **I3-20** with hydrazine hydrate in ethanol under reflux.

B. Methods

1. HTS assays

1.1 High-throughput FP assay

1.1.1 Synthesis and purification of GlcN6P-fluorescein-5-Ex

The tracer was synthesized by using a standard coupling reaction between an amine and N-hydroxysuccinimidyl ester. The reaction included: 100 mM $NaHCO_3$ (pH 8.4), 130 mM glucosamine-6-phosphate (GlcN6P) pH 8.0, 41.6% DMSO and 14 mM fluorescein-Ex, succinimidyl ester. The reaction was incubated for 1 hour at 37°C followed by an overnight incubation at room temperature with continuous stirring, the reaction was stopped by addition of Tris-HCl (pH 8.0) to a final concentration of 0.2 M. Purification of GlcN6P-fluorescein-5-Ex was carried out by high-performance liquid chromatography (HPLC) on a semi-preparative Luna C18 column (250×10 mm, 5 μm) from Phenomenex. The eluents used were 25 mM NH_4OAc (pH 5.5) (E1) and 100% methanol (E2). Elution

was performed by the following gradient: T_0= 5% (v/v) E2, T_{10}= 50% (v/v) E2, T_{30}= 50% (v/v) E2, T_{45}= 75% (v/v) E2, T_{55}= 5% (v/v) E2 at a flow rate of 4 ml/min. The fractions containing the UV-containing fractions were collected, dried using a SpeedVac, dissolved in water and stored at -20°C. The fractions containing GlcN6P-fluorescein-5-Ex were identified and confirmed by mass spectroscopy analysis. The final tracer concentration was determined by UV spectroscopy (Abs_{492}~9.2×10^4 M^{-1} cm^{-1}).

1.1.2 FP assay

All the FP experiments were performed on an EnVision multimode plate reader (Perkin Elmer) with the λ_{ex}= 485 nm and λ_{em}= 535 nm. The FP experiments were performed in 384-well, black, flat-bottom microplates at room temperature. After addition of all reagents, plates were centrifuged for 1 minute at 1000*g*, followed by measurement of the FP signals, where each well was flashed 10 times and the average values were used. All polarization values were expressed as milli-Polarization units (mP), calculated from equation 1:

$$mP = (1000) * \frac{S - G*P}{S + G*P} \qquad (1)$$

Where: *S*= fluorescence intensity measured when the excitation and emission polarizers are parallel and *P*= fluorescence intensity measured when the excitation and emission are perpendicular and *G*= grating factor that corrects for instrument bias. All the nonlinear regression analyses were performed by fitting the experimental data to the defined equations using SigmaPlot version 13.0.

1.1.3 Determination of the GlcN6P-fluorescein-5-Ex/yGsy2p equilibrium dissociation constant

The concentration of the tracer was initially varied from 0-100 nM in order to determine the optimal assay concentration. Based on total fluorescence intensity and mP values, the optimal concentration was determined to lie between 10-40 nM in the final assay. The binding affinity for the tracer for yGsy2p was determined by adding the tracer to a final concentration of 20 nM to each well in the presence of varying yGsy2p concentrations (0 to 50 μM) in a final volume of 50 μL. The final assay buffer consisted of 15 mM Tris-HCl (pH 7.8) and 15 mM NaCl, and the plate was incubated at room temperature for 10 minutes before reading. The dissociation constant K_d was calculated by fitting the experimental data to equation 2:

$$f = y_0 + \frac{a*x}{b+x} \qquad (2)$$

Where f =mP, y_0=mP_{min}, a= mP_{max}-mP_{min}, b= K_d and x = Concentration of yGsy2p. Experiments were performed in triplicate.

1.1.4 Activation of yGsy2p or hGYS1 in the presence of G6P or GlcN6P

The activation of hGYS1 or yGsy2p in the presence of G6P or GlcN6P was determined using the radiochemical assay previously described[89] and the data was fit to equation 2. However, the parameters were defined as: f = % activation, y_0 = % $activation_{min}$, a=% $activation_{max}$ - % $activation_{min}$, x= Concentration of G6P or GlcN6P and b= AC_{50}. Experiments were performed in triplicate.

1.1.5 Competitive displacement experiments

G6P was serially diluted in 15 mM Tris-HCl (pH 7.8) to provide a final concentration ranging from 0.68 μM to 40 mM. The reaction mixture contained a final

concentration of 15 mM Tris-HCl (pH 7.8), 15 mM NaCl, 20 nM GlcN6P-fluorescein-5-Ex, 4.2 μM yGsy2p and varying concentrations of G6P in a final volume of 50 μL. The plate was incubated for 10 minutes at room temperature before reading. The K_d was determined by fitting the observed mP changes to equation 3:

$$f1 = \mathrm{mP}min + \frac{(\mathrm{mP}max - \mathrm{mP}min)}{\left(1+\frac{x}{EC50}\right)\wedge(-Hillslope)} \qquad (3)$$

Where $f1$= mP, EC_{50}= K_d, x= Concentration of G6P. Experiments were performed in triplicate.

1.1.6 Determination of Z'-factor

To determine the quality of the FP-displacement assay for adaptation for HTS, the Z'-factor was calculated using equation 4:

$$Z' = 1 - \frac{3(\sigma_p + \sigma_n)}{|\mu_p - \mu_n|} \qquad (4)$$

Where σ_p and σ_n are the standard deviations of the signal for the positive and negative controls.

For the negative control, 2 μL of H_2O was added, and for the positive control, 2 μL of G6P was added to a final concentration of 2 mM in a 384-well plate. The protein sample was prepared in 25 mM Tris-HCl (pH 7.8), 25 mM NaCl, 7 μM yGsy2p, and 40 nM tracer, which was dispensed by a Multi-drop 384 liquid dispenser (Titertek) into the wells with either H_2O or G6P. The plate was spun down in a centrifuge followed by measurement of the FP signals.

1.2 High-throughput coupled GS activity assay

For the HTS, each plate had three internal control sets: 1) Columns 1 and 2 were the positive control for the plate (n=32); 2) Column 23 was a no G6P control assay, serving as a substitute for the standard positive control for inhibition (n=16); and 3) Column 24

had no hGYS1 enzyme, representing the background measurement (n=16). Prior to the HTS, a Z'-factor was calculated with these three conditions, each at $n \geq 308$, to determine the quality of the HTS for identifying hGYS1 modulators. All solutions were added using either the MultiFlo microplate dispenser (BioTek, Winooski, VT) or MultiDrop 384 (TiterTek, Pforzheim, Germany). To the 384-well assay plates containing 10 µL compound solutions, 20 µL of the appropriate 2× assay mix was added to each well followed by 10 µL of the hGYS1Δ634S8,11N enzyme (4 µg/ml) or enzyme dilution buffer. The final 40 µL hGYS1Δ634S8,11N reaction assay solution contained 1 µg/ml hGYS1Δ634S8,11N enzyme, 200 µM UDPG, 400 µM G6P, 1 mg/mL glycogen, 0 or 12.5 µM compound (1.25% DMSO) and 25 µM DTT in approximately 50 mM Tris, pH 7.8. Column 23 contained no G6P, while column 24 contained no hGYS1. The GS reaction was initiated by adding enzyme and was allowed to proceed at 30°C for 20 min, allowing approximately 20% UDPG utilization in the positive controls. Next, the plates were added to a humidified chamber at >90°C for 15 minutes to inactivate GS activity. The humidified chamber consisted of a plastic wrapped Pyrex dish lined with paper towels and a thin layer of water, which was heated in a hybridization oven. Once the assay plates had cooled to room temperature, the second enzyme, hSCAN-1 (Provided by Terence Kirley), was added and the reaction incubated at 37°C for 60 minutes. Along with the components present for the GS reaction, the 50 µL hSCAN-1 reaction assay also contained 61.6 ng/mL hSCAN-1, 0.01% Tween-20, and 5 mM $CaCl_2$. To measure the amount of Pi produced, the P_i ColorLock Gold Assay Kit (Innova Biosciences, Cambridge, UK) was used as directed, with the exception that 10 µL of Gold mix (reagent + accelerator) was used instead of 12.5 µL due to limitations of the liquid dispenser (Multidrop 384). Absorbance at 650 nm was

measured on a SpectraMax Plus 384 plate reader (Molecular Devices, Sunnyvale, CA). For the first round of screening, an activator was defined as having ≥140% activity compared to control (i.e., >40% activation), whereas an inhibitor had ≤75% activity compared to control (i.e., >25% inhibition). After one round of screening, compounds identified were rescreened twice using the same protocol. The cutoff value for activators remained at ≥140% activity, but inhibitors were selected ≥40% inhibition.

2. Expression and purification of yGsy2p and hGYS1

The His-tagged yGsy2p recombinant enzyme was expressed in BL21 (DE3) *Escherichia coli* and purified using a two-step procedure including affinity chromatography on Ni^{2+}-nitrilotriacetic acid-agarose, and ion exchange purification on a Q-sepharose column[38]. The hGYS1 expression clone in the pFL vector[93] was modified by deleting the intein-chitin binding domain fusion at the C-terminus and replacing it with a simple non-cleavable 6×His-tag at the C-terminus. Purification of the construct was achieved using Ni-NTA resin (Qiagen product #31314) following the manufacturer's instructions. Separately, a construct of hGYS1 was generated in which the C-terminus was truncated at position 634, and the N-terminal phosphorylation sites at positions 8 and 11 were simultaneously mutated to Asn residues, which avoids solubility issues associated with mutation of these residues to Ala, in order to generate the hGYS1Δ634S8,11N construct. This construct was also fused to the same C-terminal 6×His-tag for purification using Ni-NTA resin.

3. Determination of kinetic parameters

Enzyme activity of GS was determined using UDPG as a substrate through ^{14}C-glucose incorporation assay by monitoring the amount of radiolabeled glucose being

incorporated into glycogen[89]. Unless otherwise noted, yGsy2p activity was measured in reaction solution containing 0.3 mM UDPG in the absence or presence of 0.04 mM G6P. The activity of mutant hGYS1Δ634S8,11N enzyme was measured using 0.2 mM UDPG and 0.4 mM G6P, while the activity of wild-type hGYS1 was measured using 0.2 mM UDPG and 1 mM G6P. All kinetic data analyses were performed using the program package SigmaPlot (version 13.0) by fitting the data to the appropriate kinetic equation. The IC_{50} curves for **H23** and its analogs were fit to the four parameter logistic equation. Titration experiments for Michaelis-Menten curves were performed by covarying inhibitor and substrate concentrations. The reaction mixture contained 5 μg/ml yGsy2p, varied UDPG (0.2-8 mM in the absence or presence of 7.2 mM G6P) and **H23** concentrations (0-0.8 mM). All data were fit to competitive, noncompetitive and uncompetitive inhibition models in SigmaPlot (Version 13.0). An appropriate model was selected through analysis of goodness-of-fit and the residuals of those fits. All experiments include the controls contained 2% (v/v) DMSO. The values presented here are the averages ± the standard errors of the mean of three independent experiments with duplicate measurements for each data point in each experiment.

4. Crystallization and structure determination

The G6P-bound yGsy2p (wild-type) crystals were obtained using the hanging drop vapor diffusion method[38]. Briefly, the protein solution was prepared at 3 mg/ml in the buffer containing 20 mM Tris-HCl pH 8.0, 1mM β-mercaptoethanol, and 25 mM G6P. The protein solution was mixed with crystallization reservoir solution containing 0.1 M Bis-Tris, pH 5.9 and 13-15% PEG300. The crystals were soaked with compounds on sitting drop plates to obtain inhibitor-bound yGsy2p complex. The crystals were cryo-protected

in the solution containing 0.1M Bis-Tris pH 5.9, 30% PEG300, and frozen in gaseous N_2 at 100K. Diffraction data sets were collected using X-ray crystallography at the Advanced Photon Source at beamline 19-ID, operated by the Structural Biology Center at Argonne National Laboratory. The data sets were then indexed, integrated and scaled using the HKL3000[94] program package. The structures were solved by molecular replacement using PHASER MR[95], as implemented in the Collaborative Computational Project Number 4[96] (CCP4) program suite. The G6P bound yGsy2p-R589/592A2 mutant structure (pdb code: 3NB0) was used as the model for molecular replacement. The structures were initially refined with a single round of rigid body refinement for individual domains, followed by iterative rounds of restrained refinement with the application of domain-based TLS and NCS restraints using REFMAC5[97] as implemented in CCP4. COOT[98] (version 0.7.2.1) was used to visually inspect and manually adjust the refined models.

5. Analysis of GS activity from cell lysates

HEK293-PTG cells were generated by transfecting HEK293 cells[99] with the plasmid pCDH-FLAG-PTG, harboring the mouse PTG coding region and the hygromycin antibiotic resistance gene utilizing Lipofectamine following manufacturer specifications. Mixed clones were selected for ~10 days in the presence of 0.2 mg/ml hygromycin, expanded and stored in liquid N_2. Analyses of protein expression, GS activity ratio in the absence and presence of saturating concentrations of UDPG (4.4 mM) and of G6P (7.2 mM) and glycogen levels indicated that the protein was expressed, the GS activity ratio was increased 7-fold, from 0.02 in control cells to 0.15 in transfected cells, and that glycogen was increased by 90-fold. Quantitation of the expression of PTG was difficult because the basal levels were very low and undetectable under our conditions.

For lysate preparation the HEK293-PTG cells were cultured in 100 mm plates with 5.5 mM αMEM, 10% FBS, 6 μg/mL penicillin, 10 μg/mL streptomycin, and 0.2 mg/ml hygromycin. Rat-1 cells were cultured in 100 mm plates with 25 mM DMEM, 10% FBS, 6 μg/mL penicillin and 10 μg/mL streptomycin. Cells were grown for 3-4 days until confluency. Before harvest, the cells were washed twice with 5 mL ice-cold GS buffer (50 mM Tris-HCl pH 7.8, 20 mM EDTA, 25 mM KF). Then, 400 μL of GS homogenization buffer (50 mM Tris-HCl pH 7.8, 10 mM EDTA, 2 mM EGTA, 100 mM NaF) with protease inhibitor (0.1 mM TLCK, 10 μg/ml leupeptin, 1 mM benzamidine, 0.5 mM PMSF, 1 mM Na_3VO_4) and β-mercaptoethanol (0.4%) plus Triton X-100 (0.2%) were added to each 100 mm plate. Plates were frozen on liquid N_2 and scraped. Then the lysates were transferred to 2 mL Eppendorf tubes, sonicated for 15 seconds twice on ice, and placed on nutator for 10 minutes at 4 ºC. Protein concentrations were measured using the Bradford reagent. GS activity was initially measured with varying concentrations of the lysates. For monitoring the effect of small molecules on GS, HEK293-PTG cell lysates were diluted 10-fold while Rat-1 cell lysates were diluted 2-fold in homogenization buffer to achieve steady-state kinetics under the conditions we used in the ^{14}C-glucose incorporation assay[33]. GS activity in cell lysates was measured in 50 mM Tris-HCl buffer at pH 7.8 with 6.7 mg/ml glycogen, and subsaturating concentrations of UDPG (0.2 mM) and G6P (1 mM) in the absence or presence of 100 μM H23 and its analogues. All assays including the controls contained 2% (v/v) DMSO.

6. Generation of the S26A and Y513L mutants of yGsy2p

The point mutations S26A and Y513L in yGsy2p were performed using QuikChange II Site-Directed Mutagenesis Kit (Agilent Technologies). The mutants were

cloned into pET-28A yeast Gsy2p construct[44] using forward primers 5'-G GTT GGT GGT ATT TAC GCC GTG CTA AAA TCG AAG GC-3'/5'-C TAC GAG CCT TGG GGT CTC ACA CCT GCA GAA TGT AC-3' and their complements, respectively, and were confirmed by DNA sequencing using T7 or T7-ter primer sequence. The mutant proteins were purified exactly the same way as was yGsy2p. However, the yield was poor compared to WT protein. Additionally, the activity of Y513L mutant was ~10-fold lower than WT enzyme. The activity of the S26A mutant was >100-fold lower than WT enzyme. Kinetics experiments with Y513L and S26A mutants were performed under saturating G6P concentration (7.2 mM).

7. Analysis of hSCAN-1 activity towards UDPG, UDP, UMP, and G6P

High-performance anion exchange chromatography (HPAEC) was used to analyze hSCAN-1 activity on the components present in the HTS reaction mix: UMP, UDP, UDPG, and G6P. Concentrations similar to what would be present in the reaction mix were used: 400 μM for G6P and 200 μM for UMP, UDP, and UDPG, all in 50 mM Tris pH 7.8. Three incubations were set-up for each component. The first contained no additional enzymes and served as the control. The second incubation contained the hSCAN-1 enzyme at a concentration twice that used in the HTS, but otherwise prepared in the same manner as used in the HTS. The third incubation contained calf intestinal alkaline phosphatase (CIAP, Fisher Scientific-1 U/μL), diluted 1:500 in a solution containing 1 mM $MgCl_2$. The reactions were incubated at 30°C for 3 hours and terminated by boiling for 5 minutes. The solutions were passed through a centrifuge filter (Costar Spin-X, 8160), diluted 1:10, and 25 μL aliquots were loaded onto a PA1 column for separation by HPAEC using a Dionex ICS 3000 instrument and a sodium acetate gradient. UDPG, UDP, and UMP were

performed as previously described[100]. For G6P, the starting mobile phase, eluent A, consisted of 100mM NaOH and eluent B was 100 mM NaOH and 1 M sodium acetate.

8. Enzymatic assay for cellular glycogen measurement

HEK293-PTG cells were grown in 100 mm plates with 5.5 mM αMEM, 10% FBS, 6 μg/mL penicillin, 10 μg/mL streptomycin, 2 ug/ml puromycin and 0.2 mg/ml hygromycin. Rat-1 cells were cultured in 100 mm plate with 25 mM DMEM, 10% FBS, 6 μg/mL penicillin and 10 μg/mL streptomycin. When plates reached confluency, cells were washed, trypsinized, and counted with a hemocytomer. Cells were then transferred to 96-well CellBind plates with each well containing 35,000 cells. After 3 days, cells were starved to eliminate glycogen accumulation by culturing cells in medium without glucose for 48 hours. After restoring the glucose levels with addition of standard medium (5.5 mM αMEM for HEK293-PTG cells/25 mM DMEM for Rat-1 cells), there is a linear accumulation of glycogen over 6 hours, during which period test compounds (0.5% DMSO) were added to examine their ability of blocking glycogen synthesis. For determination of glycogen levels, cells were washed, fixed with methanol and incubated with amyloglucosidase to hydrolyze glycogen to free glucose. Glucose was then converted to G6P via hexokinase, followed by oxidation with G6P dehydrogenase and quantification of the resultant NADPH.

9. WST-1 assay for cellular toxicity

The WST-1 assay was used to measure compound cytotoxicity in HEK293-PTG cells. Similarly, cells were first grown in 100 mm plate and then transferred to 96-well CellBind white-wall plate with each well containing 12,500 cells. After 2 days, compounds diluted in serum- and antibiotic-free media were added to cells and incubated for 24 hours.

Four hours prior to the end of compound incubation, 2-(4-iodophenyl)-3-(4-nitrophenyl)-5-(2, 4-disulfophenyl)-2H-tetrazolium (WST-1) was added to cells. Reduction of WST-1 was quantified by measuring the absorbance of the dye at 450 nm using a microplate reader. The percentage of cell viability was calculated using equation 5, by comparing the compound-treated wells to the DMSO-treated vehicle controls after subtraction of the negative control (media + WST-1).

$$\% \text{ Cell viability} = (Abs_{sample} - Abs_{neg}) / (Abs_{DMSO} - Abs_{neg}) \times 100\% \quad (5)$$

Where Abs_{sample} denotes the absorbance value of compound-treated samples, Abs_{DMSO} denotes the absorbance value of DMSO-treated samples, and Abs_{neg} indicates the absorbance value of negative control (media + WST-1).

III. Discovery, characterization, and development of small molecule inhibitors from high-throughput FP assay

A. Results

1. Development of high-throughput FP assay

As an alternative to the ^{14}C-glucose incorporation assay, our strategy for developing a high-throughput assay ideally sought to establish an assay that is sensitive, rapid, and inexpensive[101]. We would reserve the classical radiochemical assay as the "orthogonal" assay for subsequent studies of hits emerging from any screening assay systems. Assays that measure the extent of polarized light emitted from a fluorescently labeled tracer molecule – or fluorescence polarization – can meet such HTS requirements. An FP assay utilizes a fluorescently-labeled tracer molecule that binds to a protein target and thereby forms a complex that rotates more slowly in solution than the fluorophore alone and that leads to differences in the polarization of the emitted light. Incubation of the protein-fluorophore complex with small molecules that displace the fluorescent tracer into solution

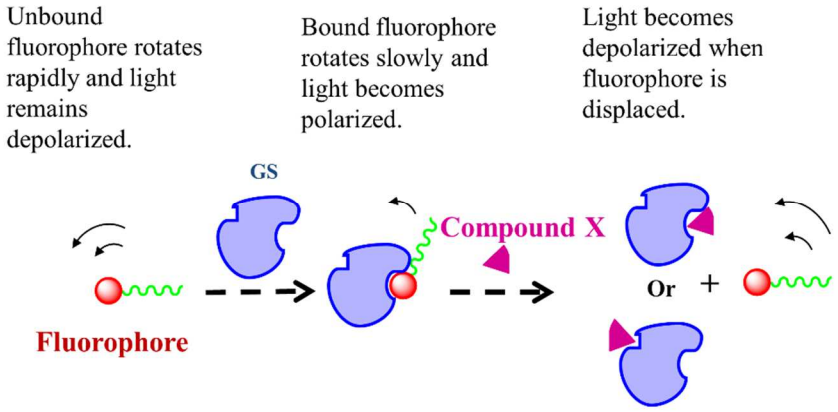

Figure 10. Principle of FP assay. An FP assay features the binding of a fluorophore to a protein target (e.g., GS) that leads to slower complex rotational motion and light polarization. Displacement of the fluorophore, either through direct competition or allosteric regulation, results in faster fluorophore rotation and light depolarization. Compounds that cause a decrease of light polarization are identified as protein modulators.

thereby produces more of the faster rotating complex and causes relative depolarization of the emitted light. Using this assay system as a vehicle for HTS, we identified small molecules that reduce the FP signal as GS-interacting agents (**Figure 10**).

The development of any FP assay involves the design and synthesis of a functional, fluorescent probe. Although G6P is a well-known, allosteric activator of GS, the selective coupling to what would be similarly reactive hydroxyl groups in G6P presented an synthetic challenge. Because glucosamine-6-phosphate (GlcN6P) also activates GS[102] and possesses a single, reactive amine group at the 2'-position, its selection as a molecular probe on which to tag a fluorophore is an attractive alternative to G6P. In addition, close inspection of the Gys2p crystal structure with bound G6P[38] indicates that the 2'-OH is solvent exposed and thus may not impede binding of the probe if this position is modified. Herein, we synthesized a fluorophore-modified GlcN6P (aka GlcN6P-fluorescein-5-Ex) using GlcN6P and the N-hydroxysuccinimidyl ester of fluorescein-5-Ex (**Figure 11A**), purified the fluorophore by HPLC and confirmed the expected molecular mass by mass spectrometry (MS) in which it displayed a $M+H^+$ peak at *m/z* 735.1267 consistent with $[C_{31}H_{31}N_2O_{15}PS + H]^+$ with calculated exact mass within acceptable limits (*i.e.*, calculated *m/z* 735.1256) (**Figure 11B**).

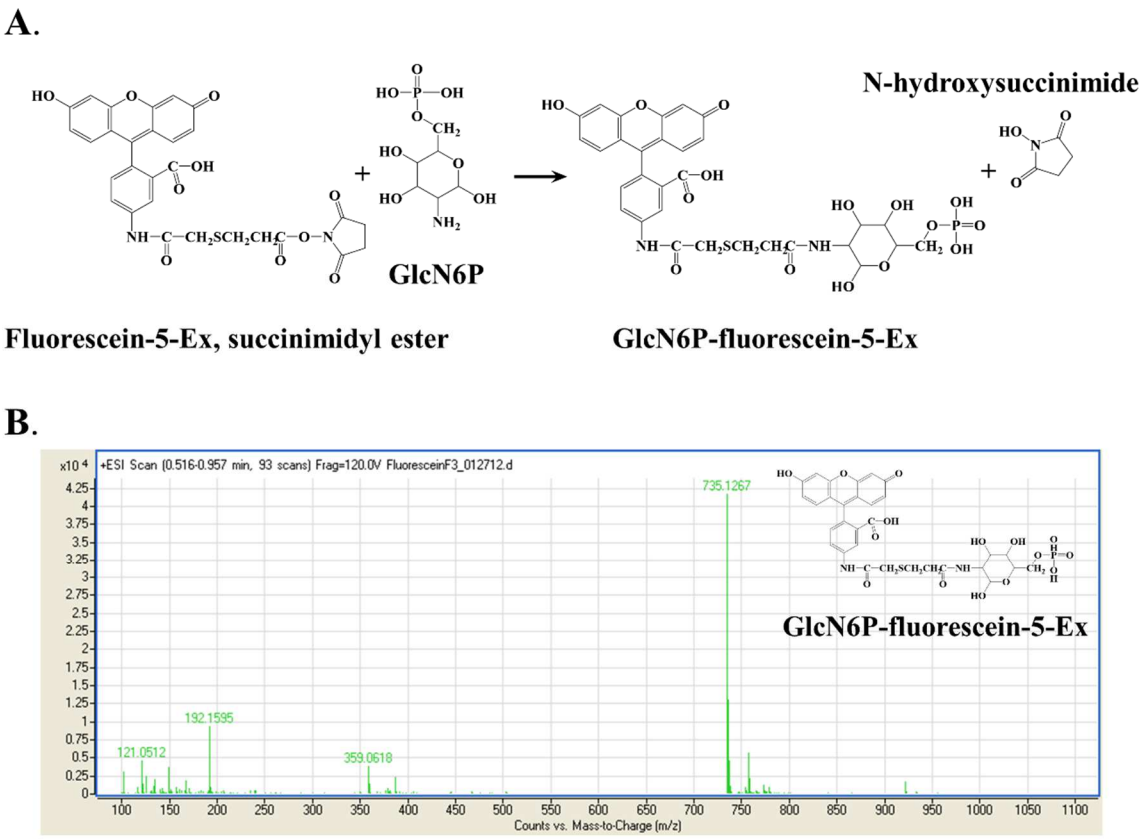

Figure 11. Synthesis, purification, and validation of GlcN6P-fluorescein-5-Ex. **(A)** Schematic representation of the coupling reaction of Fluorescein-5-Ex, succinimidyl ester and GlcN6P to form GlcN6P-fluorescein-5-Ex. **(B)** The HPLC-purified product of fluorophore coupling reaction, GlcN6P-fluorescein-5-Ex, was confirmed by MS demonstrating *m/z* of 735.1267. (This data was generated by Dr. Vimbai M. Chikwana.)

We next examined the binding of the GlcN6P-fluorescein-5-Ex probe to GS by adding the tracer to varying concentrations of yGsy2p to generate a saturation binding curve, which led to a calculated dissociation constant of 7.6 ± 0.7 μM (**Figure 12A**). Furthermore, the competitive displacement by G6P (K_d = 70.9 ± 3.6 μM) demonstrated that the tracer molecule bound to the G6P allosteric site (**Figure 12B**). In comparison, we determined yGsy2p activation by G6P using the standard ^{14}C-glucose incorporation assay which yielded an AC_{50} of 98.1 ± 3.1 μM (**Figure 12C**). We also tested the binding of GlcN6P-fluorescein-5-Ex and displacement by G6P using hGYS1. While the GlcN6P-

coupled fluorophore and the fluorophore alone bound to hGYS1, G6P was unable to displace either compound, a finding that suggested nonspecific binding of the fluorophore to hGYS1. For this reason, we used yGsy2p and not hGYS1 for HTS. The high conservation of residues within the G6P allosteric site, the active site and overall protein sequence identity (~55%) between yGsy2p and hGYS1 supported the decision to use the yeast enzyme as a screening surrogate for the human enzyme (**Figure 13**). The robustness of the FP assay for HTS was assessed by determining the Z′-factor, a parameter reflective of both the signal dynamic range and data variability[103]. While the ideal Z′-factor is 1, a Z′-factor between 0.5 and 1 is considered excellent and suitable for screening assays. The FP values for the positive controls (maximal binding, without G6P) and negative controls (fully displaced tracer, with G6P) were 109.23 ± 1.97 and 26.48 ± 1.93 (mean ± SD) from the 384-wells, respectively. The Z′-factor for this assay was determined as 0.86, indicating that this assay is well suited for HTS (**Figure 12D**).

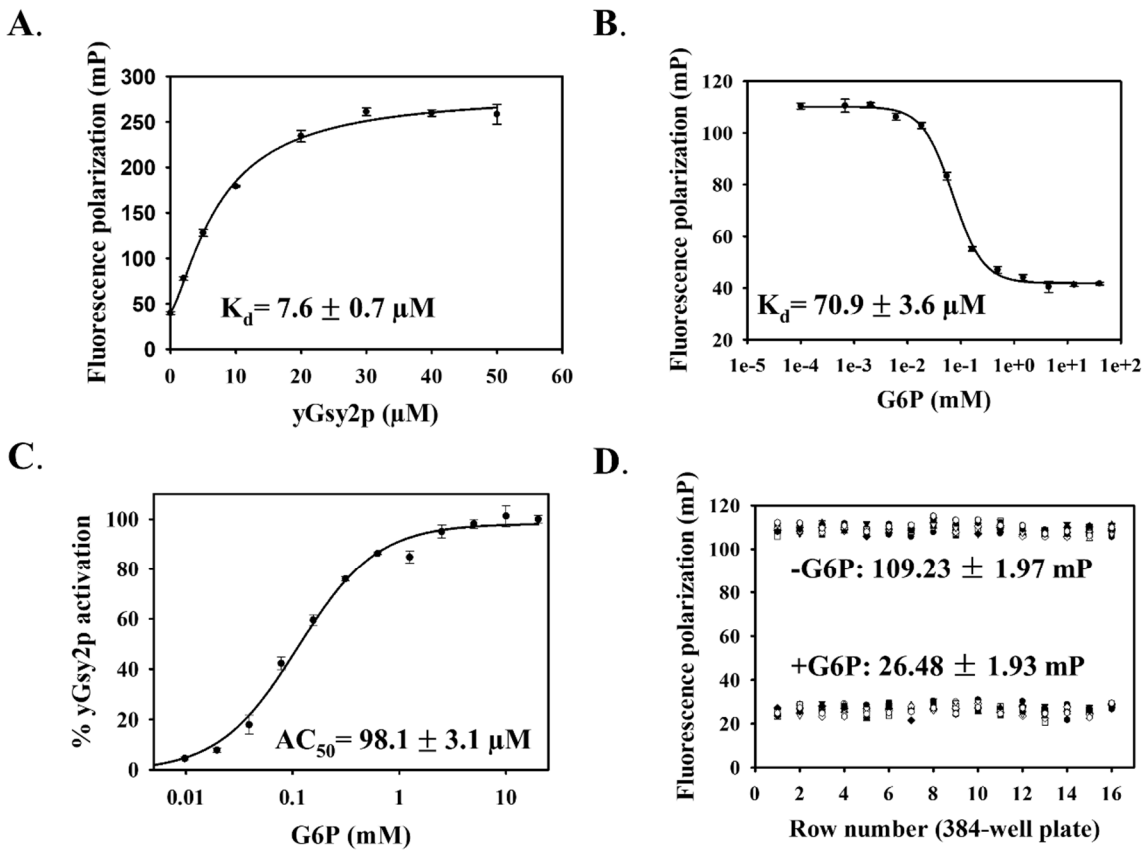

Figure 12. Development of FP assay for HTS. **(A)** Saturation binding isotherm for GlcN6P-fluorescein-5-Ex binding to yGsy2p. The binding affinity was determined by adding GlcN6P-fluorescein-5-Ex to a final concentration of 20 nM in the presence of varying yGsy2p concentrations (0 to 50 µM). K_d= 7.6 ± 0.7 µM. Averages of triplicate assays ± SEM are shown. **(B)** Displacement of GlcN6P-fluorescein-5-Ex binding to yGsy2p by G6P. A mixture of yGsy2p and GlcN6P-fluorescein-Ex was added to various G6P concentrations (0.68 µM to 40 mM). K_d= 70.9 ± 3.6 µM. Averages of triplicate assays ± SEM are shown. **(C)** Yeast Gsy2p activation in the presence of varying concentrations of G6P. AC_{50} was determined as 98.1 ± 3.1 µM. Averages of triplicate assays ± SEM are shown. **(D)** Z′-factor determination: fluorescence polarization values of the bound (-G6P), and the free (+2 mM G6P) GlcN6P-fluorescein-5-Ex are shown, for the 16 rows with each row containing 12 columns of either the bound or free state. The graphs depict a representative experiment from at least three independent experiments. (This data was generated by Dr. Vimbai M. Chikwana.)

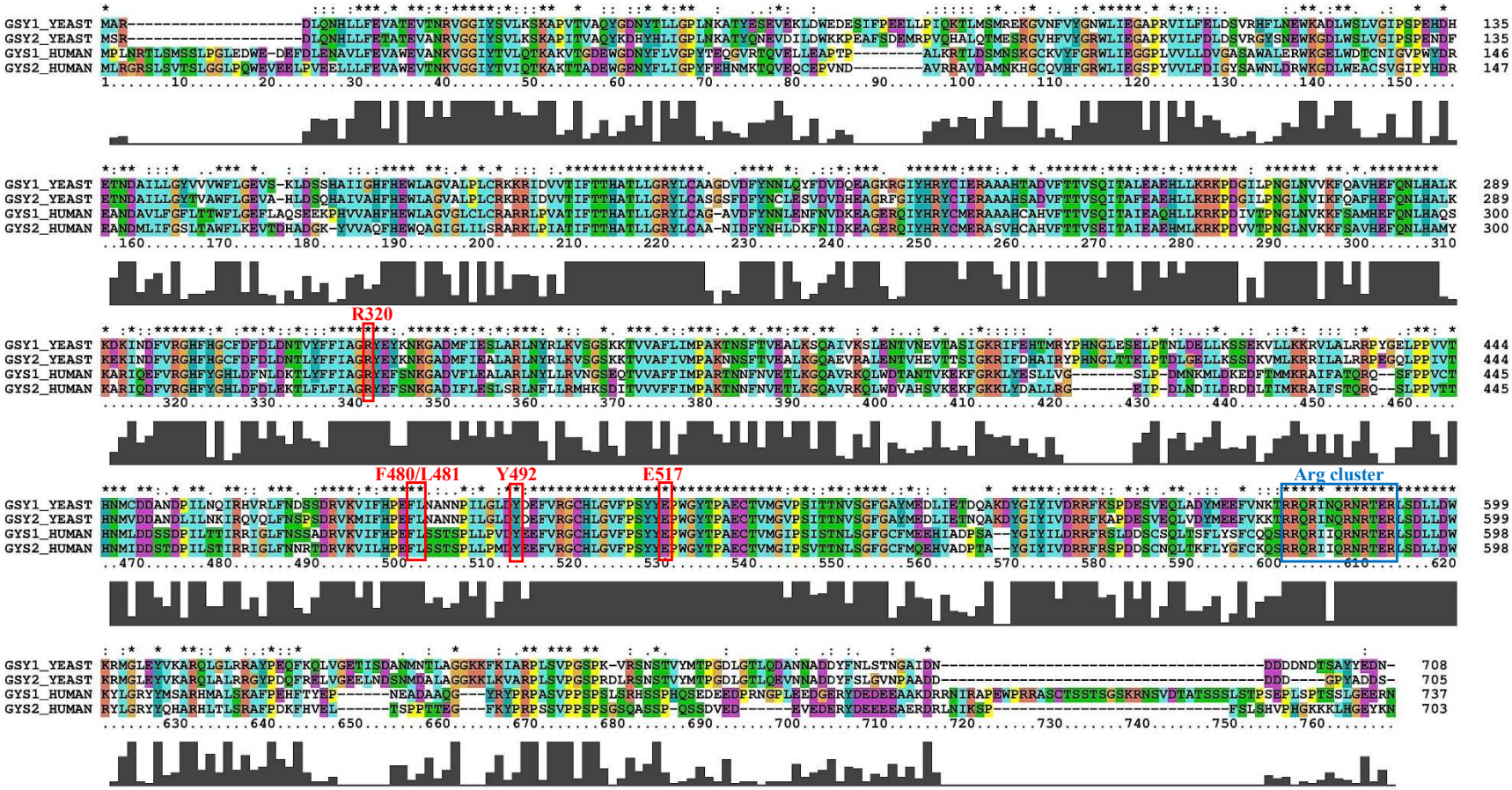

Figure 13. Sequence alignment of yeast and human GS. The overall sequence identity between yGsy2p and hGYS1 is around 55%. Residues that form the active site, including R320/F480/L481/Y492/E517 (shown in red box), and G6P binding site (Arg cluster, shown in blue box) are highly conserved across yeast and human species. The sequence alignment was generated using ClustalX.

2. Hit identification and validation

Dr. Vimbai M. Chikwana performed the HTS against the yGsy2p enzyme using the 50K ChemBridge DIVERSet library at 10 μM concentration (**Table 2**). The HTS was adapted to the 384-well plate format using three columns for the DMSO negative controls and one column for the unlabeled G6P as the positive control, resulting in a total of 157 screening plates. We used a Z'-score threshold of -1, corresponding to a separation of 3 standard deviations between μ_c (means of the control DMSO signal) and μ_s (means of the library sample signal) as a cutoff (**Figure 14**). These standards produced 117 hits and an overall 0.23% hit rate. Initial stock availability led to re-ordering of 110 compounds

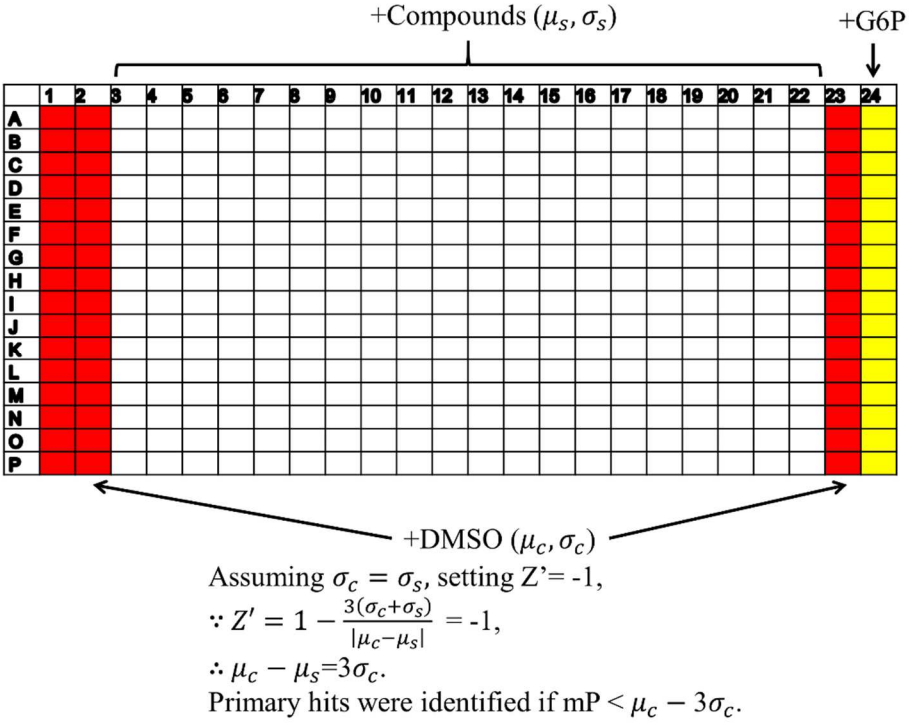

Figure 14. 384-well plate layout for FP HTS. Each screening plate has one column for unlabeled G6P as the positive control, three columns for the DMSO negative controls, and 20 columns for compounds. Z'-score threshold of -1, corresponding to a separation of 3 standard deviations between μ_c (means of the control DMSO signal) and μ_s (means of the library sample signal), was chosen as a signal cutoff for hit selection. The 50K compounds from ChemBridge DIVERSet library were applied to 157 screening plates, resulting in the identification of 117 primary hits.

Table 2. FP HTS protocols.

Category	Parameter	Description
Assay	Type of assay	*In vitro*
	Target	Gsy2p, Saccharomyces cerevisiae
	Primary measurement	Detection of fluorescence polarization
	Key reagents	Purified yeast synthase Gsy2p (3 μM), synthesized and purified fluorophore GlcN6P-fluorescein-5-Ex (20 nM)
	Assay protocol	The FP experiments were described in Methods
Library	Library size	50,000
	Library composition	The Library is selected from ChemBridge's EXPRESSPick. Collection stock of more than 480,000 handcrafted compounds.
	Source	ChemBridge Corporation
Screen	Format	384-well plate
	Concentration tested	10 μM, 1.2 % DMSO
	Plate controls	For the negative controls 10 μL of DMSO (6%) was added and for the positive controls 10 μL of G6P was added for a final concentration of 2 mM to 40 μL reaction mixture in a 384-well plate.
	Reagent/compound dispensing system	Multi-drop 384 liquid dispenser (Titertek)

	Detection instrument	EnVision® Multilabel plate reader (PerkinElmer)
Post-HTS analysis	Assay validation/QC	Plate corrected individual Z'-scores
	Hit criteria	Z'-score threshold of -1, equivalent to a separation of 3 standard deviations between μ_c (means of the control signal) and μ_s (means of the library sample signal)
	Hit rate	0.23%
	Additional assay(s)	Hits were validated using standard ^{14}C-glucose incorporation assay against yGsy2p, using 100 μM compounds in triplicate
	Confirmation of hit purity and structure	LC/MS or NMR

(designated **H1**-**H110**) from ChemBridge and validation of their activity using the standard ^{14}C-glucose incorporation assay at 100 μM concentration. This approach validated 16 hits with greater than 40% inhibition of yGsy2p activity (**Figure 15A**).

Since the yGsy2p enzyme was used as a screening surrogate for the hGYS1 enzyme, I next examined if the 16 validated compounds were also active as inhibitors of hGYS1 activity. To accomplish this necessary confirmation, we redesigned the hGYS1 construct to create a constitutively active enzyme through deletion of the C-terminal phosphorylation domain (residues 635-737) and through the substitution of the two N-terminal phosphorylation sites (Ser8, Ser11) with Asn residues (designated hGYS1Δ634S8,11N). Purification of this truncated form of GS in significant quantity led to an enzyme that exhibited an activation state of ~0.2, a ratio of GS activity in the absence of as compared to the activity in the presence of G6P as an index of the phosphorylation state of the enzyme[45]. Unlike the heavily phosphorylated, full-length enzyme produced in insect cells that had an activation state of <0.01[93], this truncated form of GS was well suited for screening assays designed to look for inhibitors because the enzyme was neither overly inhibited by phosphorylation nor rendered insensitive to the effects of G6P. At a test concentration of 100 μM, only 1 hit, namely a substituted imidazole, (*rac*)-2-methoxy-4-(1-(2-(1-methylpyrrolidin-2-yl)ethyl)-4-phenyl-1*H*-imidazol-5-yl)phenol (**H23**), demonstrated greater than 20% inhibition using this truncated hGYS1 (**Figure 15B)**.

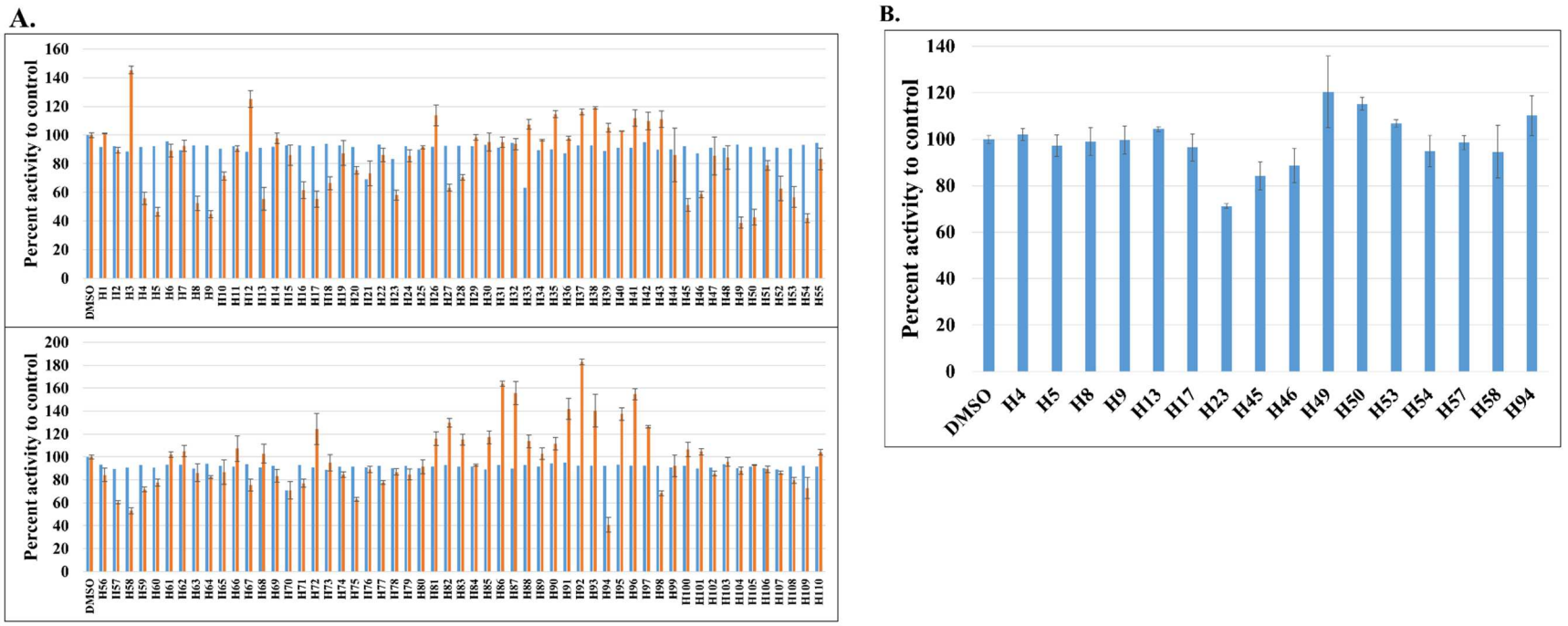

Figure 15. Hit identification and validation. **(A)** In the FP assay, setting a Z'-score threshold of -1 gave 117 initial hits, out of which 110 (designated **H1-H110**) were re-purchased and tested. The blue column represents the percentage of FP signal to control. The hits were screened at 10 μM in single measurement. The orange column is the percentage of yGsy2p activity to control measured through ^{14}C-glucose incorporation assay. The hits were tested at 100 μM. Averages of triplicate assays ± SEM are shown. **(B)** Percentage of hGYS1Δ634S8,11N activity to control measured through ^{14}C-glucose incorporation assay. The hits were tested at 100 μM. Averages of triplicate assays ± SEM are shown.

3. Crystal structure of the H23-yGsy2p complex

There are no mammalian GS crystal structures, but the structures of two eukaryotic enzymes, namely yGsy2p from *Saccharomyces cerevisiae*[38] and GS from *Caenorhabditis elegans*[39] provide a basis for structural studies of our small molecule inhibitors. As previously described, yeast Gsy2p existed as tetramer in the crystal structure, and each subunit contained two Rossmann-fold domains with the catalytic site in the interdomain cleft[38]. In the crystal packing environment in crystals of the activated form of GS, one of the four subunits appeared 13.3º more closed than the other three subunits[41]. I successfully determined the crystal structure of the **H23**-yGsy2p (wild-type) complex to a resolution of 2.85 Å (**Table 3**), and observed **H23** binding in three of the four subunits, all of which corresponded to the more "open" domain subunits (**Figure 16B**). The structure showed **H23** bound within the active site of GS in a location that overlapped with the binding site for UDPG (**Figure 16C** and **16D**). Structural alignment of the R589/592A2·UDP complex to the WT·**H23** complex using their C_α carbons generated an overall root mean square deviation of 0.36 Å, indicating a high degree of similarity. The binding of **H23** to yGsy2p was mediated by hydrogen-bond formation between the phenolic hydroxyl group of **H23** and the nitrogen backbone of Leu481, hydrophobic π-stacking interactions of the 2-methoxyphenol sandwiched between Tyr492 and Phe480, dynamic van der Waals interactions of the stilbene-like double bond with the side chains of Phe480 and Arg320, and additional van der Waals interactions of the *N*-methylpyrrolidine moiety with Tyr492, Thr514, and Glu517 (**Figure 16D**).

Table 3. Structural data and refinement statistics for H23-yGsy2p crystal.

Data collection		**Refinement**	
Space group	I222	No. reflections	95326
Cell dimensions		R_{work}/R_{free}	0.20/0.26
a, b, c (Å)	192.3, 206.6, 205.0	r.m.s. deviations	
α, β, γ	90.0, 90.0, 90.0	Bond lengths (Å)	0.010
Resolution	50-2.85	Bond angles (º)	1.44
R_{merge}	0.091 (0.766)	Ramachandran plot	
R_{meas}	0.100 (0.843)	Preferred/Allowed (%)	99.01
R_{pim}	0.040 (0.347)	Outliers (%)	0.99
CC1/2	0.999 (0.857)	B-factors	
I/σ(I)	20.3 (2.0)	Protein	Chain A, 80.1; B, 83.7;
Completeness (%)	99.7 (100)		C, 91.9; D, 94.6
Redundancy	6.3 (5.5)	Ligand (**H23**)	Chain A, 100.9; C, 128.3; D, 107.5

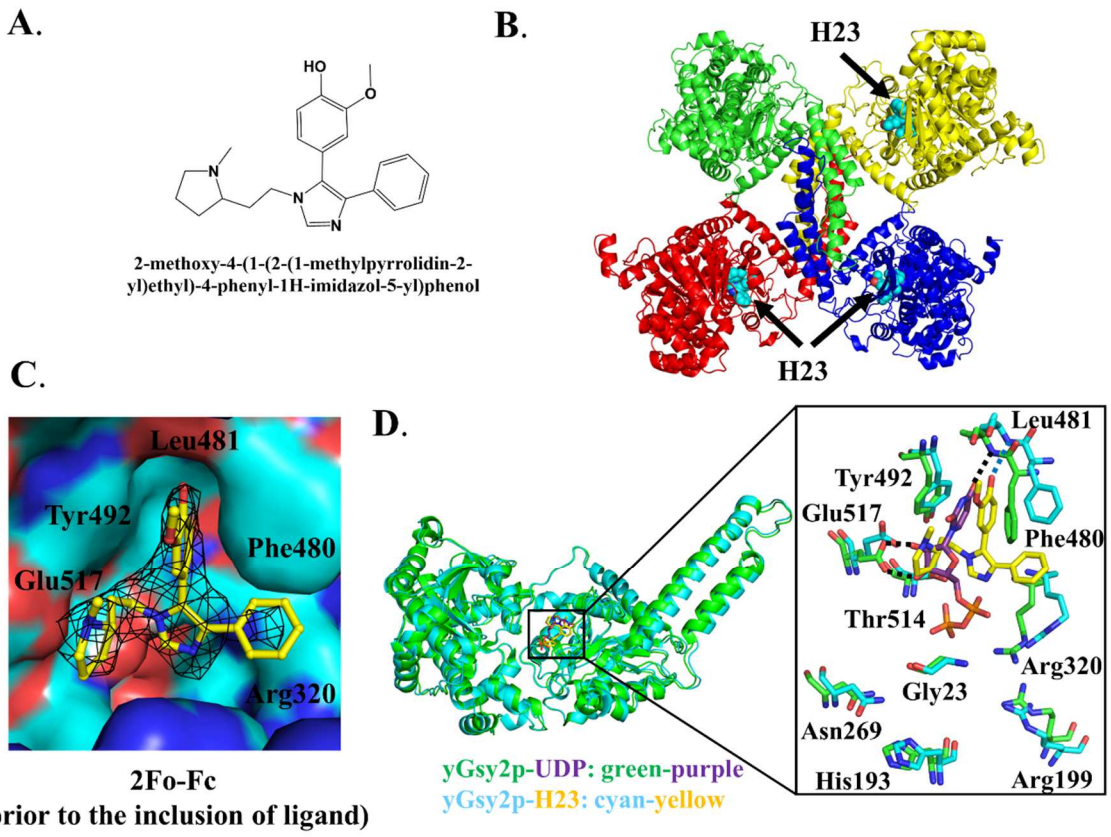

Figure 16. Crystal structure of the H23-yGsy2p complex (PDB: 6U77). **(A)** Chemical structure of **H23**. **(B)** Ribbon diagram representation of the crystal structure of **H23**-yGsy2p complex. **H23** is represented by space-filling models in cyan, and binds to three subunits of yGsy2p which are colored differently. **(C)** The electron density for **H23** prior to the inclusion of the ligand in refinement. The map shown is the original unbiased 2Fo-Fc map contoured at 1 standard deviation. **(D)** Stick representation of the superposed UDP (purple) and **H23** (yellow) structures and their interactions with the surrounding amino acids.

4. Kinetic characterization of H23

In a study of the inhibitory potential for **H23** against yeast and human GS using the standard ^{14}C-glucose incorporation assay, **H23** exhibited IC_{50} values of 280 µM and 263 µM in the absence and presence, respectively, of G6P for yGsy2p (**Figure 17A**). The similarity in IC_{50} values indicated **H23** was not in direct competition with G6P. Under subsaturating G6P concentrations, the IC_{50} values of **H23** against either hGYS1Δ634S8,11N or wild-type hGYS1 was 161 µM and 875 µM, respectively (**Figure**

17B). Even though the presence or absence of G6P did not impact **H23** potency, the activity state of the human GS enzyme had a five-fold effect on the binding of **H23**.

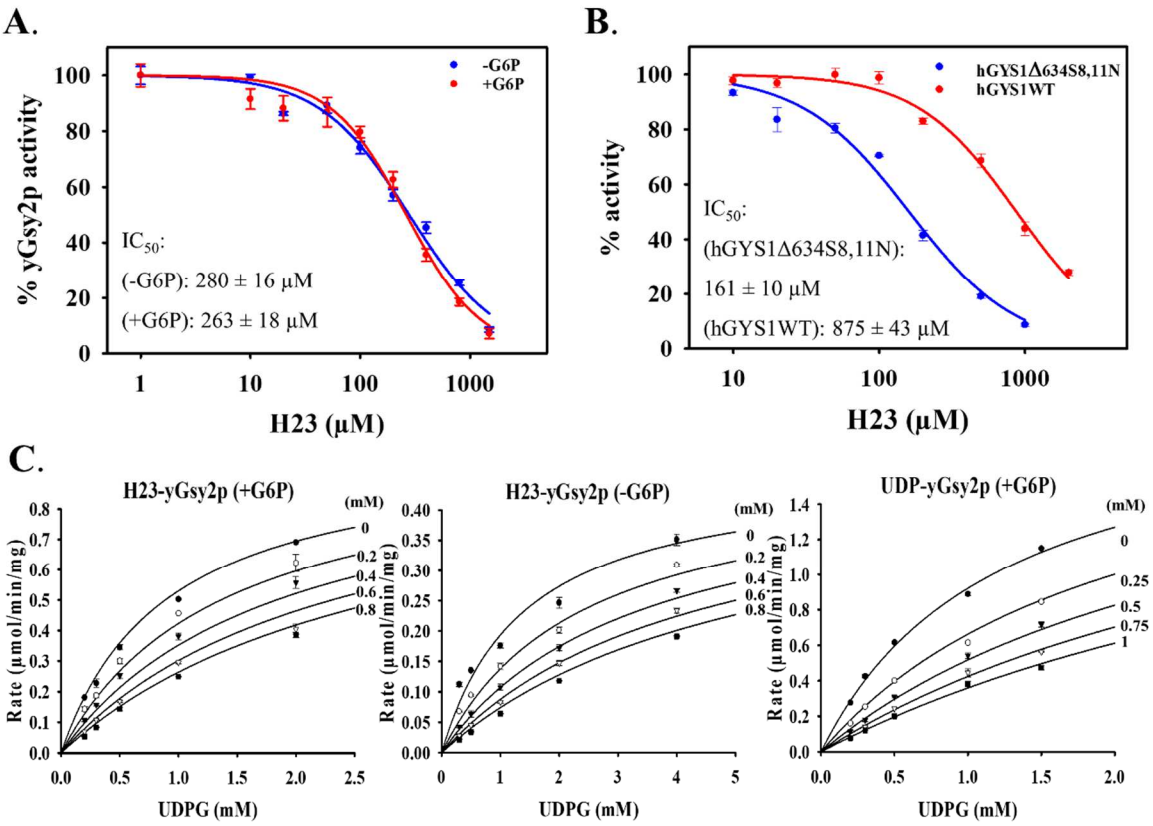

Figure 17. Kinetic characterization of **H23**. **(A)** Inhibition of **H23** to yGsy2p in the absence or presence of G6P. **(B)** Inhibition of **H23** to hGYS1Δ634S8,11N and hGYS1 wild-type. All IC_{50} curves represent one of three experiments performed using triplicate measurements for each condition, with mean ± SEM shown. **(C)** Michaelis-Menten curves fit to the competitive inhibition equation for varied **H23** versus UDPG. **H23** has a K_i of 370 ± 30 µM in the presence of G6P and a K_i of 290 ± 20 µM in the absence of G6P. UDP is used as a positive control for competitive inhibition against varied UDPG for yGsy2p, which displayed a K_i of 350 ± 10 µM. The reported K_i values are the mean ± SEM from three independent experiments in duplicate.

To understand the mode of **H23** inhibition, I performed co-variation experiments by varying the concentrations of UDPG at different fixed concentrations of **H23** and fitting the kinetic data against the equations for competitive, non-competitive, and uncompetitive inhibition. The inhibition data with **H23** was consistent with a competitive inhibition mode

with respect to varied UDPG for yGsy2p, with K_i values of 0.37 mM in the presence of G6P, and 0.29 mM in the absence of G6P. UDP displayed a similar competitive mode of inhibition with a K_i value of 0.35 mM (**Figure 17C**).

5. Development of SAR for H23 analogs toward hGYS1

The overall protein sequence alignment shows 55% sequence identity between yGsy2p and hGYS1. Because the amino acids in the binding site for **H23**, including Arg320, Phe480, Leu481, Tyr492, and Glu517 in yGsy2p, were completely conserved across yeast and human species (**Figure 13**), the structural information derived from the **H23**-yGsy2p crystal structure provided a useful guide for SAR studies focused on hGYS1. We examined a total of 491 analogs that shared at least 50% structural similarity with **H23**, and tested their activities against yGsy2p, hGYS1Δ634S8,11N, and wild-type hGYS1 using the ^{14}C-glucose incorporation assay. My initial kinetic studies showed that a five-membered, heteroaryl (HA) core with a phenyl group at the A_1 position, and a second, vicinal phenyl group were essential elements of **H23** (**Table 4**). Consequently, analog development modified the HA core, A_1 and substructures at R_1-R_7 positions shown in the structure in **Table 4**. In this study, all **H23** analogs possessed one of the following HA cores: imidazole (designated as HA_1, **IM**), pyrrole (designated as HA_2, **PR**) or pyrazole (designated as HA_3, **PZ**). Active compounds appeared in structures with any of these three cores, but the most potent compounds had a pyrazole (HA_3) scaffold. Commercial libraries were the source of HA_1 and HA_2 compounds in **Table 4**, and a three-step synthesis provided the HA_3 compounds as outlined in **Scheme 1**.

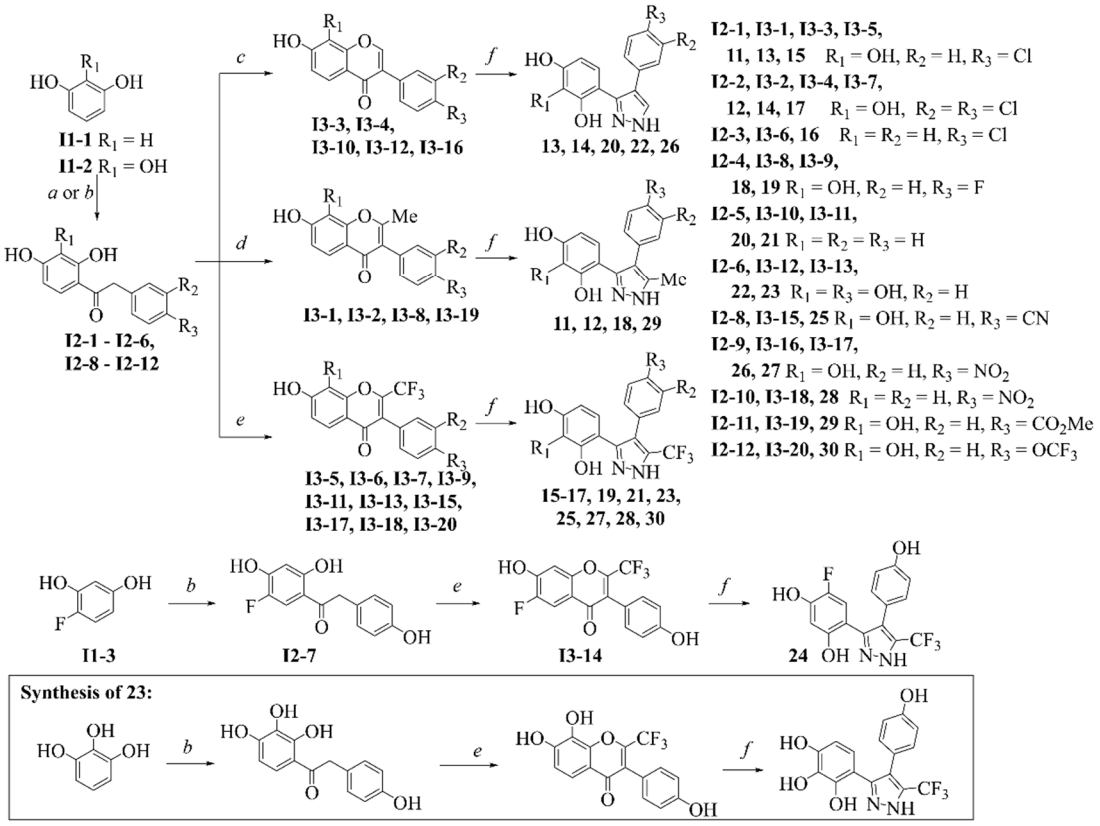

Scheme 1. Synthesis of pyrazoles **PZ11-30**. Reagents and conditions: **(*a*)** (i) arylacetonitrile, $BF_3{\cdot}Et_2O$, HCl (gas), rt, 6-8 h, (ii) H^+/H_2O, 0.5-2 h; **(*b*)** (i) arylacetic acid, $BF_3{\cdot}Et_2O$, 80-90 ^{0}C, 2 h, (ii) H_2O; **(*c*)** (i) DMF, $BF_3{\cdot}Et_2O$, $POCl_3$, 50-60 ^{0}C, 2 h, (ii) H_2O; **(*d*)** (i) Ac_2O, KOAc, reflux, 8 h, (ii) H_2SO_4, EtOH, reflux, 0.5 h; **(*e*)** (i) $(CF_3CO)_2O$, pyridine, rt, 48-120 h, (ii) H_2O; **(*f*)** $N_2H_4{\cdot}H_2O$, reflux, 0.5-6 h. (This synthetic work was performed in Dr. Mykhaylo S. Frasinyuk's laboratory at NAS of Ukraine and Dr. David S. Watt's laboratory at University of Kentucky.)

We took a step-by-step strategy to modify positions in **H23** to augment or diminish interactions with substituents between **H23** and relevant residues in yGsy2p. Briefly, starting from the imidazole core (HA_1), we determined that the R_1 hydroxyl group that formed a hydrogen bond with the peptide nitrogen of Leu481 was essential to retain good inhibitory activity (i.e., compare **H23** versus **IM1** in **Table 2**). The addition of an extra methylene unit to the R_7 chain eliminated inhibitory potential (**IM4** versus **IM3**). In a similar fashion, the most potent of the pyrrole HA_2 compounds also had a hydroxyl group

at the R_1 position (**PR7** versus **PR9** or **PR10**). Interestingly, substitution of a carboxyl group at the R_7 position improved the potency to hGYS1 by 2-fold (IC_{50} values for **H23** versus **PR7**), a finding that suggested different conformational binding modes for **H23** and **7** for hGYS1.

Because none of the analogs within the HA_1 or HA_2 series generated noteworthy improvements in potency, we explored a different set of compounds based on a pyrazole core (HA_3). Within the HA_3 series, my SAR studies demonstrated the importance of a hydrogen bond acceptor at the R_1 position as displayed in the following order of potency: -OH > $-NO_2$ > -CN > -F > -H > -Cl (i.e., **PZ23** versus **PZ27**, **PZ25**, **PZ19**, **PZ21** and **PZ15**). When a chlorine is present at the R_1 position, adding a second chlorine substituent at the R_2 position improved potency (**PZ12** versus **PZ11** or **PZ14** versus **PZ13** or **PZ17** versus **PZ15**). The most potent compounds in this series had a pyrogallol group at the $R_{4\text{-}6}$ positions, and the hydroxyl groups on this substituent conferred inhibition to GS even if the R_1 position was non-optimal. For instance, **PZ11** was 16-fold more potent than **H23**. Strikingly, the meta-hydroxyl group (R_5) was critical to binding. Substitution of this hydroxyl group with hydrogen decreased potency significantly (**PZ16** versus **PZ15** or **PZ28** versus **PZ27**). The SAR studies also indicated that substituents at the R_7 position had an effect on activity in the following order of $-CF_3$ > -H > $-CH_3$ (**PZ15** or **PZ13** versus **PZ11**; **PZ17** or **PZ14** versus **PZ12**). In summary, analog development initiated from the substituted imidazole **H23** led to a substituted pyrazole, namely 4-(4-(4-hydroxyphenyl)-3-(trifluoromethyl)-1H-pyrazol-5-yl)pyrogallol (**PZ23**) that had an *in vitro* IC_{50} value of 2.75 μM, an improvement in potency toward hGYS1 of more than 300-fold.

Table 4. SAR for **H23** analogs.

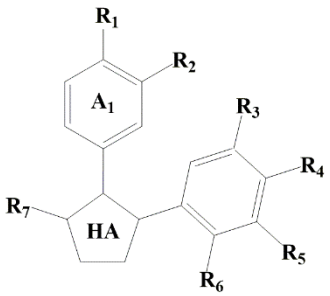

HA_1 (Imidazole, IM)

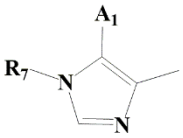

HA_2 (Pyrrole, PR)

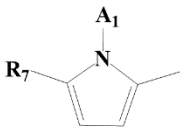

HA_3 (Pyrazole, PZ)

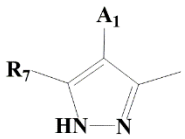

										%Activity @ 300µM compound			IC_{50} (µM)
Compound	HA	A_1	R_1	R_2	R_3	R_4	R_5	R_6	R_7	yGsy2p	hGYS1Δ 634S8,11N	hGYS1	hGYS1
H23	HA_1		OH	OCH_3	H	H	H	H	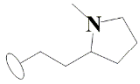	36.5±0.6	46.5±0.4	77.1±1.2	875±43
IM1	HA_1		H	H	H	H	H	H	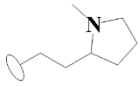	NI	93.3±1.5	NI	ND
IM2	HA_1	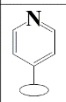	H	H	H	H	H	H	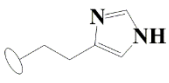	72.7±0.4	94.4±2.2	NI	ND
IM3	HA_1		OH	H	H	H	H	H	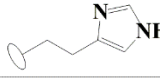	66.6±1.3	56.6±1.3	93.4±2.8	ND
IM4	HA_1		OH	H	H	H	H	H	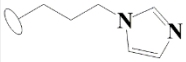	94.8±2.9	NI	NI	ND
PR5	HA_2		OH	H	H	H	H	H	CH_3	79.7±1.0	84.3±0.5	NI	ND
PR6	HA_2		OH	H	H	H	H	H	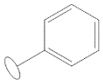	86.0±3.1	NI	NI	ND
PR7	HA_2		OH	H	H	H	H	H	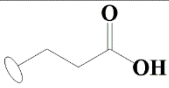	40.1±0.9	40.1±0.4	58.9±0.3	384±28
PR8	HA_2		OH	H	H	OCH_3	H	H	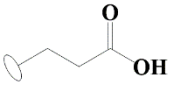	34.5±0.4	50.6±3.0	84.0±0.1	ND
PR9	HA_2		$CONH_2$	H	H	H	H	H	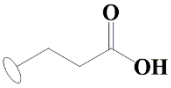	49.3±0.6	40.6±0.1	78.7±0.9	ND
PR10	HA_2		F	H	H	H	H	H	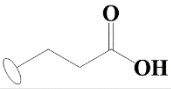	84.7±0.1	72.1±4.1	87.5±0.4	ND
PZ11	HA_3		Cl	H	H	OH	OH	OH	CH_3	3.52±0.67	6.47±0.09	4.34±0.94	52.9±3.8

										% Activity @ 20 µM compound			IC_{50} (µM)
Compound	**HA**	**A_1**	**R_1**	**R_2**	**R_3**	**R_4**	**R_5**	**R_6**	**R_7**	**yGsy2p**	**hGYS1Δ 634S8,11N**	**hGYS1**	**hGYS1**
PZ11	**HA_3**		**Cl**	**H**	**H**	**OH**	**OH**	**OH**	**CH_3**	**NI**	**NI**	**91.8±0.3**	**52.9±3.8**
PZ12	**HA_3**		**Cl**	**Cl**	**H**	**OH**	**OH**	**OH**	**CH_3**	**NI**	**81.7±2.7**	**84.7±2.5**	**ND**
PZ13	**HA_3**		**Cl**	**H**	**H**	**OH**	**OH**	**OH**	**H**	**NI**	**79.4±0.9**	**85.4±0.1**	**ND**
PZ14	**HA_3**		**Cl**	**Cl**	**H**	**OH**	**OH**	**OH**	**H**	**76.7±0.5**	**26.4±2.3**	**52.5±4.4**	**19.5±1.3**
PZ15	**HA_3**		**Cl**	**H**	**H**	**OH**	**OH**	**OH**	**CF_3**	**51.5±0.4**	**11.8±2.4**	**47.5±1.7**	**19.8±0.5**
PZ16	**HA_3**		**Cl**	**H**	**H**	**OH**	**H**	**OH**	**CF_3**	**NI**	**87.9±1.5**	**NI**	**ND**
PZ17	**HA_3**		**Cl**	**Cl**	**H**	**OH**	**OH**	**OH**	**CF_3**	**47.4±4.4**	**5.28±0.16**	**12.2±1.3**	**13.7±0.6**
PZ18	**HA_3**		**F**	**H**	**H**	**OH**	**OH**	**OH**	**CH_3**	**NI**	**89.0±1.5**	**94.0±2.4**	**ND**
PZ19	**HA_3**		**F**	**H**	**H**	**OH**	**OH**	**OH**	**CF_3**	**45.7±12.4**	**11.7±0.1**	**47.8±7.0**	**14.1±0.8**
PZ20	**HA_3**		**H**	**H**	**H**	**OH**	**OH**	**OH**	**H**	**NI**	**25.2±1.6**	**84.7±2.7**	**ND**
PZ21	**HA_3**		**H**	**H**	**H**	**OH**	**OH**	**OH**	**CF_3**	**51.8±1.8**	**5.68±0.16**	**47.2±1.2**	**16.4±0.6**
PZ22	**HA_3**		**OH**	**H**	**H**	**OH**	**OH**	**OH**	**H**	**6.21±0.59**	**23.0±1.9**	**22.6±0.4**	**9.82±1.06**
PZ23	**HA_3**		**OH**	**H**	**H**	**OH**	**OH**	**OH**	**CF_3**	**0.97±0.01**	**-1.01±0.37**	**-0.26±0.34**	**2.75±0.08**
PZ24	**HA_3**		**OH**	**H**	**F**	**OH**	**H**	**OH**	**CF_3**	**65.2±2.4**	**74.2±4.0**	**78.4±0.9**	**72.4±6.5**
PZ25	**HA_3**		**CN**	**H**	**H**	**OH**	**OH**	**OH**	**CF_3**	**51.2±1.5**	**8.14±0.65**	**42.0±1.5**	**10.1±0.8**

										% Activity @ 20 µM compound			IC_{50} (µM)
Compound	**HA**	**A_1**	**R_1**	**R_2**	**R_3**	**R_4**	**R_5**	**R_6**	**R_7**	**yGsy2p**	**hGYS1Δ 634S8,11N**	**hGYS1**	**hGYS1**
PZ26	**HA_3**		**NO_2**	**H**	**H**	**OH**	**OH**	**OH**	**H**	**78.4±5.1**	**85.0±2.6**	**66.8±3.7**	**34.0±7.6**
PZ27	**HA_3**		**NO_2**	**H**	**H**	**OH**	**OH**	**OH**	**CF_3**	**18.8±0.5**	**10.5±0.1**	**1.43±0.13**	**6.54±0.09**
PZ28	**HA_3**		**NO_2**	**H**	**H**	**OH**	**H**	**OH**	**CF_3**	**82.3±7.5**	**92.7±1.6**	**89.2±6.4**	**ND**
PZ29	**HA_3**			**H**	**H**	**OH**	**OH**	**OH**	**CH_3**	**90.6±5.8**	**NI**	**80.1±3.6**	**ND**
PZ30	**HA_3**		**OCF_3**	**H**	**H**	**OH**	**OH**	**OH**	**CF_3**	**91.6±0.6**	**40.3±2.3**	**81.4±2.1**	**ND**

For HA_3 Scaffold, IC_{50}(S) were determined using a cut-off of 70% activity to hGYS1. Compound **PZ24** is an exception since it has a unique F at R_3 position. NI: no inhibition, greater than 95% activity; ND: not determined. Values are the mean ± SEM from at least three independent experiments in duplicate.

6. Kinetic characterization of compound PZ23

In order to understand the molecular features of our most potent analog, compound **PZ23**, I examined the kinetic characteristics of its interaction with GS (**Figure 18A**). **PZ23** has a competitive mode of inhibition, with a K_i value of 1.31 ± 0.14 µM (**Figure 18B**). In light of the SAR and kinetic studies, we hypothesized that the binding of **PZ23** to the active site of yGsy2p resembled the binding of **H23** in the active site. In this model, the hydroxyl group at R_1 position formed a hydrogen bond with the nitrogen backbone of Leu481. The three hydroxyl groups in the pyrogallol subunit formed hydrogen bonds with Thr514 or Glu517. Additional structural flexibility of hydrogen-bond formation depended on the relative position of **PZ23** in the binding pocket. As my SAR study showed, the hydroxyl group at the R_5 position was important to confer inhibition, and an additional hydrogen-

bond formation between Arg320 and the pyrazole ring may also strengthen binding, particularly when an electron-withdrawing trifluoromethyl group was present, and diminish binding when electron-donating methyl group was present in the same position in the pyrazole ring (**Figure 18C**).

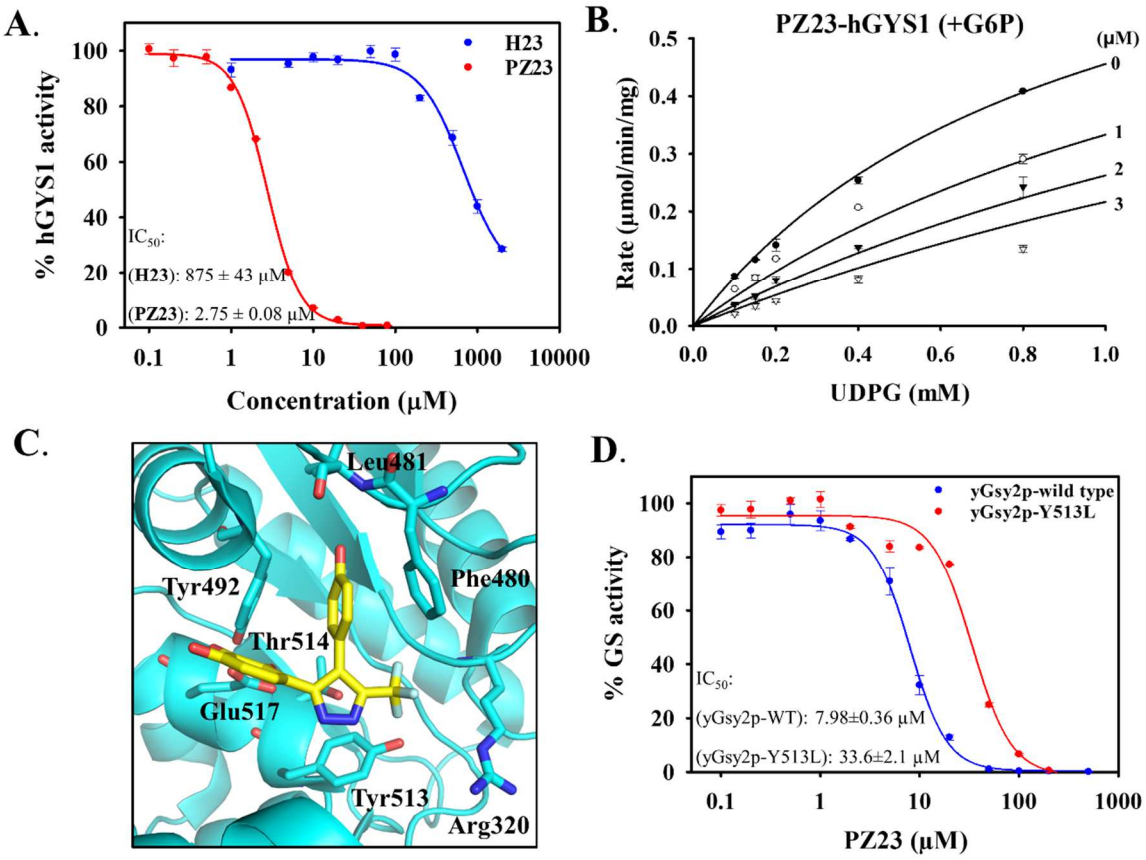

Figure 18. Kinetic characterization of **PZ23**. **(A)** Dose response curves for parent compound **H23** and the most potent analog **PZ23** against wild-type hGYS1. **(B)** Michaelis-Menten curve of competitive inhibition for **PZ23** versus UDPG. **PZ23** shows a K_i of 1.31 ± 0.14 μM under the tested condition. K_i value for **PZ23** is the mean ± SEM from three independent experiments performed using duplicate measurements for each condition. **(C)** Hypothetical binding model of **PZ23** to GS in the active site. Manual docking of **PZ23** in the active site was performed based on SAR and mode of inhibition studies. **(D)** Validation of **PZ23** binding in the active site. **PZ23** showed decreased potency against the active-site mutant Y513L compared with wild-type yGsy2p. All IC_{50} curves represent one of three experiments performed using triplicate measurements for each condition, with mean ± SEM shown.

To validate whether compound **PZ23** bound within the active site as modelled, I substituted Y513 with L513. This substitution, Y513L, did not abolish GS activity. Unlike other active site mutations that almost completely eliminated enzyme activity, the Y513L mutant decreased GS catalytic activity by only 10-fold. Consistent with my modelled mode of binding, I found that inhibition by **PZ23** toward Y513L was compromised compared to wild-type (**Figure 18D**).

7. Inhibition of GS activity in cell lysates

I next examined whether **H23** analogs could inhibit GS activity in cell lysates. Cultured cells normally do not accumulate large amounts of glycogen, largely due to the high levels of phosphorylation and the resulting low activity state of GS[53]. Lysates from two cell lines were prepared for GS activity measurement: the HEK293-PTG overexpressing *PTG*, a regulatory subunit of PP1, that recruits the phosphatase to glycogen where it promotes the dephosphorylation and activation of GS[104,105], and glycogen accumulation; and the Rat-1 fibroblasts which have detectable GS activity and glycogen as previously described[106,107]. The HEK293-PTG cells have a seven-fold increase in the GS activity ratio from 0.02 to 0.15. To determine GS activity in lysates and optimize the conditions for measurement, I measured the incorporation of ^{14}C-glucose into glycogen at 0.2 mM UDPG and 1 mM G6P initially as a function of different lysate concentrations. I observed a linear increase in GS activity within the range of 0.075-1.5 mg/ml lysate. Under the conditions of the assay, the lysate from the HEK293-PTG cells had 10-fold more activity than the Rat-1 cell lysate (**Figure 19A**). To limit substrate utilization to under 10%, I used 0.15 mg/mL HEK293-PTG lysate and 0.75 mg/mL Rat-1 lysate with imidazole **H23**, pyrrole **PR7** and pyrazoles **PZ15**, **PZ19**, **PZ27** and **PZ23**. When tested at 100 μM, **H23**

and **PR7** did not significantly inhibit GS activity in lysates. However, the remaining four substituted pyrazoles, namely **PZ15**, **PZ19**, **PZ27** and **PZ23**, reduced synthase activity in both HEK293-PTG and Rat-1 cell lysates by >30%. Consistent with its greatest potency toward purified enzyme, **PZ23** exhibited almost complete inhibition of synthase activity in lysates (**Figure 19B**). In summary, these analogs targeted GS activity in the context of the glycogen particles present in cellular lysates with potencies similar to those observed in purified enzyme preparations.

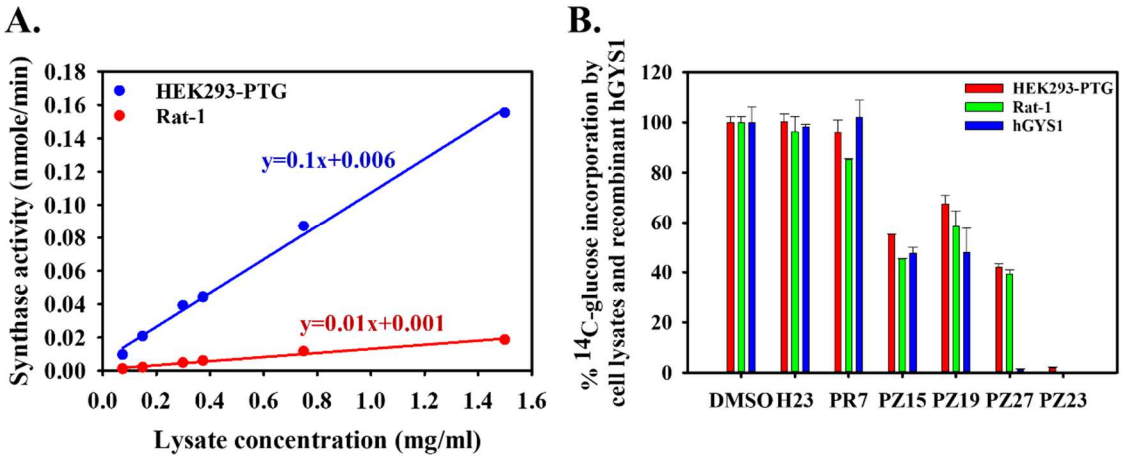

Figure 19. Inhibition of GS activity in cell lysates. **(A)** Synthase activity in HEK293-PTG and Rat-1 cell lysates in the presence of 0.2 mM UDPG and 1 mM G6P. The data was fit to linear regression line with equations showing synthase activity rate (nmole/min, y-axis) under various lysate concentrations (mg/ml, x-axis). The data represent averages of triplicate assays ± SEM. **(B)** Percent of ^{14}C-glucose incorporation to control (DMSO) by cell lysates and recombinant hGYS1 in the presence of **H23** and its analogs. For cell lysates and recombinant hGYS1, 100 µM and 20 µM compounds were used respectively. Averages of triplicate assays ± SEM are shown.

8. SAR for isoflavones toward hGYS1

In a three-step synthetic procedure, pyrazoles were made by the recyclization reaction of isoflavones with hydrazine hydrate (**Scheme 1**). A close inspection of the chemical structures of isoflavones and pyrazoles revealed their structural similarity with the difference present in the ring opening of chromones for the conversion of the pyrazole

scaffold. Nonetheless, I examined the inhibitory potential of those precursory isoflavones to hGYS1 using the ^{14}C-glucose incorporation assay. Strikingly, a number of isoflavones demonstrated low micromolar potency toward wild-type hGYS1, an observation comparable to the effect of their counterpart pyrazoles.

Therefore, I performed SAR studies to determine the substructures within the isoflavone (**IF**) scaffold for their inhibitory effects against wild-type hGYS1 (**Table 5**). Based on the availability of our in-house synthesized compounds and commercial stock, I examined substructures at $R_{1\text{-}5}$ positions. Notably, the isoflavone scaffold was prioritized with a hydroxyl group at the R_1 position, and showed the order of potency as follows: -OH > -H > -F > -NO_2 > -Cl > -CF_3 > -OCF_3 (**IF9** versus **IF5**, **IF12**, **IF29**, **IF15**, **IF33** and **IF36**). As the synthetic precursor of **PZ23**, which possesses the most potent inhibition among the pyrazole series (**Table 4**), **IF9** appears as the best isoflavone inhibitor, with an IC_{50} value of 1.56 μM toward hGYS1. However, unlike the pyrazole scaffold which prefers a hydrogen bond acceptor, R_1 position in isoflavones does not require this interaction. In contrast, a substituent that can function both as a hydrogen bond acceptor and a hydrogen bond donor seems to confer better inhibition (–OH in **IF9** versus –NO2 in **IF29**). Variability at $R_{2\text{-}3}$ is achieved via placement of chlorine at these two positions, but the impact on potency is negligible (**IF12** versus **IF26** or **IF15** versus **IF20**, **IF23**). At the R_4 position, the electron withdrawing –CF_3 group produces the best inhibition, whereas the electron donating –CH_3 group generates the least inhibition (**IF5** versus **IF1**, **IF4** or **IF12** versus **IF10**, **IF11** or **IF15** versus **IF13**, **IF14**), an observation consistent with the effect of substructures flanking the pyrazole ring. Interestingly, the R_5 position can only tolerate a hydroxyl group, since substitution of this hydroxyl group to even hydrogen, or larger

structures such as ethylmorpholine or ethylpyrrolidine abolished inhibition under the assay condition (**IF1** versus **IF3** or **IF5** versus **IF6** or **IF15** versus **IF16**, **IF17**).

Table 5. SAR for isoflavones.

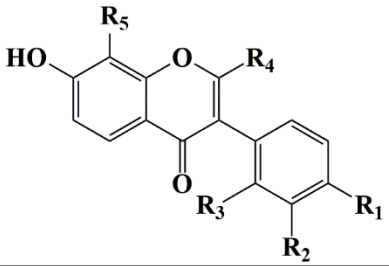

Isoflavone (IF)

Compound	R_1	R_2	R_3	R_4	R_5	% hGYS1 activity @25 μM compound	IC_{50} (μM)
IF1	H	H	H	H	OH	26.3±1.9	9.98±1.22
IF2	H	H	H	H	CH_3	NI	ND
IF3	H	H	H	H	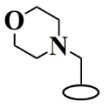	NI	ND
IF4	H	H	H	CH_3	OH	53.8±3.3	29.2±3.6
IF5	H	H	H	CF_3	OH	0.59±0.08	5.60±0.12
IF6	H	H	H	CF_3	H	NI	ND
IF7	OH	H	H	H	OH	33.4±1.9	ND
IF8	OH	H	H	CH_3	OH	4.50±0.21	ND
IF9	OH	H	H	CF_3	OH	0.50±0.10	1.56±0.06
IF10	F	H	H	H	OH	3.09±0.27	ND
IF11	F	H	H	CH_3	OH	73.5±5.9	ND
IF12	F	H	H	CF_3	OH	2.12±0.10	8.19±0.40
IF13	Cl	H	H	H	OH	10.6±0.6	ND
IF14	Cl	H	H	CH_3	OH	73.4±0.7	ND
IF15	Cl	H	H	CF_3	OH	3.64±0.24	12.0±1.0
IF16	Cl	H	H	CF_3	H	NI	ND
IF17	Cl	H	H	CF3	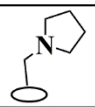	NI	ND

Compound	R_1	R_2	R_3	R_4	R_5	% hGYS1 activity @25 μM compound	IC_{50} (μM)
IF18	Cl	Cl	H	H	OH	NI	ND
IF19	Cl	Cl	H	CH_3	OH	73.9±6.1	ND
IF20	Cl	Cl	H	CF_3	OH	0.99±0.16	11.8±1.2
IF21	Cl	H	Cl	H	OH	51.8±0.60	ND
IF22	Cl	H	Cl	CH_3	OH	84.5±6.3	ND
IF23	Cl	H	Cl	CF_3	OH	9.33±0.75	11.7±0.5
IF24	F	H	Cl	H	OH	28.1±2.0	ND
IF25	F	H	Cl	CH_3	OH	83.3±0.5	ND
IF26	F	H	Cl	CF_3	OH	23.2±0.8	12.4±0.6
IF27	NO_2	H	H	H	OH	15.2±0.5	ND
IF28	NO_2	H	H	CH_3	OH	66.6±1.4	ND
IF29	NO_2	H	H	CF_3	OH	11.3±0.4	11.4±0.5
IF30	NO_2	H	H	CF_3	H	NI	ND
IF31	CF_3	H	H	H	OH	65.0±5.5	ND
IF32	CF_3	H	H	CH_3	OH	86.2±1.6	ND
IF33	CF_3	H	H	CF_3	OH	34.8±1.8	13.2±1.1
IF34	OCF_3	H	H	H	OH	73.1±1.5	ND
IF35	OCF_3	H	H	CH_3	OH	85.3±3.6	ND
IF36	OCF_3	H	H	CF_3	OH	43.7±3.2	16.5±1.1

NI: no inhibition; ND: not determined. Values are the mean ± SEM from at least three independent experiments in duplicate.

9. Kinetic characterization of isoflavones

To understand the mode of inhibition of isoflavones toward hGYS1, I chose **IF1** as a representative compound to perform the kinetic titration experiments, since **IF1** displayed

an approximate hill-slope value of -1, whereas other compounds showed cooperativity in the dose response assays (**Table 5**). Similar to **H23** and **PZ23**, **IF1** appears as a competitive inhibitor versus UDPG, with a K_i value of 13.2 μM, similar to its 10 μM IC_{50} value (**Figure 20A**). Additionally, mutagenic studies using two active site mutants Y513L and Y513F on yGsy2 showed reduced **IF9** potency to the mutant enzymes, compared with its potency to wild-type yGsy2 (**Figure 20B**). Furthermore, I examined whether active site accessibility affects compound inhibitory potential. Here, I utilized two active-state mutants, the R580A3 basal-state state mutant and the R589A2 inhibited state mutant. In the absence of G6P, **IF9** displayed IC_{50} values of 11.0 μM, 16.1 μM, and 19.9 μM toward R580A3, wild-type, and R589A2 mutants, respectively. In the presence of G6P, **IF9** showed an IC_{50} value of 11.3 μM, resembling the effect toward basal state R580A3 mutant (**Figure 20C**). These data suggest that greater active site accessibility confers better potency for **IF9**. Based on the previous SAR study and my kinetic data, we proposed a model for the binding of **IF9** in the active site of GS. In this model, the R_1 hydroxyl group forms a hydrogen bond with Leu481. The R_4 position is prioritized with electron-withdrawing $–CF_3$ group, possibly to facilitate an additional hydrogen bond formation between the oxygen element and Arg320. Furthermore, the hydroxyl group at R_5 position appears to be critical to interact with residue Tyr513, since either loss of this hydroxyl group or mutation of Tyr513 to leucine or phenylalanine led to significant reduction of inhibition (**Figure 20D**).

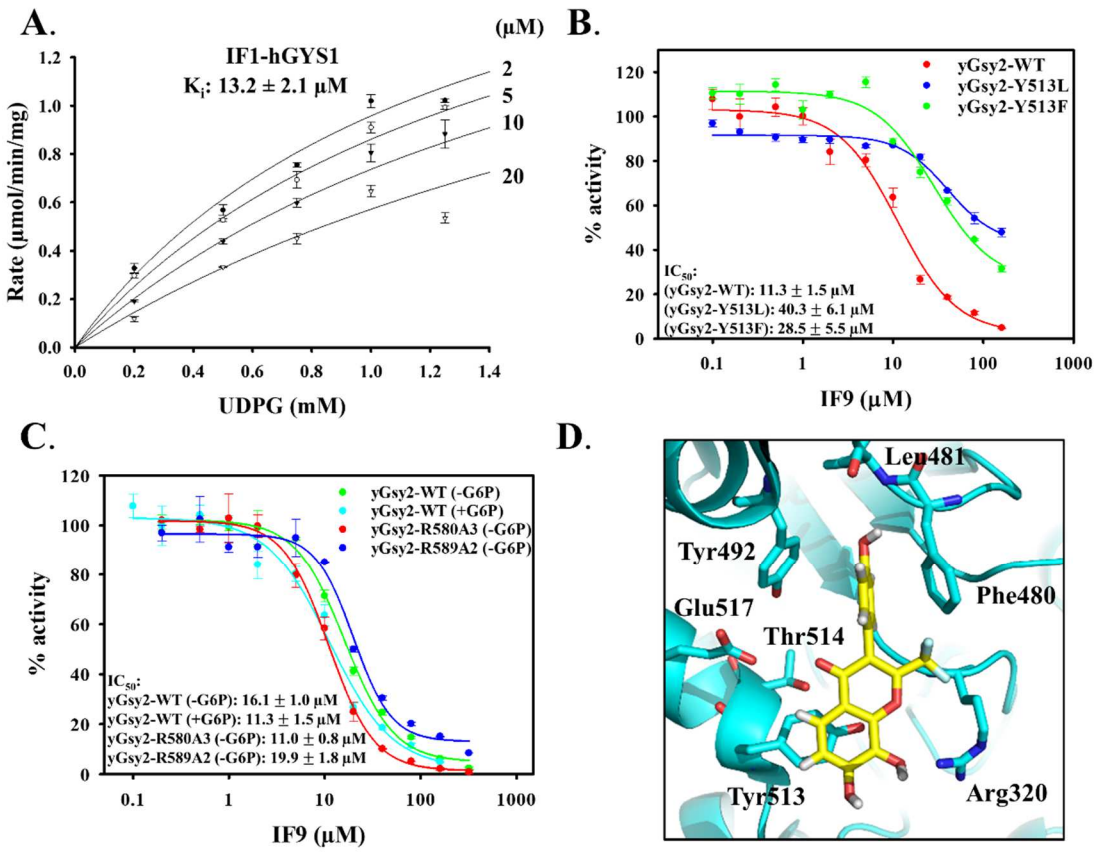

Figure 20. Kinetic characterization of isoflavones. **(A)** Michaelis-Menten curve of competitive inhibition for **IF1** versus UDPG. **IF1** shows a K_i of 13.2 ± 2.1 μM under the tested condition. K_i value for **PZ23** is the mean ± SEM from three independent experiments performed using duplicate measurements for each condition. **(B)** Dose response curves for **IF9** against wild-type, Y513L, and Y513F yGsy2 enzymes. **(C)** Dose response curves for **IF9** against wild-type, R580A3, and R589A2 yGsy2 enzymes, either in the presence or absence of G6P. **(D)** Hypothetical binding model of **IF9** to GS in the active site. Manual docking of **IF9** in the active site was performed based on SAR and kinetic studies. All IC_{50} curves represent one of three experiments performed using triplicate measurements for each condition, with mean ± SEM shown.

10. Cellular glycogen accumulation

I next considered whether these low micromolar inhibitors for the two chemical scaffolds, i.e., pyrazoles and isoflavones, would suppress glycogen accumulation in cells. However, cultured cells normally do not accumulate large amounts of glycogen. Here, we have engineered the HEK293 cells to overexpress the *PTG* gene, which were denoted as

HEK293-PTG cell line. The *PTG* gene is known to increase glycogen accumulation in cells and in mice by recruiting PP1 to glycogen where it can facilitate the dephosphorylation and activation of GS[104,105]. The HEK293-PTG overexpressing cell line has an enhanced GS activity ratio (indicative of active enzyme), and significantly increased levels of glycogen compared with non-transfected HEK293 cells. We utilized a starvation-refeeding protocol to examine the ability of the compounds to alter cellular glycogen accumulation. In brief, cells were first starved in no-glucose DMEM medium for 48 hours, during which period cellular glycogen stores are almost completely depleted. Then glucose-containing αMEM medium (5.5 mM) was refed to cells for another 6 hours. Meanwhile, compounds were added upon refeeding and incubated with cells for 6 hours. Since compounds were added after starvation and at the same time of refeeding, this assay directly evaluated the ability of compounds to inhibit glycogen re-synthesis. First, I validated whether this assay protocol is effective of identifying compounds that alter glycogen metabolism. I utilized as a positive control the widely-used glucose lowering T2D drug, metformin, which is known to inhibit glycogenesis and gluconeogenesis[108]. As shown in **Figure 21A**, metformin demonstrated dose-dependent inhibition of glycogen accumulation in HEK293-PTG cells with an EC_{50} of 9.9 mM, an observation consistent with its high working concentrations examined in various physiological conditions[109,110,111]. With the validation of this cellular glycogen assay, I next examined whether **H23** analogs developed in **Table 4** could suppress glycogen accumulation at a single dose of 25 μM. Interestingly, none of these molecules showed any inhibition of glycogen amount (**Figure 21B**). I also examined a number of isoflavones described in **Table 5** for their cellular efficacy. Surprisingly, I found 5 compounds (**IF15**, **IF20**, **IF23**, **IF29** and **IF36**) that demonstrated over 50% reduction

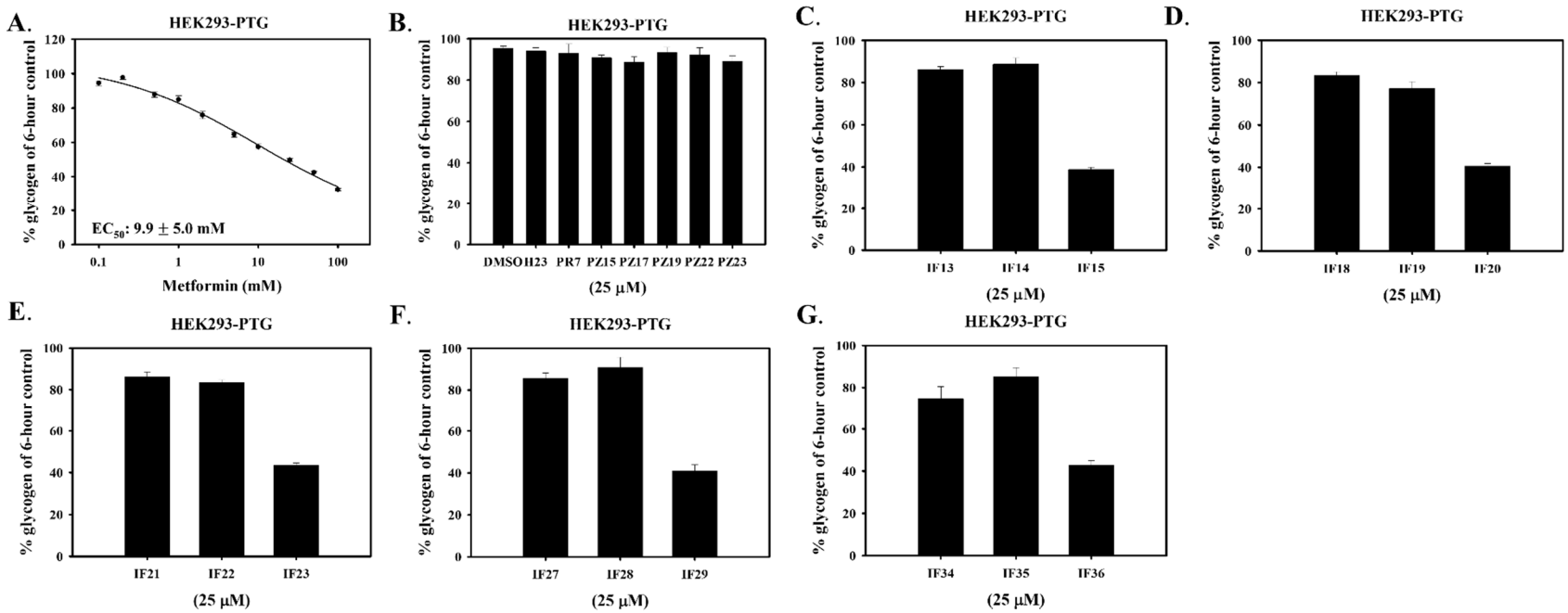

Figure 21. Screening of compounds for glycogen accumulation in HEK293-PTG cells. **(A)** Test of metformin using the starvation-refeeding protocol. Metformin showed cellular efficacy of suppressing glycogen accumulation with an EC_{50} value of 9.9 ± 5.5 mM. **(B)** Screening of representative imidazole, pyrrole, and pyrazole compounds at a single dose of 25 μM in cells. (C-G) Screening of isoflavones at a single dose of 25 μM in cells. Data for efficacious compounds, including **IF15 (C)**, **IF20 (D)**, **IF23 (E)**, **IF29 (F)**, **IF30 (G)** and their counterpart compounds are shown. Values are the mean ± SEM from two independent experiments in duplicate or triplicate.

of glycogen accumulation at 25 μM. Notably, all of these compounds possess a $–CF_3$ group at R_4 position, whereas their counterpart analogs with a –H or $–CH_3$ group at R_4 position, did not show any cellular effect (Figure **21C-G**). The cellular efficacy of these 5 isoflavones was further validated through dose response experiments, with compounds being incubated in cells for 6 hours (**Figure 22A**). To see if longer time treatment triggers more profound inhibition, I dosed the cells with compounds for 24 hours. The results showed more significant inhibitory effect of glycogen storage when the isoflavones were incubated for longer time in cells (**Figure 22B**). Taken together, these data identified five isoflavones as efficacious compounds bearing cellular efficacy of suppressing glycogen synthesis in a dose- and time-dependent manner.

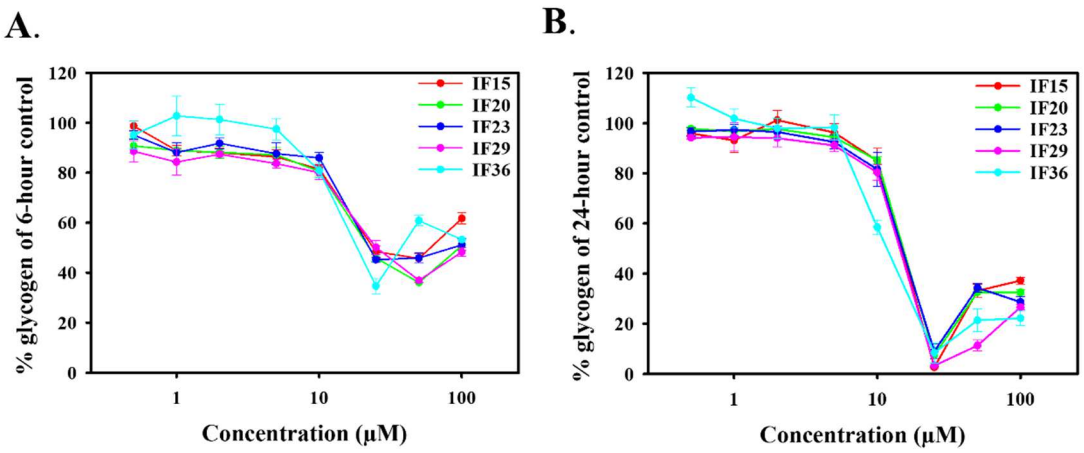

Figure 22. Concentration-dependent response for selected isoflavones in HEK293-PTG cells. Compounds were incubated in cells for 6 hours **(A)** or 24 hours **(B)**. The data represent averages of triplicate assays ± SEM.

11. Cellular toxicity assay

Live cells normally maintain a reducing environment that can convert the stable tetrazolium salt WST-1 to its soluble form formazan through a complex cellular mechanism that is dependent on the glycolytic production of NAD(P)H in viable cells[112].

This bioreduction process is accompanied by the color change of yellow WST-1 to purple formazan, which can be quantified through colorimetric measurement as a reflection of viable cells present. Using this WST-1 assay, I measured cellular toxicity of metformin and the five isoflavones in HEK293-PTG cells incubated for 24 hours. Metformin did not show any cytotoxicity until concentration went up to 50 mM which showed ~75% cell viability, and 100 mM which showed ~35% cell viability (**Figure 23A**). For isoflavones, at 25 μM, **IF36** caused around 50% cell death, whereas none of the other isoflavones (i.e., **IF15**, **IF20**, **IF23**, and **IF29**) did showed any noticeable changes in cell viability. However, all compounds demonstrated cellular toxicity at 50 μM and 100 μM concentrations (**Figure 23B**). Since the isoflavones demonstrated a profound effect of suppressing glycogen accumulation at 25 μM within 6-hour treatment, we suggest that their cellular efficacy was not likely to be caused by toxicity. However, the cellular glycogen data derived from high compound concentrations (i.e., 50 μM and 100 μM) should be analyzed cautiously because of the potential cytotoxic effect.

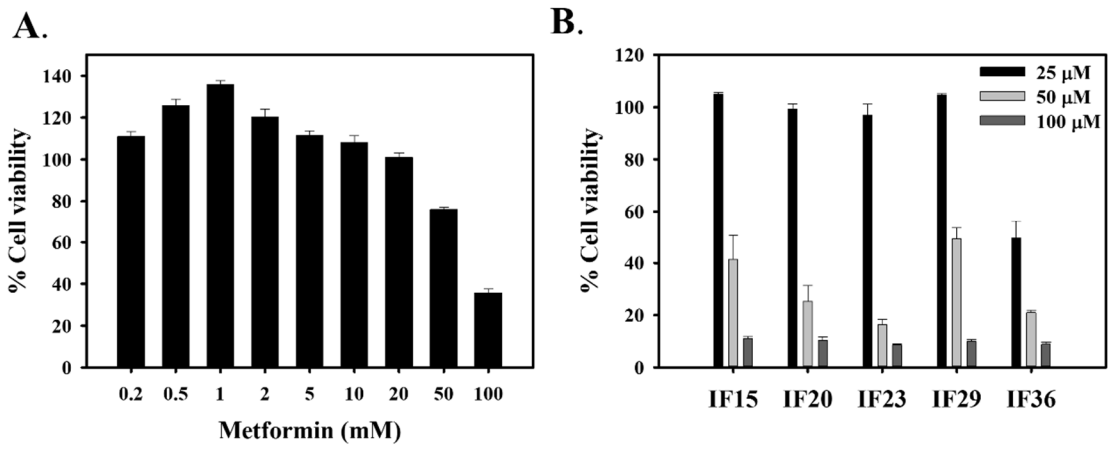

Figure 23. Effect of metformin and isoflavones on cell viability. Metformin **(A)** and the five isoflavones (i.e., **IF15**, **IF20**, **IF23**, **IF29**, and **IF36**) **(B)** were incubated in HEK293-PTG cells for 24 hours to evaluate their cytotoxicity using WST-1 assay. The data represent averages of triplicate assays ± SEM.

B. Discussion

Excess glycogen accumulation in cells leads to impaired autophagy and glycophagy, dysregulated mitochondrial metabolism, and eventually cell death. These defects are pathological for a number of GSDs. Accumulating evidence suggests that suppression of glycogen accumulation through inhibition of GS, the rate-limiting enzyme in glycogen biosynthesis, is therapeutically effective for treating various types of GSDs. For instance, knocking out *GYS1* in Pompe disease mouse models led to significant improvement of metabolic and neurologic defects[113]. Similar results were observed in LD mouse models where genetic depletion of *GYS1* alleviated LB formation and epileptic symptoms[63,85]. Silencing *GYS2* expression using an RNAi approach also effectively prevented hepatomegaly and hepatic steatosis in mouse models of Cori and Von Gierke disease, respectively[88]. These results demonstrated that GS is a therapeutically viable target without obvious organismal toxicity.

An FP assay for the screening of small molecule inhibitors of GS was developed in our laboratory. The FP assay utilized a GlcN6P-coupled fluorophore, i.e., GlcN6P-fluorescein-5-Ex which binds in the G6P allosteric site of GS. This assay was used to screen compounds that can displace the fluorophore. A Z'-factor of 0.86 indicated the robustness and adaptation of this FP assay for HTS. Through a HTS of 50,000 compounds from the ChemBridge DIVERSet chemical library against yGsy2, we identified 110 primary hits by setting a Z'-score of -1. Those 110 hits were rescreened against yGsy2 using the orthogonal ^{14}C-glucose incorporation assay, and the number of hits dropped dramatically to 16 by setting a minimum cut-off value of 40% inhibition. The final validation occurred by testing

the 16 hits against hGYS1 using the radiochemical assay which identified **H23** as the only inhibitor. The screening triaging strategy is summarized in **Figure 24**.

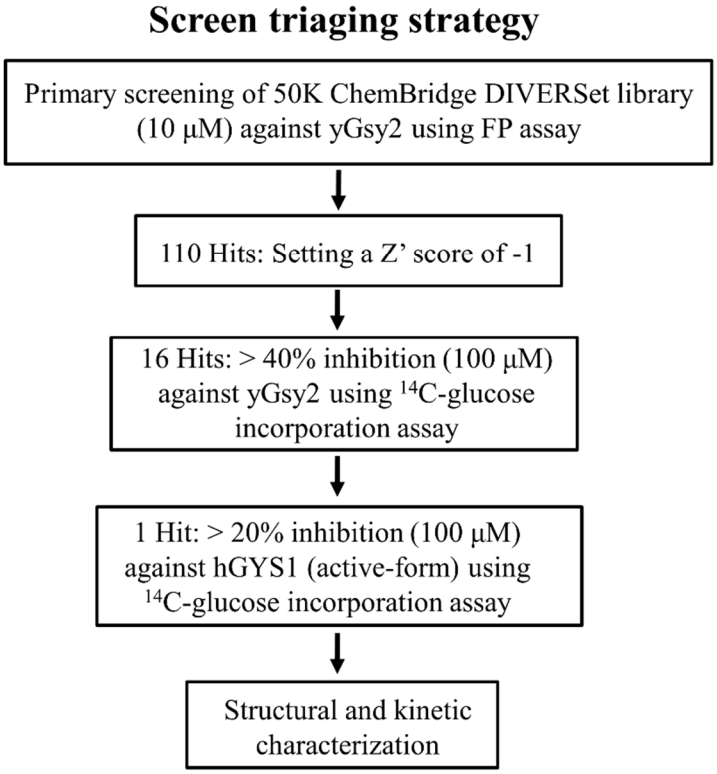

Figure 24. Screening triaging strategy. The high-throughput FP assay was utilized to screen 50,000 compounds from ChemBridge DIVERSet library. A Z' score of -1 was applied to identify 110 primary hits from the FP assay. Hit validation was achieved by a two-step testing against yGsy2 and then hGYS1 using the radiochemical ^{14}C-glucose incorporation assay.

Notably, there is a relatively low yield of hits when the compounds were examined using the FP assay and the ^{14}C-glucose incorporation assay. The loss of hits might lie in the nature of these two assay systems, since the FP assay is affinity-based whereas the radiochemical assay is activity-based. Thus, it is possible to identify compounds that could displace the fluorophore without inducing an effect on enzyme activity. We also noticed the poor translation of hits when testing moved from yeast to human GS. One possible explanation is that the kinetic aspects of the two enzyme systems differ. Consider, for

instance, the impact of regulatory input on the enzymes results in different enzymatic outcomes. Regulation of yeast GS by G6P primarily impacts k_{cat}, whereas in mammalian systems the impact is primarily on K_m for substrate[44,114]. Thus, the discrepancy in hits between yGsy2 and hGYS1 could also be affected by the different manners in which the kinetic steps in catalysis are impacted by regulatory input. A more sensitive assay directly targeting hGYS1 activity is likely to offer a better screening outcome.

Unfortunately, the HTS FP assay was not suitable for use on hGYS1. Unlike yGsy2, both the uncoupled and GlcN6P-coupled fluorophore bound to hGYS1 (**Figure 25**). However, addition of competitive binders such as G6P, UDP, or short glucose polymers were not capable of displacing the fluorophores. These data suggest the fluorophores don't bind to any known sites in hGYS1, such as the G6P allosteric site, glycogen-binding sites, or active site. The non-specific fluorophore binding, combined with the fact that hGYS1 produced in insect cells results in a heavily phosphorylated enzyme that requires very high concentrations of G6P for activity measurements, makes the full-length recombinant human enzyme unsuitable for an assay designed to displace G6P. Therefore, we used yGsy2p instead of hGYS1 for screening purpose.

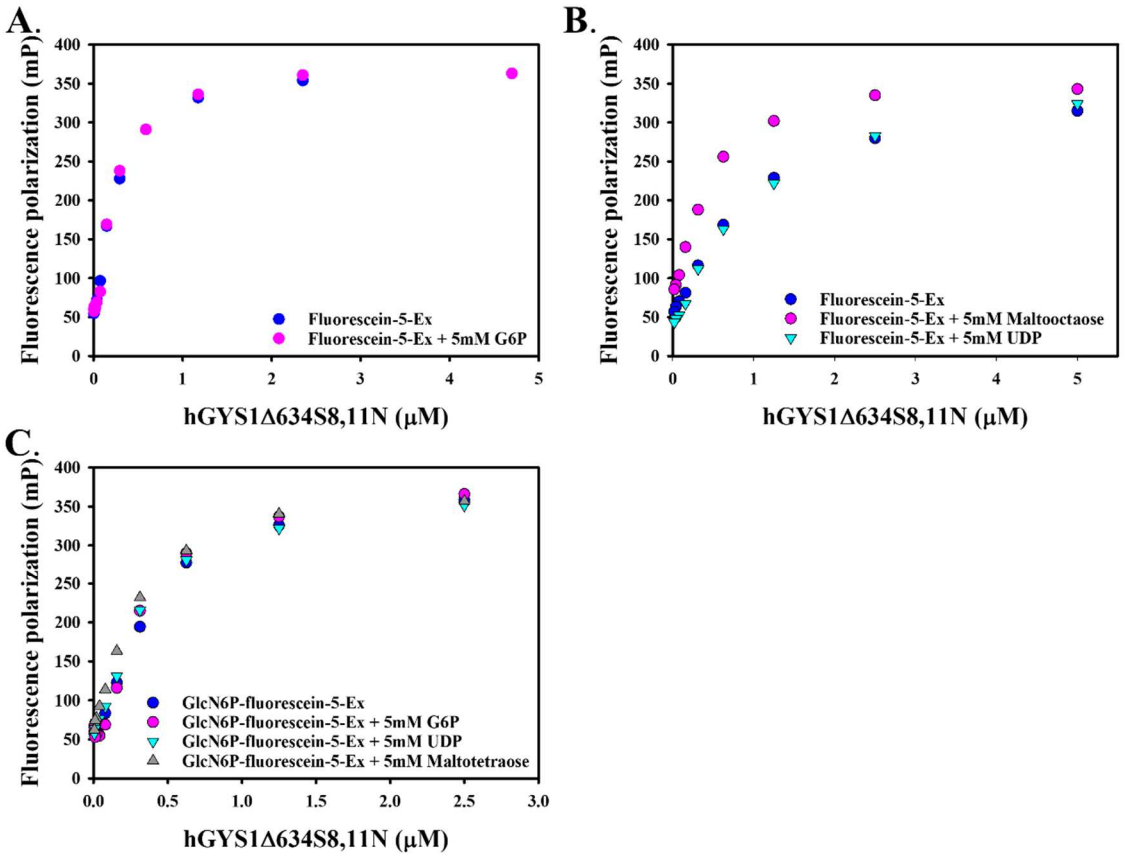

Figure 25. Binding of the uncoupled and GlcN6P-coupled fluorophore to hGYS1. FP assay was utilized to examine the binding and displacement of fluorescein-5-Ex to hGYS1 by G6P **(A)**, maltooctaose, and UDP **(B)**, as well as the binding and displacement of GlcN6P-fluorescein-5-Ex to hGYS1 by G6P, UDP, and maltotetraose **(C)**. The data represent a single measurement for each point.

Nonetheless, our FP assay provided a novel HTS assay, and did indeed identify a competitive inhibitor of UDPG, namely (*rac*)-2-methoxy-4-(1-(2-(1-methylpyrrolidin-2-yl)ethyl)-4-phenyl-1*H*-imidazol-5-yl)phenol (**H23**), that bound within the active site of yGsy2. This outcome was determined by both an X-ray structure and by kinetic studies using **H23** and analogs developed in a subsequent SAR study. However, the site of binding was a surprise to us because the assay was designed to identify small molecules that displace G6P binding. Upon close inspection of the known eukaryotic GS structures we note that the UDPG and G6P binding sites reside on opposing ends of the same alpha-helix,

with Tyr492 stacked against the uracil ring of UDP and His500 forming a hydrogen bond with the phosphate moiety of G6P (**Figure 26A**). Considering this structural proximity and the cooperative nature of the structural transitions in GS, it was not surprising that binding at one site could transmit structural information to the other site and that under the subsaturating conditions of our HTS assay, binding of compounds within the active site might promote displacement of the fluorophore from the G6P site. To test this hypothesis, I determined whether UDP could competitively displace the tracer molecule, GlcN6P-fluorescein-5-Ex. Whereas, G6P showed a K_d of 71 μM, which is consistent with the published AC_{50} value of ~100 uM for enzyme activation, UDP was able to partially displace the fluorophore, but at concentrations >3-fold over the K_i value for UDP inhibition of yGsy2p (**Figure 26B**). This data lends support to our contention that the G6P and UDP sites are structurally linked and binding at one site can influence binding at the other, albeit not through direct competition for the same site and at lower binding efficiencies.

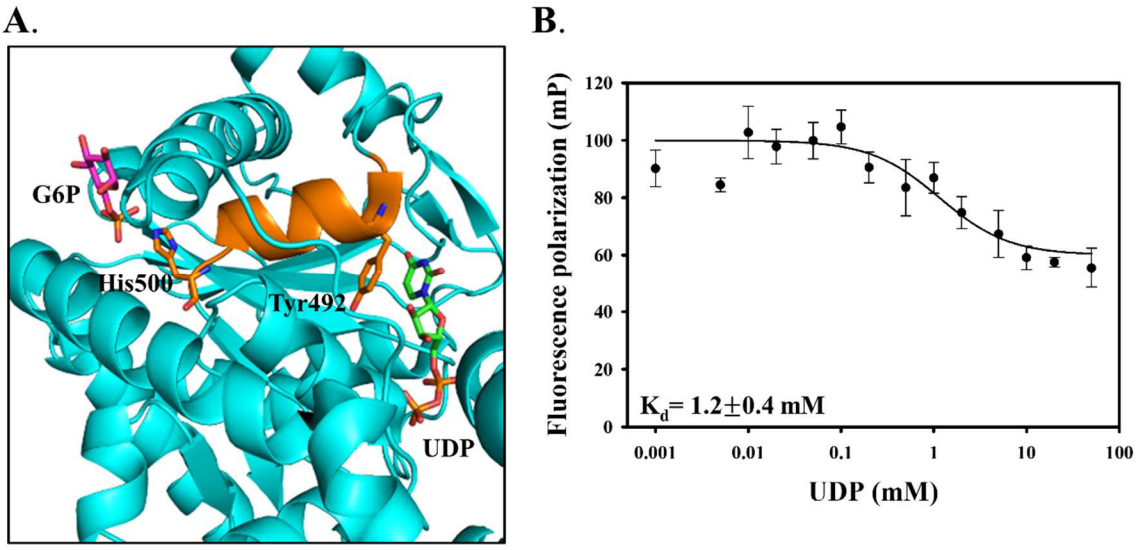

Figure 26. Displacement of fluorophore through active site inhibitors. **(A)** Structural overview of the binding sites for allosteric activator G6P and substrate UDPG. The UDP and G6P binding sites lie on opposing ends of the same alpha-helix (orange), with Tyr492 contacting the uracil ring of UDP (green) and His500 contacting the phosphate of G6P (magenta). **(B)** Displacement of GlcN6P-fluorescein-5-Ex by UDP in FP assay. The data represent averages of triplicate assays ± SEM.

Our focused medicinal chemistry effort with around 500 analogs showed stepwise improvement of potency toward wild-type hGYS1 (**Figure 27**). Although none of the imidazole and pyrrole compounds displayed large changes in potency, the pyrazole and isoflavone scaffolds demonstrated significant improvement of potency. Remarkably, the most potent pyrazole compound, **PZ23**, showed over 300-fold improvement of potency over **H23**, and the most potent isoflavone compound, **IF9**, showed over 500-fold improvement of potency, compared with the IC_{50} value of **H23**. Those newly developed pyrazoles and isoflavones both possess a catechol substructure, a chemical moiety that appears as a promiscuous compound in many biochemical HTS[115]. Catechol could undergo reversible redox reaction to form 1,2-benzoquinone, presenting toxicity issues. Nonetheless, detailed kinetic, enzyme mutagenic, and SAR studies validated those pyrazoles and isoflavones are actual inhibitors of GS. Those data provide valuable information to understand the kinetic and structural mechanisms of GS inhibition upon compound binding.

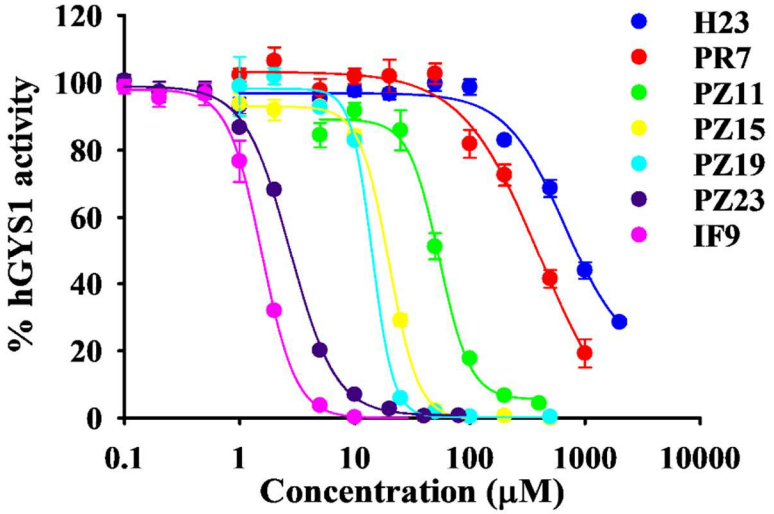

Figure 27. Improvement of potency toward wild-type hGYS1 through SAR studies. Medicinal chemistry effort with ~500 analogs showed stepwise improvement of compound potency toward wild-type hGYS1. Dose response curves of representative analogs from each of the four chemical scaffold (i.e., imidazole, pyrrole, pyrazole, and isoflavone) are shown.

Those potent pyrazole and isoflavone compounds were further tested in cells to assess their abilities to suppress cellular glycogen accumulation. Our collaborator, Dr. Anna A. DePaoli-Roach developed an assay where cells were first depleted of glycogen through starvation, and then replenished with glucose-containing medium to reinitiate glycogen synthesis. Simultaneous with glucose refeeding, our inhibitory compounds were added during the 6-hour incubation. This starvation-refeeding protocol was designed to directly assess the capacity of compounds in suppressing cellular glycogen biosynthesis. Surprisingly, at a test concentration of 25 μM, none of the pyrazole compounds showed any inhibition of glycogen accumulation. However, several pyrazole compounds were capable of suppressing GS activity that are present in the context of cellular lysates with comparable inhibition profile shown in the ^{14}C-glucose incorporation assay (**Figure 19**). The data suggest potential cellular permeability or metabolic stability issues that are associated with those pyrazoles which warrant further exploration. Nonetheless, the cellular assay identified 5 isoflavone analogs that suppressed cellular glycogen accumulation by $\geq$50% at 25 μM (**Figure 21**). Furthermore, we noticed that all the efficacious compounds possess an electron withdrawing -CF_3 group at the R_4 position of the isoflavone scaffold. However, for analogs which have an electron donating -CH_3 group, or hydrogen at the R_4 position, we did not see any reduction of glycogen level, an observation consistent with their lower potency toward hGYS1 that may also indicate transport or metabolic differences.

To further validate their cellular efficacy, the 5 most potent isoflavones were re-examined in cells for concentration-dependent effects. With 6-hour treatment, all compounds demonstrated dose-dependent inhibition of glycogen accumulation up to 25

μM concentration. When compounds were treated for 24-hour in cells, a more profound effect on glycogen accumulation was observed (**Figure 22**). These data suggest that the compounds' cellular efficacy is both dose- and time-dependent. The 24-hour incubations showed a rebound effect on glycogen accumulation above 50 μM. One explanation is that the compounds became insoluble and precipitated out of solution as a consequence of higher concentrations, resulting in lower working concentrations in solution. Secondly, as glycogen being the primary intracellular energy source in these experiments, cells may trigger some protective mechanisms for glycogen replenishment when levels get too low. Future target engagement experiments, such as using biotinylated compounds or cellular thermal shift assays, will be necessary to investigate whether those isoflavones induced cellular efficacy through binding directly to GS, or through off-target effect that in turn led to such rebound phenomenon.

IV. Discovery and characterization of small molecule inhibitors from a coupled GS activity assay adapted to HTS

Glycogen synthase activity can be analyzed by either following glucose incorporation into glycogen as one product of the enzymatic reaction, or you can follow the production of the other product, UDP. Over 50 years ago, coupling the phosphorylation of UDP from phosphopyruvate via the enzyme pyruvate kinase to either the oxidation of NADH, which can be measured spectrophotometrically or fluorometrically, or the use of dinitrophenylhydrazine, a colorimetric reagent that acts on pyruvate, was used to measure the amount of UDP produced[116,117,118]. Alternatively, the hydrolysis of UDP by inosine diphosphatase-generated P_i could be measured via molybdate-based assays[116,119]. Consequently, it is likely that following either the phosphorylation of UDP or its hydrolysis to UMP and P_i provides a better strategy to develop an HTS assay for hGYS1 activity, since it is produced stoichiometrically with glucosyl transfer to glycogen. To achieve this approach, we utilized a novel, well-characterized human nucleotidase to generate inorganic P_i from UDP. The human soluble calcium-activated nucleotidase-1 (hSCAN-1) is an apyrase enzyme that hydrolyzes nucleotide di- and triphosphate, with guanosine diphosphate (GDP)/UDP/inosine diphosphate (IDP) as the preferred substrates to their respective mono-phosphates[120]. In the defined *in vitro* assay for GS, there is only UDP present and its production will increase as a function of GS activity. Importantly, hSCAN-1 does not hydrolyze its product UMP. Therefore, the amount of P_i produced should be stoichiometric with the amount of UDP generated during the GS reaction, and by extension, would equal the amount of glucose incorporated into glycogen. By coupling this hSCAN-1 with GS, it is possible to substitute the standard radioactive ^{14}C-glucose assay for HTS

targeting hGYS1 directly. This assay was developed and optimized by Dr. Anna A. DePaoli-Roach and deployed by Dr. Cynthia A. Morgan in an HTS assay. I will review the optimization of conditions for the HTS assay and its successful application for the identification of small molecule modulators of hGYS1 from a 10K chemical library. I will also then summarize the work I performed to characterize the hits identified from this screen using various biochemical, biophysical, and cellular assays.

A. Results

1. Assay development

With UDP being one product of the GS reaction and the availability of UDPase hSCAN-1, the development of such an assay based on UDP hydrolysis and P_i quantification becomes feasible. Under ideal conditions, the amount of inorganic phosphate produced should be equivalent to the amount of UDP released as glucose is added to glycogen. The HTS assay contained four major steps: 1) the GS reaction where UDPG serves as the glucosyl donor to glycogen and releases the product UDP; 2) heat inactivation of the GS enzyme; 3) addition of hSCAN-1 to hydrolyze UDP to UMP and P_i; and 4) the quantification of P_i present using the P_i ColorLock Gold Assay (**Figure 28**). Key objectives for optimizing the GS reaction conditions were: 1) concentrations of UDPG and G6P; 2) enzyme concentration to keep the reaction within the linear range of P_i detection; and 3) selecting an incubation time to hold substrate consumption to less than 15-20% of available UDPG. Items 2 and 3 are co-dependent variables, since selection of one influences the choices for the other. For HTS, we utilized the truncated form of hGYS1, hGYS1Δ634S8,11N, for screening purposes. This modified hGYS1 enzyme can be purified in significant quantity and possesses an activation state (-/+ glucose-6-P) of ~0.2

under standard assay conditions, which provided a more suitable screening assay since the target enzyme was neither overly inhibited due to phosphorylation, nor rendered insensitive to the effects of G6P.

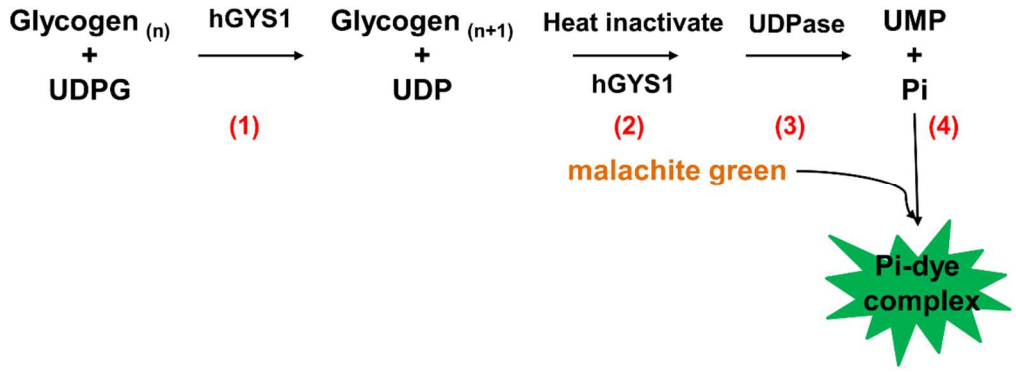

Figure 28. Development of high-throughput coupled GS activity assay. A four-step procedure is featured in this assay, including **(1)** GS catalytic reaction, **(2)** heat inactivation of the GS enzyme, **(3)** hydrolysis of UDP to UMP and P_i via the hSCAN-1 enzyme, and **(4)** quantification of P_i via ColorLock Gold Assay. (This assay was developed by Dr. Anna A. DePaoli-Roach.)

We first examined the half-maximal activity values for both UDPG and G6P using the standard ^{14}C-glucose incorporation assay by varying one component while using saturating amounts of the other. The K_m value for UDPG was 270 ± 60 µM, and the AC_{50} value for G6P was 337 ± 24 µM. Based on these values, we utilized 200 µM UDPG and 400 µM G6P in the screening assay. Varying amounts of glycogen were present in our hGYS1Δ634S8,11N enzyme preparations and we noted no change in enzyme activity whether we added additional glycogen or not. Therefore, for the HTS we used 1 mg/mL glycogen. Once the substrate parameters were established, linearity versus enzyme concentration was determined for the enzyme preparation. Although it was in the upper linear range of enzyme concentration, a concentration of 1 µg/ml was selected to enable the identification of both inhibitors and activators, while still producing a robust signal versus background. The final step in optimizing the GS reaction was determining reaction

time, with 20 minutes at 30°C allowing for approximately 20% UDPG utilization or less. Complete inactivation of GS after the 20 minutes reaction was necessary to prevent additional UDP production. In a 1.5 mL microcentrifuge tube, complete inactivation of GS occurred by heating in a water bath for 5 minutes at >80°C. In order to get complete and nearly even inactivation across a 384-well plate, we used a humidified chamber within a hybridization oven at >90°C for 15 minutes, resulting in enzyme inactivation. Although the outside rows and columns heated faster, there was very little difference in overall enzyme activity between the interior, and exterior wells on the plate, and thus little to no edge effects were observed.

Further analysis of the substrate selectivity for hSCAN-1 was conducted to verify previous results that indicated the enzyme's selectivity for UDP compared to the other components present in the assay mix[100,120,121]. In particular, using HPAEC, we verified that hSCAN-1 did not hydrolyze UDPG, UMP, or G6P to any measurable degree, whereas CIAP was able to generate P_i (**Figure 29**). The hSCAN-1 enzyme hydrolyzed UDP to UMP. Most critically, there was no hydrolysis of UMP, and therefore no additional P_i release in the presence of hSCAN-1. CIAP was able to liberate P_i from both UDP and UMP that went untouched by hSCAN-1. In a similar manner, G6P did not liberate an appreciable amount of P_i in the presence of hSCAN-1, but glucose was detected in G6P incubated with CIAP; thus, any P_i released from G6P or glycogen would also be present in the background measurement. To best measure GS activity, we wanted all of the UDP produced in the GS reaction to be hydrolyzed by hSCAN-1 to UMP and P_i. Therefore, this step in the assay was optimized to ensure the reaction went to completion. Using HTS assay conditions, 10 ng/mL of hSCAN-1 for 30 minutes at 37°C hydrolyzed over 95% of available UDP. For

the HTS, we selected 61.6 ng/mL hSCAN-1 for 60 minutes to ensure over 99% of UDP present was hydrolyzed.

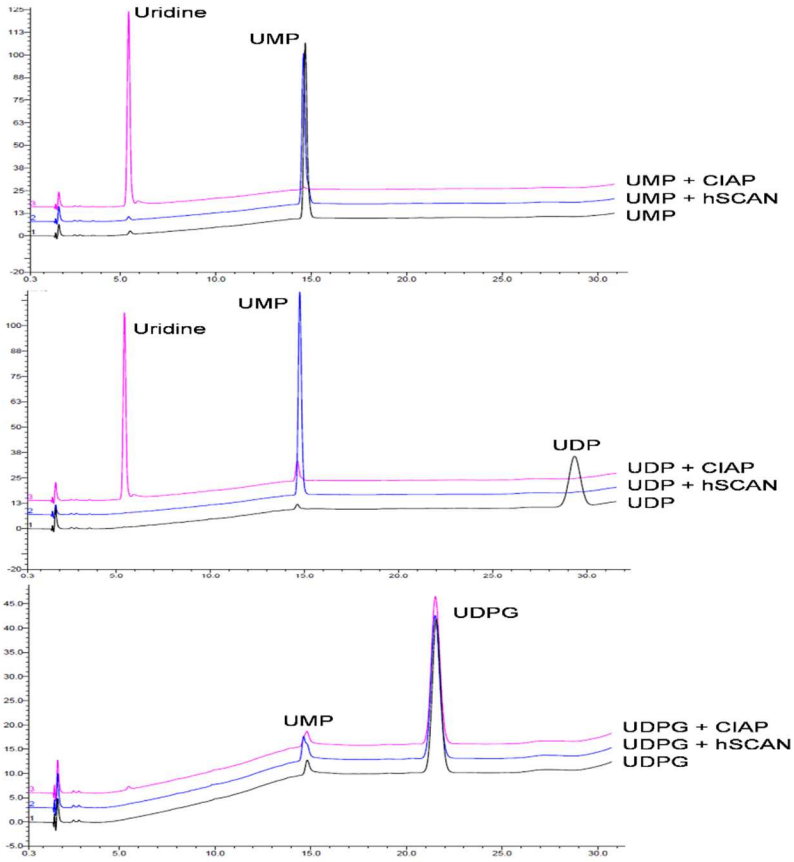

Figure 29. HPAEC analysis of hSCAN-1 activity. UMP, UDP, and UDPG were incubated with either hSCAN-1 or CIAP. Only UDP was hydrolyzed by hSCAN-1, whereas CIAP was able to hydrolyze both UMP and UDP. UDPG was not affected by either enzyme. (This data was generated by Dr. Christopher J. Contreras.)

The P_i ColorLock Gold assay was used to quantify the amount of P_i produced from UDP through the hSCAN-1 enzymatic reaction. This highly sensitive assay was able to detect the low nanomoles of P_i released in our HTS assay. The standard curve for P_i indicated that the assay was linear up to 3.5 nanomoles, but began to saturate above that point. Based on our assay components, the maximum amount of P_i that could be produced was 8 nanomoles, which would occur if all of the available UDPG in the reaction was

consumed. However, we optimized the conditions such that for the control, approximately 20% UDPG was utilized, and therefore the control reactions should produce approximately 1.6 nanomoles of P_i, well within the linear range of the P_i ColorLock Gold assay. As such, this assay would identify both activators and inhibitors and could distinguish between a 90% inhibitor and a 50% inhibitor, but it would not distinguish a 2-fold activator from a 5-fold activator.

For confirmation of the quality of the HTS protocol to identify hGYS1 modulators from a single replicate, a Z'-factor score was calculated to compare the no-hGYS1 positive controls (i.e., maximum inhibition) versus the DMSO negative controls. The Z'-factor of 0.84 between the positive and negative controls indicated this assay would be very effective at identifying hGYS1 inhibitors (**Figure 30**).

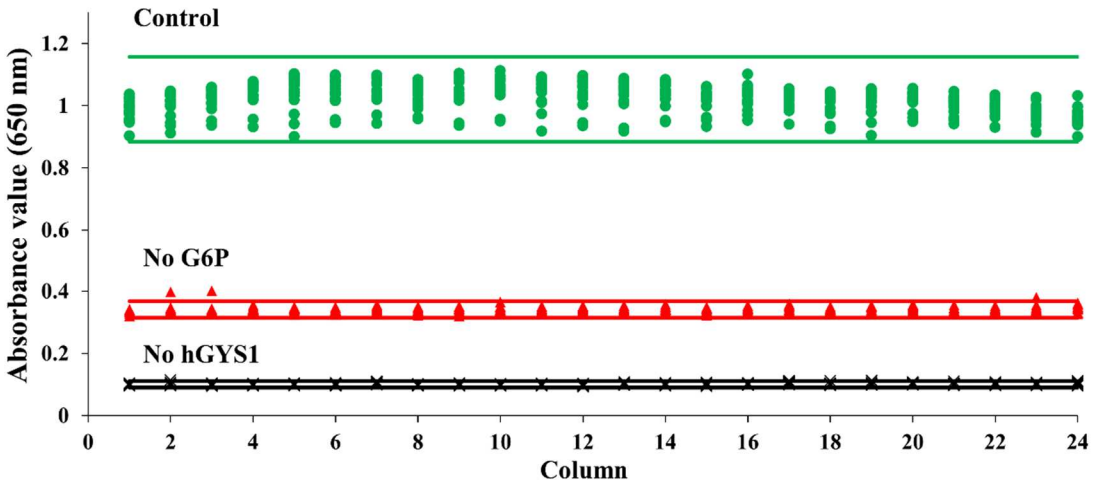

Figure 30. Z'-Factor determination for high-throughput coupled GS activity assay. Each point represents the absorbance value at 650 nm of a reaction. Green data points represent the assay control. Black data points represent the no hGYS1 control. Red data points represent the no-G6P control. The corresponding lines represent 3× standard deviation from each control average. The Z'-factor for the control versus no hGYS1 control is determined as 0.84. (This data was generated by Dr. Cynthia A. Morgan.)

2. Compound screening from 10K chemical library

As proof-of-principle for the HTS assay, Dr. Cynthia A. Morgan screened a 10,000-compound library comprised of known drugs, bioactives, and natural products. Primary hits were selected as those compounds exhibiting ≥25% inhibition or ≥40% activation compared to the intraplate controls. All hits were also outside of 3× standard deviation from the control average established for each plate. Approximately half of the plates contained at least one compound that met our selection criteria. Primary screening in singlicate identified 60 inhibitors and 59 activators. These 119 compounds were then cherry-picked and re-tested in duplicate. Selection criteria for activators remained at ≥40% activation, while a more stringent criteria of ≥ 40% inhibition was used to identify inhibitors. Of the 119 cherry-picked compounds, 3 activators and 46 inhibitors remained after the second round of screening. Overall the HTS gave a hit rate of approximately 1% after primary screening, with over one-third of these hits re-confirmed in secondary screening. These 49 unique compounds identified in the HTS as modulators of hGYS1Δ634S8,11N represent a diverse spectrum of compounds and included opioids, anti-parasitics, ion-channel blockers, and dyes. The largest group contained flavonoids, including epigallocatechin-3-monogallate (EGCG), gossypol, katacine, and 6,2'-dimethoxyflavone. Various anti-parasitics and disinfectants including hexachlorophene (HCLP), closantel, and tetracycline were also identified.

3. Titration experiments with selected HTS hits

Of the 46 inhibitors, 6 hits were ordered to validate whether the identified compounds also inhibit GS using the standard ^{14}C-glucose incorporation assay. These compounds were EGCG, HCLP, closantel, 4,4'-diisothiocyanato-2,2'-stilbenedisulfonic

acid (DIDS), tetracycline, and zonisamide, which were selected based on their degree of inhibition during re-screening, commercial availability, and diversity of scaffold. We first tested these compounds on both wild-type hGYS1 and hGYS1Δ634S8,11N at a single dose of 20 μM. Tetracycline and zonisamide were weak inhibitors in the HTS and showed little to no inhibition on either the WT-hGYS1 or the truncated enzyme using the radiochemical assay. The remaining four compounds inhibited both of these enzymes, ranging from ~30% inhibition of wild-type hGYS1 with HCLP to ≥95% inhibition of both enzymes with EGCG (**Figure 31A**). This data showed comparability of inhibition to both enzyme species of hGYS1, demonstrating the effectiveness of using hGYS1Δ634S8,11N as a screening surrogate for wild-type hGYS1. IC_{50} curves were produced for each of these four compounds using the hGYS1 WT. Their values ranged from 1.5±0.3 μM for DIDS to 21.5±1.9 μM for HCLP (**Figure 31B**). I further examined mode of inhibition of two compounds through titration experiments by co-varying UDPG and inhibitor concentrations using the 14C-glucose incorporation assay. As demonstrated in the Michaelis-Menten curves, EGCG was a noncompetitive inhibitor (K_i = 23.1±1.0 μM) whereas HCLP was a mixed-type inhibitor versus UDPG (K_i = 25.2 ± 7.8 μM) (**Figure 31C**). The higher K_i value EGCG produced in the titration assay than its IC50 value (2.8±0.4 μM) derived from the dose-response assay was likely caused by different glycogen concentrations (6.7 mg/ml versus 1 mg/ml) in the assays, which was further examined in the following section.

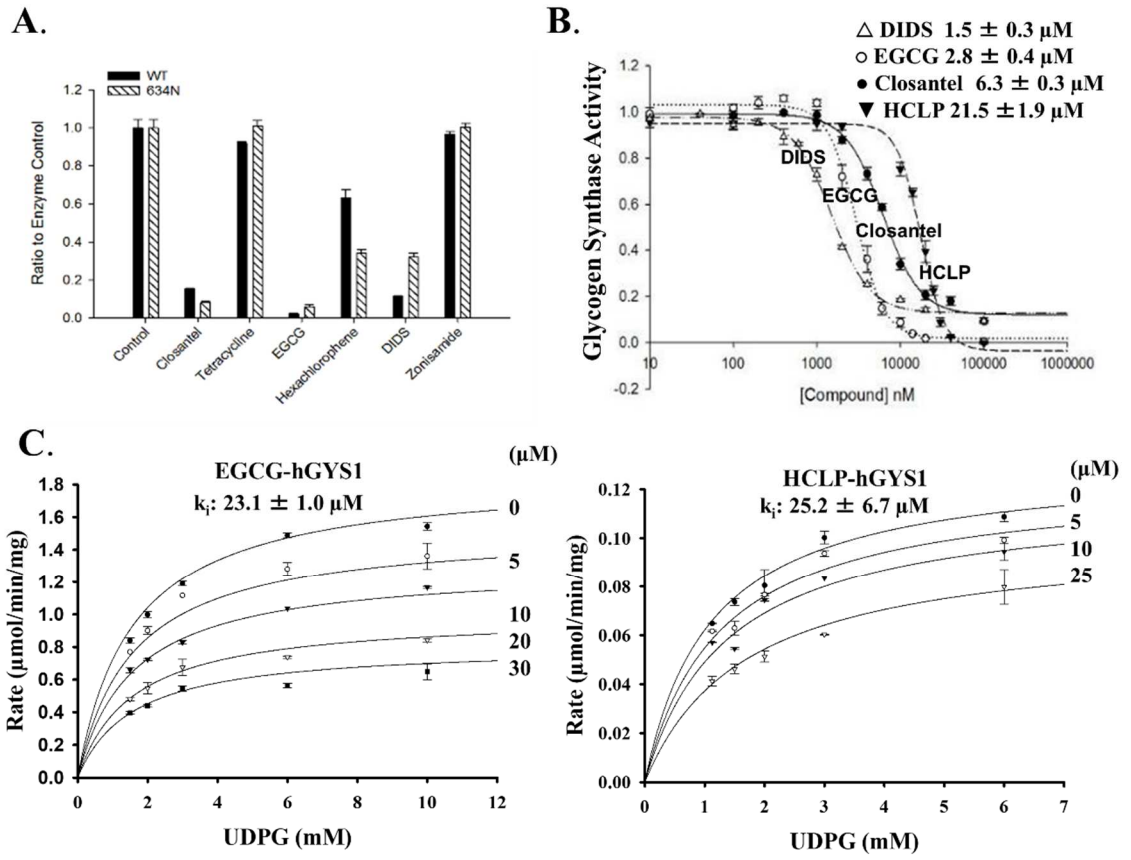

Figure 31. Titration experiments with selected HTS hits. **(A)** Effect of HTS hits on hGYS1 WT and hGYS1Δ634S8,11N. A single dose of 20 μM of each compound was tested on both wild-type and mutant hGYS1. **(B)** Dose response assays were done from 0 to 100 μM to determine the IC_{50} values for EGCG, DIDS, closantel, and HCLP. Each assay contains 0.2 mM UDPG, 0.4 mM G6P, and 1 mg/ml glycogen. A minimum of three assays (each at n=3) were performed for each compound and a representative curve for each compound is shown below. The IC_{50} value shown is the average ± SEM for all assays. **(C)** Mode of inhibition of EGCG and HCLP against wild-type hGYS1. Each assay contains saturating G6P (7.2 mM) and glycogen (6.7 mg/ml) concentrations. The reported K_i values are the mean ± SEM from three independent experiments in duplicate.

4. Kinetic characterization of EGCG

As EGCG showed a noncompetitive inhibition mode versus UDPG, we hypothesize EGCG may bind to glycogen-binding sites on GS since it has multiple hydroxyl groups that could competitively displace glycogen, which is also rich in hydroxyls. Four glycogen-binding sites (designated S1/S2/S3/S4) have been identified from structural and mutagenesis studies of yGsy2p[40]. For example, mutation of conserved

residues in contact with maltodextrin binding on site 1 (S1A3, W118A/W149A/H156A) decreased *in vitro* GS catalytic efficiency by 40-fold and cellular glycogen accumulation by 6-fold[40]. I examined the potency of EGCG toward the S1A3 enzyme and determined that EGCG showed a 23-fold reduction in potency toward S1A3 (**Figure 32A**. Whether EGCG impacts binding at other glycogen-binding sites needs further investigation. The similarity in IC_{50} values derived from different G6P concentrations makes it less likely that EGCG interacts near the G6P site (**Figure 32A**). Additionally, two structurally similar analogs of EGCG, epigallocatechin (EGC) and epicatechin (EC), were examined for their potency to yGsy2. While EGCG had an IC_{50} value of 6.62 µM, EGC showed a 2-fold decrease of potency, whereas EC showed no inhibition to yGsy2 (**Figure 32B**). This data further supports the idea that the number of hydroxyl units on these green tea extracts could play a key role in conferring inhibition toward GS.

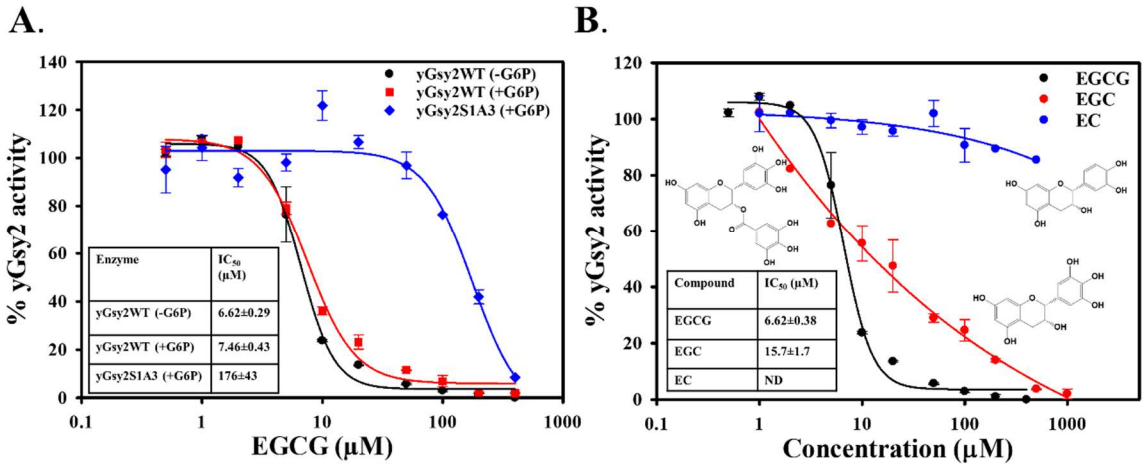

Figure 32. Kinetic characterization of EGCG. **(A)** Dose response curves of EGCG to wild-type yGsy2 and S1A3 mutant in the absence or presence of 7.2 mM G6P. **(B)** Dose-response curves of EGCG, EGC, and EC to wild-type yGsy2 in the absence of G6P. The IC_{50} values are averages of triplicate assays ± SEM.

5. Structural and kinetic characterization of HCLP

To understand how compounds physically interact with GS, I used X-ray crystallography in an attempt to determine the structure of the HCLP-enzyme complex. The structural data and refinement statistics are outlined in **Table 6**. The presence of HCLP was confirmed by 2Fo-Fc map contoured at 1 standard deviation prior to the inclusion of ligand (**Figure 33A**). I superposed this yGsy2p (WT)-HCLP structure with the yGsy2p-UDP•G structure (PDB code: 4KQM) in the active site, and found that UDPG and HCLP existed in somewhat overlapping, yet distinct, binding modes. As shown in the cartoon representation, UDPG and HCLP bound in orthogonal orientations within the GS active site (**Figure 33B**). A close inspection of the binding structure revealed that HCLP was

Table 6. Structural data and refinement statistics for HCLP-yGsy2p crystal.

Data collection		**Refinement**	
Space group	I222	No. reflections	68635
Cell dimensions		R_{work}/R_{free}	0.20/0.26
a, b, c (Å)	191.7, 203.5, 205.3	r.m.s. deviations	
α, β, γ	90.0, 90.0, 90.0	Bond lengths (Å)	0.01
Resolution (Å)	50-3.15	Bond angles (°)	1.8
R_{merge}	0.125 (0.77)	Ramachandran plot	
R_{meas}	0.141 (0.870)	Preferred/Allowed (%)	98.7
R_{pim}	0.065 (0.406)	Outliers (%)	1.3
CC1/2	0.999 (0.761)	B-factors	
I/σ(I)	12.4 (1.9)	Protein	Chain A, 73.8; B, 81.2;
Completeness (%)	99.5 (99.2)		C, 87.9; D, 89.9
Redundancy	4.6 (4.5)	Ligand (HCLP)	Chain B, 121.8

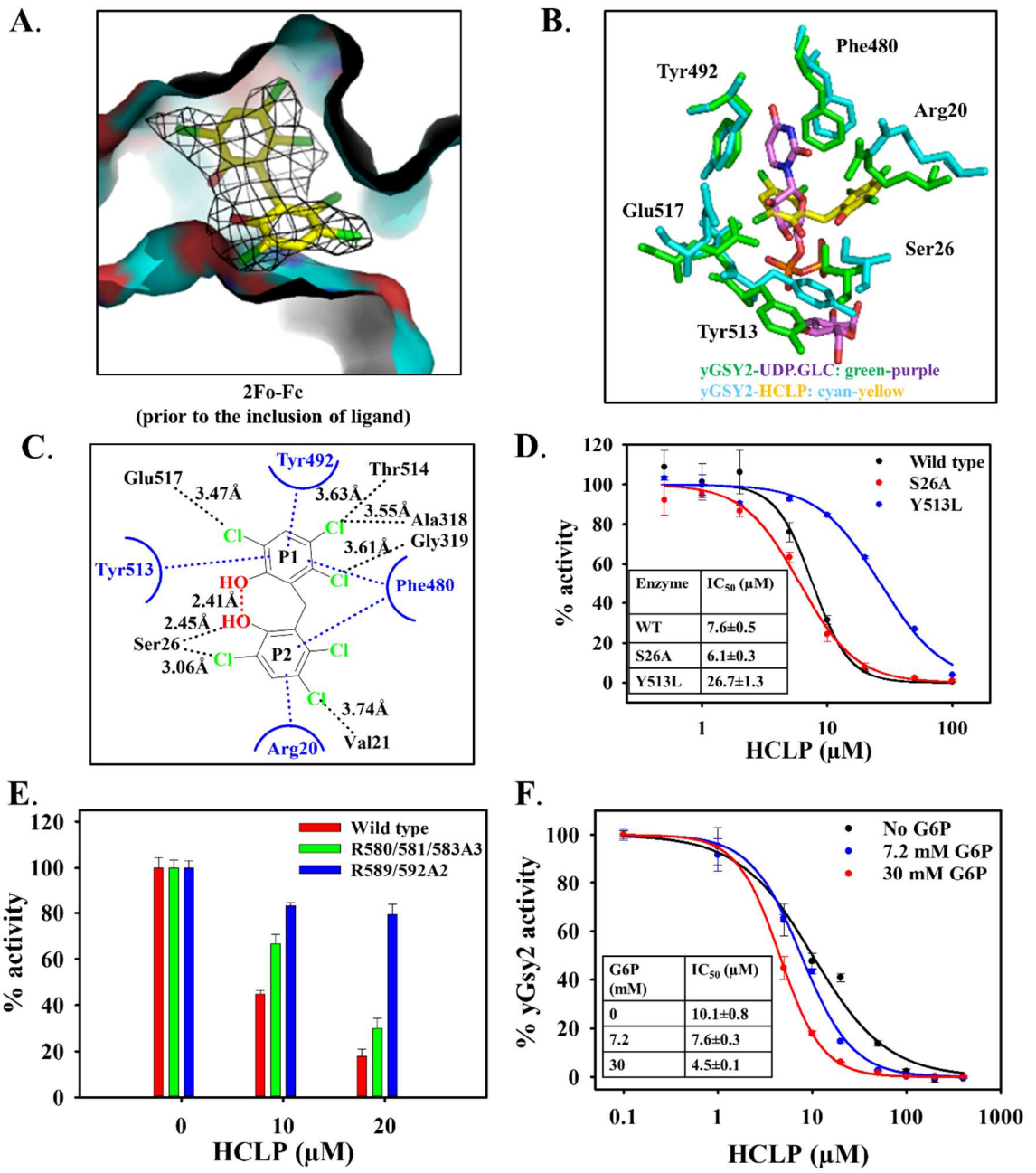

Figure 33. Characterization of HCLP. **(A)** The electron density for HCLP prior to the inclusion of the ligand in refinement. The map shown is the original unbiased 2Fo-Fc map contoured at 1 standard deviation. **(B)** Stick representation of the superposed UDP•G (purple) and HCLP (yellow) structures in the active site of GS. **(C)** Molecular interactions of HCLP with surrounding residues. **(D)** Inhibition of HCLP to WT, S26A, and Y513L mutants of yGsy2. **(E)** Inhibition of HCLP to WT, the basal state mutant (R580A3), and the inhibited state mutant (R589A2) of yGsy2. **(F)** Dose response curves of HCLP against yGsy2 under various concentrations of G6P.

mainly stabilized by hydrophobic interactions, including one phenyl ring (P1) being stabilized by π- π stacking with Phe480, Tyr492, and Tyr513, while the other ring (P2) is stabilized by aromatic interactions with Phe480 and Arg20. The chlorines formed to form multiple hydrophobic interactions with Val21, Ala318, Gly319 as well as polar interactions with Ser26, Thr514, and Glu517. Additionally, the hydroxyl group on P2 was in close contact with GS and was likely to form a hydrogen bond with Ser26. The two hydroxyl groups were also in close proximity (2.4 Å) and appeared to form an intramolecular hydrogen bond, which maybe critical for keeping the two aromatic rings in a relative planar conformation[122] (**Figure 33C**).

To understand the molecular interactions that confer HCLP binding to GS, enzyme mutagenic studies were performed to examine two key residues predicted to be important for binding. The Ser26 hydroxyl is 2.45 Å from the hydroxyl group of the P2 ring and putatively forms a hydrogen bond, and the Tyr513 side chain oriented more inwardly into the binding pocket in the HCLP-bound conformation to facilitate parallel π-stacking interaction with the P1 ring. While HCLP inhibited the S26A mutant nearly equipotently as wild-type yGsy2, it exhibited a 4-fold reduction of potency against the Y513L mutant (**Figure 33D**). These data suggest that the hydrophobic interactions, rather than hydrogen bonds, were most important for the binding of HCLP in the catalytic site.

Next, I validated the binding of HCLP in the active site by testing its inhibition against different activity-state mutants of yGsy2, including the basal state mutant R580A3 and the inhibited state mutant R589A2. Compared with the basal state mutant, HCLP showed less inhibition to the inhibited state mutant (**Figure 33E**). When tested under different concentrations of G6P, I observed increased potency when G6P concentration

was increased from 0, 7.2 mM, to 30 mM (**Figure 33F**), indicating the more activated the enzyme is, the better potency HCLP produces. Taken together, these data clearly demonstrated that HCLP is an active-site interactor of GS.

6. SAR for HCLP analogs

I further probed the SAR profile of HCLP using 15 structurally similar analogs (designated as **HC1**-**HC15**), and tested their inhibition against GS. These analogs showed comparable inhibitory effect across yeast and human GS species (**Table 7**). Among these analogs, compound **HC1** (bithionol) demonstrated the greatest potency against hGYS1. Bithionol has two fewer chlorines than HCLP in the *meta* positions and a sulfur atom linking the two aromatic rings. When this sulfur was replaced by sulfur monoxide, I observed a 3-fold decrease of potency to hGYS1 (**HC1** versus **HC3**), possibly due to increased steric hindrance or conformational constraints caused by the sulfur monoxide. Compound **HC4** has two less chlorines at the *ortho* positions compared with bithionol, and showed around 5-fold decrease in potency. Analog **HC2** has two bromines instead of chlorines at the *ortho* positions, and a carbon instead of sulfur between the two aromatic rings, which exhibited more than 2-fold decrease of potency compared with bithionol. Additionally, removal of the two bromines further reduced inhibitory effect (**HC2** versus **HC5**). Since both aromatic rings form hydrophobic interactions in the active site, I hypothesize that the chlorines function as electron-withdrawing groups to improve stacking interactions[123]. Consequently, loss of chlorines or substituting chlorines with bromines diminish this electron-withdrawing effect, and lead to decreased binding efficiency and inhibition. The two hydroxyl groups which formed intramolecular hydrogen-bond in

HCLP seems to be critical to confer inhibition, as compounds **HC7-HC13** totally abolished inhibition at 25 μM when either hydroxyl group was absent.

Table 7. SAR for HCLP analogs.

Compound	Structure	% yGsy2 activity @ 12.5 μM	% hGYS1 activity @ 25 μM	IC_{50} (μM) against yGsy2	IC_{50} (μM) against hGYS1
HCLP (Hexachlorophene)	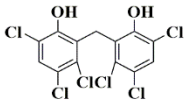	**39.4±2.0**	**50.3±0.2**	**10.1±1.6**	**27.1±1.3**
HC1 (Bithionol)	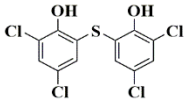	**41.0±4.9**	**56.3±1.4**	**12.4±2.5**	**37.8±4.1**
HC2 (Bromochlorophen)	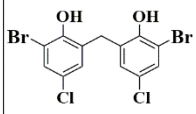	**42.3±1.9**	**77.4±8.1**	**ND**	**83.8±18.1**
HC3 (Bithionoloxide)	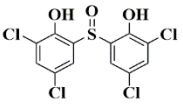	**82.1±5.6**	**86.4±8.2**	**ND**	**106±22**
HC4	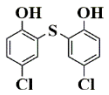	**89.4±2.7**	**84.9±2.2**	**ND**	**172±20**
HC5 (Dichlorophen)	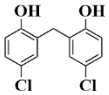	**81.8±2.0**	**86.1±6.0**	**ND**	**257±34**
HC6	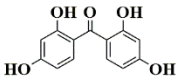	**91.2±4.1**	**109.8±4.8**	**ND**	**315±40**
HC7 (Triclosan)	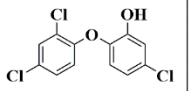	**106.2±6.0**	**88.1±9.0**	**ND**	**NI**
HC8	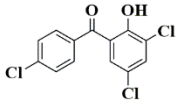	**96.9±1.8**	**100.4±11.3**	**ND**	**ND**

Compound	Structure	% yGsy2 activity @ 12.5 µM	% hGYS1 activity @ 25 µM	IC_{50} (µM) against yGsy2	IC_{50} (µM) against hGYS1
HC9	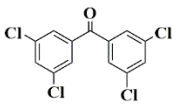	**105.6±3.8**	**93.3±7.7**	**ND**	**ND**
HC10	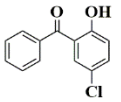	**96.5±3.1**	**89.6±4.1**	**ND**	**ND**
HC11	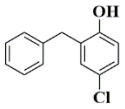	**90.4±8.2**	**95.1±0.7**	**ND**	**ND**
HC12	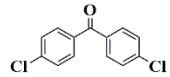	**93.0±2.7**	**86.8±7.4**	**ND**	**NI**
HC13	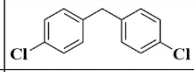	**88.7±3.3**	**91.8±4.1**	**ND**	**ND**
HC14	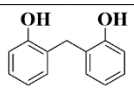	**93.9±3.8**	**91.8±16.0**	**ND**	**ND**
HC15	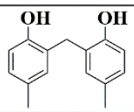	**88.3±6.4**	**ND**	**ND**	**ND**

NI: no inhibition up to 1 mM; ND: not determined. Values are the mean ± SEM from at least three independent experiments in duplicate.

7. Analysis of HCLP and its analogs in cells

As a proof-of-principle study, we selected three compounds to further examine their ability to suppress glycogen accumulation in the engineered HEK293-PTG cell-based assay. These compounds were HCLP, **HC1** (bithionol), and their counterpart compound **HC3** (bithionoloxide), which were selected based on their comparable potency to hGYS1 and structural similarity. Using the starvation-refeeding protocol described earlier, I observed dose-dependent inhibition of glycogen accumulation when HEK293-PTG cells were treated with increasing concentrations of HCLP and bithionol, but not bithionoloxide (**Figure 34A**). To further validate their cellular effects, I tested the compounds in Rat-1 fibroblast cells. Rat-1 fibroblast cells demonstrated measureable GS activity[31,106], and therefore were also applicable for cellular glycogen assay. The results indicated that except

for bithionoloxide, both HCLP and bithionol reduced glycogen accumulation in a dose-dependent manner, an observation consistent with the cellular efficacy as shown in HEK293-PTG cells (**Figure 34B**). To understand whether the decreased glycogen accumulation was associated with cellular toxicity, the WST-1 assay as described previously was performed to assess cell viability. HEK293-PTG cells were incubated with three concentrations (10 μM, 25 μM, and 50 μM) of HCLP, bithionol, and bithionoloxide for 24 hours. As the results indicated, HCLP did not show cellular toxicity at 10 μM, whereas bithionoloxide did not show any cellular toxicity even at 50 μM concentration (**Figure 34C**). While HCLP and bithionol were effective at reducing glycogen levels in cells, these results suggest these effects may relate primarily to the cytotoxicity of these compounds to cells; however, further studies are warranted on a larger set of analogs to make more definitive conclusions.

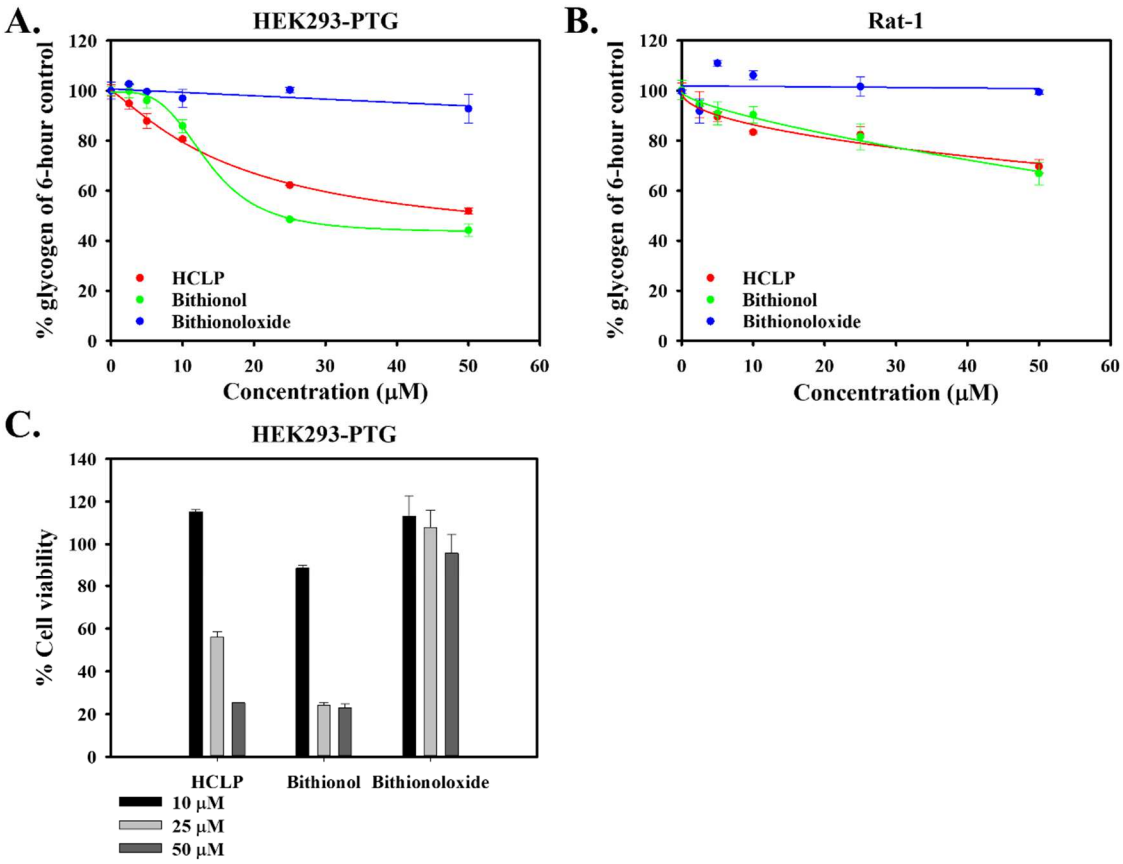

Figure 34. Analysis of HCLP, bithionol, and bithionoloxide in cells. Concentration-dependent response for HCLP, bithionol, and bithionoloxide in HEK293-PTG **(A)** and Rat-1 **(B)** cells. Compounds were incubated for 6 hours. The data represent averages of triplicate assays ± SEM. **(C)** Effect of HCLP, bithionol, and bithionoloxide on cell viability. The three compounds were incubated in HEK293-PTG cells for 24-hour to measure their toxicity using WST-1 assay. All data are averages of triplicate assays ± SEM.

B. Discussion

In this section, I demonstrated how our laboratories developed a nonradioactive high-throughput assay for the identification of small molecule modulators of human GS activity. In this assay, glycogen catalytic activity is coupled to the production of UMP and P_i. It is worth noting that there may not be an exact 1:1 relationship between glucose incorporated into glycogen and the P_i measured. UDPG can be non-productively hydrolyzed to glucose and UDP without successful transfer of the glucose residue into glycogen, yet this reaction still produces UDP. However, comparison of this assay with the standard ^{14}C-glucose incorporation assay suggests that, in general, this non-productive turnover of UDPG is low and where a large difference is observed, may offer insight into how the compound is impacting enzyme catalysis. Modulators of hSCAN-1 could also be identified via the HTS, even though a saturating hSCAN-1 enzyme concentration (61.6 ng/mL, 6 times than needed) was used in the assay. Based on the results with zonisamide and tetracycline, these compounds may have an effect on hSCAN-1, since both had modest inhibition using this HTS assay but little to no inhibition in the ^{14}C-glucose incorporation assay. In this regard, the orthogonal ^{14}C-glucose assay serves as an effective validation assay for the discrimination of false positive hits that target hSCAN-1.

Using this assay, we identified 46 inhibitors of hGYS1. This 10K chemical library consisted of drugs, natural products, and semi-synthetic natural compounds. As many hits included large polyphenols such as tannins, theaflavin mono- and digallates, the stains hematein and gentian violet, plus the metal chelator dimercaptosuccinic acid, and have been recognized as pan-assay interference compounds (PAINS – e.g. EGCG, gossypol, and myricetin)[124,125], they may not be suitable for further drug development; however, they may

still prove useful as molecular probes to study GS structure, function, and inhibition. Various drugs were also identified in the HTS, including the antimicrobials tetracycline, closantel, HCLP, ion channel blockers including calmidazolium chloride and DIDS, plus the thyroid hormone analog tiratricol. Most of these drugs are known to affect multiple biological pathways and most are not approved for use in humans by the FDA. Interestingly, this assay also identified 3 small molecule activators of human GS. Although their activation has not been validated through dose response assay or ^{14}C-glucose incorporation assay, once confirmed these molecules would be of great interest to be studied further for their mechanism of activation, binding mode, affinity, etc.

Despite the nature of this compound library, results from ^{14}C-glucose incorporation assay confirmed that EGCG, HCLP, closantel, and DIDS inhibit human GS with low micromolar IC_{50} values (**Figure 31B**). Kinetic snalyses showed EGCG and HCLP are noncompetitive and mixed-type inhibitors against hGYS1, respectively (**Figure 31C**), demonstrating the capacity of this assay for finding compounds with different binding modes. Such an outcome was expected since this high-throughput coupled assay was an activity-based approach; thus, any compounds that could decrease GS activity by blocking glycogen-, UDPG-, or G6P-binding, either competitively or allosterically, would be identified. To further validate whether the primary hits were true GS-binders, a crystal structure of HCLP-complexed with yGsy2 was obtained, which unambiguously identified HCLP bound in the catalytic cleft of GS. Enzyme mutagenic data, along with SAR studies, lend further support to such a binding mode (**Figure 32**, **Table 7**). These biochemical and biophysical studies together confirmed the hits derived from this high-throughput colorimetric assay were actual interactors of GS.

Consistent with their comparable potency toward hGYS1 in the ^{14}C-glucose incorporation assay, both HCLP and bithionol exhibited dose-dependent inhibition of glycogen accumulation in two cell lines, whereas bithionoloxide did not (**Figure 33**). However, HCLP and bithionol were found to be generally cytotoxic to HEK293-PTG cells, which could be the driving factor in glycogen reductions. This may not be surprisingly since they are known to affect a number of intracellular proteins[126,127,128] and trigger pleiotropic biological activities, including antiviral[129] and anticancer[130,131,132] effects. HCLP was once widely used as a disinfectant, anti-bacterial agent in medicine and bactericide in agriculture. Further animal and clinical studies indicated the application of HCLP was associated with the development of specific lesions in the CNS[133]. However, the alternative organochlorine, bithionol, does not appear to damage the CNS and was suggested as a possible substitute for HCLP[134]. In fact, bithionol has received approval from Food and Drug Administration as an orally administered medication for the treatment of helminthic infections and has been safely dosed in humans at 25 mg/kg body weight per day[135]. The drug has also proven to be effective in preclinical cancer models and safe in non-cancer patients[131]. Detailed toxicology and pharmacokinetics of bithionol are available at Toxnet (U.S. National Library of Medicine). Although the polypharmacology of HCLP and bithionol makes them unsuitable for drugs toward GSDs, the unique binding pattern, mechanism of inhibition, and SAR studies provide important insights for the further development of GS-modulating drugs.

In summary, this 10K HTS yielded 119 primary hits, possessing a hit rate of around 1%. Rescreening of those 119 hits validated 49 hits, including 46 inhibitors and 3 activators. A further validation assay was performed by examining 6 of the 49 compounds

using the ^{14}C-glucose incorporation assay, selected based on degree of inhibition during rescreening, availability, drug-like properties, and diversity of scaffold. As a consequence, 4 out of the 6 compounds showed the desired biochemical effect, i.e., with low micromolar potency to wild-type hGYS1. Compared with the high-throughput FP assay, this high-throughput coupled assay presented a few advantages. Firstly, this assay was designed to screen for inhibitors of human GS directly, rather than yeast GS. Secondly, in our pioneering studies, two thirds of hits were validated in the standard radiochemical assay, demonstrating a good transition of hit rates between these two assays, whereas the FP assay demonstrated a relatively low transition (14.5%) to ^{14}C-glucose incorporation assay. Thirdly, only 14 nM hGYS1 enzyme was needed to achieve a measurable signal in the HTS assay, while in the FP assay 3 μM yGsy2 enzyme was used. The high-throughput coupled activity assay thus demonstrated a great improvement in assay sensitivity. Based on these observations, we conclude that this novel, two-step enzymatic, and colorimetric assay is capable of identifying small molecule modulators of human GS. This assay is rapid, robust, and nonradioactive, representing a marked improvement over the current radiochemical method for the identification of lead compounds. Based on these results, we are confident that our novel high-throughput coupled activity assay with human GS can be used for further large-scale drug discovery.

V. Conclusions and future directions

The suppression of glycogen accumulation has emerged as an attractive therapeutic approach for GSDs whose etiology is derived from excessive glycogen accumulation. Animal models support an approach where genetic or chemical depletion of glycogen in mouse models of Lafora disease[63,84,85,86,136], of Pompe disease[87], and of Cori disease alleviates the disease symptoms[88]. Interestingly, recent studies suggested that T2D might also possess disease characteristics similar to some GSDs, such as glycogen accumulation in pancreatic β cells under hyperglycemic conditions contributing to β-cell dysfunction[62,70].

Only a few studies have identified molecules that target glycogen accumulation, including the widely-used glucose lowering T2D drug metformin[108,111], the mTORC1 inhibitor, rapamycin, that indirectly suppress GS activity through signaling regulation[87], use of RNAi to mediate reduction of GYS2[88], and a newly developed antibody-enzyme fusion that can directly degrade polyglucosan[136]. However, these molecules either targeted glycogen synthesis in an indirect manner, or presented a separate challenge for the delivery of the therapeutic to the central nervous system. Here, we have established two robust, rapid, and nonradioactive methods as HTS vehicles for the discovery, characterization, and development of small molecule inhibitors of GS.

In our first approach, we adopted a high-throughput FP assay to screen for small molecule inhibitors that can displace a G6P-coupled fluorophore that binds to the allosteric site of yGsy2. Screening the ChemBridge DIVERSet library which contains 50,000 compounds yielded 110 primary hits, and through the ^{14}C-glucose incorporation assay only 1 hit (**H23**, (*rac*)-2-methoxy-4-(1-(2-(1-methylpyrrolidin-2-yl)ethyl)-4-phenyl-1*H*-imidazol-5-yl)phenol) was identified as hGYS1 inhibitor. This outcome was supported by

both an X-ray structure and by kinetic studies using **H23** and analogs as part of a robust SAR study. The binding at the UDP site was surprising because the assay was designed to identify small-molecule inhibitors that displaced G6P binding. However, a close inspection of the known, eukaryotic GS structures demonstrates that the UDPG and G6P binding sites resided on opposing ends of the same alpha-helix, with Tyr492 stacked against the uracil ring of UDP and His500 forming a hydrogen bond with the phosphate moiety of G6P. Considering this direct structural linkage and the cooperative nature of the structural transitions in GS, it was not surprising that binding at one site could transmit structural information to the other site and that under the subsaturating conditions of our HTS assay, binding of compounds within the active site could promote displacement of the fluorophore from the G6P site. This was further confirmed by the observation that UDP can displace the fluorophore at high concentrations **(Figure 26B)**.

Extensive medicinal chemistry efforts led to the identification of potent analogs with low micromolar potency to hGYS1 possessing two chemical scaffolds, i.e., pyrazole and isoflavone. Representative compounds from each scaffold, **PZ23** and **IF9**, demonstrated over 300- and 500-fold marked improvement of potency compared with the potency of parent compound **H23**. Mode of inhibition and enzyme mutagenic studies suggested these analogs bind in the active site of GS with similar binding mode of **H23**. Based on the existing data, manual docking of **PZ23** and **IF9** were performed to model their binding. Considering the multiple activity states and dynamics of GS conformation, obtaining crystal structures of ligand-enzyme complex is necessary to further understand the molecule interactions conferring binding. Particularly, isoflavones, a class of phytoestrogen chemicals, demonstrated cellular efficacy of suppressing glycogen

accumulation. This encouraging data validated our biochemical and medicinal approaches for the development of small molecule inhibitors as a means to suppress cellular glycogen accumulation.

Due to the poor outcome and low translation of the high-throughput FP assay to ^{14}C-glucose incorporation assay, we sought an alternative HTS approach by developing a coupled colorimetric assay for the identification of small molecule modulators of hGYS1. The second assay, based on malachite green detection of P_i, was designed to measure UDP production derived from UDPG following glucosyl transfer. The specificity of hSCAN-1 to hydrolyze UDP to UMP and P_i played a key role in the successful implementation of this coupled assay in a high-throughput fashion. An excellent Z'-factor of 0.84 demonstrated the robustness of this screening assay. In proof-of-principle for this HTS assay, we screened 10,000 compounds from the ChemBridge Microsource library from which we identified and validated four compounds with micromolar potency toward hGYS1. The high sensitivity, translatability, and reproducibility of this high-throughput coupled assay demonstrated great improvement over the FP assay as a HTS platform for the identification of small molecule modulators of human GS.

Humans have two isoforms of GS, namely hGYS1 and hGYS2. The fact that hGYS1 is universally expressed in most tissues while hGYS2 is restrictively expressed in liver prompted us to identify inhibitors against hGYS1 in the hope of diminishing brain glycogen stores, aberrantly accumulated in some GSDs such as Lafora disease[53]. The high sequence homology between hGYS1 and hGYS2 enzymes could make it difficult to develop isoform-specific inhibitors. Nonetheless, inhibition of hGYS2 might aid in the therapeutic efficacy of GSDs with excessive glycogen accumulation in liver that would

ultimately lead to liver damage. Recently, Pursell *et al.* showed that GYS2 inhibition with RNAi prevents liver injury in mouse models of Corwedisease and had no adverse effects[88].

Mutations in GYS1[137] or GYS2[138] in rare GSDs lead to decreased glycogen in muscle and liver respectively. Disruption of the mouse GYS1 gene resulted in 90% perinatal lethality, likely due to cardiac developmental problems during embryogenesis, but the surviving mice were ostensibly normal and lived normal lifetimes[139]. Disruption of GYS2 in mice largely mimicked the phenotype of human GSD0 patients, namely tendencies to post-prandial hyperglycemia and to hypoglycemia upon fasting but compatible with a relatively normal life[138,140]. Given that small molecule inhibition will not have the penetrance of genetic defects, inhibition of GS activity by small molecules is unlikely to elicit extreme phenotypes, and small-molecule inhibition remains as a potentially valuable means of treating these devastating diseases.

In summary, this study described two strategies of assay development for the screening of small molecule inhibitors of GS, the binding modes of **H23** and HCLP validated through both X-ray crystallographic and kinetic data; and SAR study leading to analogs, such as pyrazole **PZ23** and isoflavone **IF9**, with low micromolar potency. These outcomes suggest that targeting GS with small molecule inhibitors represents an attractive approach for developing new therapeutics for diseases in the GSD family. Unlike other enzyme-based strategies where complete inhibition is the ultimate objective, a partial reduction of GS activity may be sufficient to alleviate unwanted and damaging levels of glycogen deposition in the neural tissue of patients suffering from Lafora disease[63,84,86]. The challenges of developing any therapeutic, nevertheless, remain the same, and the gulf that stretches between our identification of small molecule inhibitors with activity in the

low micromolar range and a therapeutic candidate is wide and deep. Initial efforts will involve microsomal studies to evaluate anticipated pharmacokinetic concerns about unwanted redox reactions of **PZ23** to 4-(4*H*-pyrazol-4-ylidene)- or 2,3-dihydroxy-4-(3*H*-pyrazol-3-ylidene)cyclohexa-2,5-dien-1-ones, or **IF9** to 7-, or 8-hydroxy-3-phenyl-4H-8l5-chromene-4,8-dione. We will use a combination of synthesis (*i.e.*, SAR studies) and computational modeling to identify analogs that avoid this concern and retain desired physiochemical properties (*i.e.*, water solubility; bioavailability); we will evaluate any promising, new leading structures for potential toxicity issues (*e.g.*, hERG studies); and we will explore biotinylated analogs to confirm the specificity of these pyrazole analogs for the desired target. These initial, encouraging results bode well for the future development of small molecule strategies to study and potentially treat GSDs.

References

1. Imberty, A.; Buleon, A.; Tran, V.; Perez, S., Recent advances in knowledge of starch structure. *Starch-Starke* **1991,** *43* (10), 375-384.

2. Roach, P. J.; Depaoli-Roach, A. A.; Hurley, T. D.; Tagliabracci, V. S., Glycogen and its metabolism: some new developments and old themes. *The Biochemical journal* **2012,** *441* (3), 763-787.

3. Hers, H. G., The control of glycogen metabolism in the liver. *Annual review of biochemistry* **1976,** *45*, 167-189.

4. Dringen, R.; Gebhardt, R.; Hamprecht, B., Glycogen in astrocytes: possible function as lactate supply for neighboring cells. *Brain research* **1993,** *623* (2), 208-214.

5. Nielsen, J.; Ortenblad, N., Physiological aspects of the subcellular localization of glycogen in skeletal muscle. *Applied physiology, nutrition, and metabolism* **2013,** *38* (2), 91-99.

6. Nielsen, J.; Schroder, H. D.; Rix, C. G.; Ortenblad, N., Distinct effects of subcellular glycogen localization on tetanic relaxation time and endurance in mechanically skinned rat skeletal muscle fibres. *The Journal of physiology* **2009,** *587* (Pt 14), 3679-3690.

7. Cardell, R. R., Jr., Smooth endoplasmic reticulum in rat hepatocytes during glycogen deposition and depletion. *International review of cytology* **1977,** *48*, 221-279.

8. Ishikawa, T.; Pel, Y. F., Intramitochondrial glycogen particles in rat retinal receptor cells. *The Journal of cell biology* **1965,** *25*, 402-407.

9. Lentz, T. L., Intramitochondrial glycogen granules in digestive cells of Hydra. *The Journal of cell biology* **1966,** *29* (1), 162-167.

10. Mori, M.; Dempo, K.; Abe, M.; Onoe, T., Electron microscopic study of intranuclear glycogen. *Journal of electron microscopy* **1970,** *19* (2), 163-169.

11. Hartl, P.; Olson, E.; Dang, T.; Forbes, D. J., Nuclear assembly with lambda DNA in fractionated Xenopus egg extracts: an unexpected role for glycogen in formation of a higher order chromatin intermediate. *The Journal of cell biology* **1994,** *124* (3), 235-248.

12. Ragano-Caracciolo, M.; Berlin, W. K.; Miller, M. W.; Hanover, J. A., Nuclear glycogen and glycogen synthase kinase 3. *Biochemical and biophysical research communications* **1998,** *249* (2), 422-427.

13. Sun, R. C.; Dukhande, V. V.; Zhou, Z.; Young, L. E. A.; Emanuelle, S.; Brainson, C. F.; Gentry, M. S., Nuclear glycogenolysis modulates histone acetylation in human non-small cell lung cancers. *Cell metabolism* **2019,** *30* (5), 903-916 e7.

14. Gunja-Smith, Z.; Marshall, J. J.; Mercier, C.; Smith, E. E.; Whelan, W. J., A revision of the Meyer-Bernfeld model of glycogen and amylopectin. *FEBS letters* **1970,** *12* (2), 101-104.

15. Melendez, R.; Melendez-Hevia, E.; Canela, E. I., The fractal structure of glycogen: A clever solution to optimize cell metabolism. *Biophysical journal* **1999,** *77* (3), 1327-1332.

16. Melendez-Hevia, E.; Waddell, T. G.; Shelton, E. D., Optimization of molecular design in the evolution of metabolism: the glycogen molecule. *The Biochemical journal* **1993,** *295 (Pt 2)*, 477-483.

17. Prats, C.; Graham, T. E.; Shearer, J., The dynamic life of the glycogen granule. *The Journal of biological chemistry* **2018,** *293* (19), 7089-7098.

18. Buschiazzo, A.; Ugalde, J. E.; Guerin, M. E.; Shepard, W.; Ugalde, R. A.; Alzari, P. M., Crystal structure of glycogen synthase: homologous enzymes catalyze glycogen synthesis and degradation. *The EMBO journal* **2004,** *23* (16), 3196-3205.

19. Wolfsdorf, J. I.; Weinstein, D. A., Glycogen storage diseases. *Reviews in endocrine & metabolic disorders* **2003,** *4* (1), 95-102.

20. Whelan, W. J., Pride and prejudice: the discovery of the primer for glycogen synthesis. *Protein science : a publication of the Protein Society* **1998,** *7* (9), 2038-2041.

21. Gibbons, B. J.; Roach, P. J.; Hurley, T. D., Crystal structure of the autocatalytic initiator of glycogen biosynthesis, glycogenin. *Journal of molecular biology* **2002,** *319* (2), 463-477.

22. Testoni, G.; Duran, J.; Garcia-Rocha, M.; Vilaplana, F.; Serrano, A. L.; Sebastian, D.; Lopez-Soldado, I.; Sullivan, M. A.; Slebe, F.; Vilaseca, M.; Munoz-Canoves, P.; Guinovart, J. J., Lack of glycogenin causes glycogen accumulation and muscle function impairment. *Cell metabolism* **2017,** *26* (1), 256-266 e4.

23. Roach, P. J., Glycogen and its metabolism. *Current molecular medicine* **2002,** *2* (2), 101-120.

24. Cohen, P., The Croonian Lecture 1998. Identification of a protein kinase cascade of major importance in insulin signal transduction. *Philosophical transactions of the Royal Society of London. Series B, Biological sciences* **1999,** *354* (1382), 485-495.

25. Printen, J. A.; Brady, M. J.; Saltiel, A. R., PTG, a protein phosphatase 1-binding protein with a role in glycogen metabolism. *Science* **1997,** *275* (5305), 1475-1478.

26. Hajduch, E.; Litherland, G. J.; Hundal, H. S., Protein kinase B (PKB/Akt)--a key regulator of glucose transport? *FEBS letters* **2001,** *492* (3), 199-203.

27. Zorzano, A.; Palacin, M.; Guma, A., Mechanisms regulating GLUT4 glucose transporter expression and glucose transport in skeletal muscle. *Acta physiologica Scandinavica* **2005,** *183* (1), 43-58.

28. Jiang, G.; Zhang, B. B., Glucagon and regulation of glucose metabolism. *American journal of physiology. Endocrinology and metabolism* **2003,** *284* (4), E671-678.

29. Dietz, M. R.; Chiasson, J. L.; Soderling, T. R.; Exton, J. H., Epinephrine regulation of skeletal muscle glycogen metabolism. Studies utilizing the perfused rat hindlimb preparation. *The Journal of biological chemistry* **1980,** *255* (6), 2301-2307.

30. Baskaran, S.; *Structure and Regulation of Yeast Glycogen Synthase*. Doctoral dissertation, Indiana University. **2010**.

31. Skurat, A. V.; Peng, H. L.; Chang, H. Y.; Cannon, J. F.; Roach, P. J., Rate-determining steps in the biosynthesis of glycogen in COS cells. *Archives of biochemistry and biophysics* **1996,** *328* (2), 283-288.

32. Coutinho, P. M.; Deleury, E.; Davies, G. J.; Henrissat, B., An evolving hierarchical family classification for glycosyltransferases. *Journal of molecular biology* **2003,** *328* (2), 307-317.

33. Breton, C.; Snajdrova, L.; Jeanneau, C.; Koca, J.; Imberty, A., Structures and mechanisms of glycosyltransferases. *Glycobiology* **2006,** *16* (2), 29R-37R.

34. Browner, M. F.; Nakano, K.; Bang, A. G.; Fletterick, R. J., Human muscle glycogen synthase cDNA sequence: a negatively charged protein with an asymmetric charge distribution. *Proceedings of the National Academy of Sciences of the United States of America* **1989,** *86* (5), 1443-1447.

35. Nuttall, F. Q.; Gannon, M. C.; Bai, G.; Lee, E. Y., Primary structure of human liver glycogen synthase deduced by cDNA cloning. *Archives of biochemistry and biophysics* **1994,** *311* (2), 443-449.

36. Farkas, I.; Hardy, T. A.; Goebl, M. G.; Roach, P. J., Two glycogen synthase isoforms in Saccharomyces cerevisiae are coded by distinct genes that are differentially controlled. *The Journal of biological chemistry* **1991,** *266* (24), 15602-15607.

37. Farkas, I.; Hardy, T. A.; DePaoli-Roach, A. A.; Roach, P. J., Isolation of the GSY1 gene encoding yeast glycogen synthase and evidence for the existence of a second gene. *The Journal of biological chemistry* **1990,** *265* (34), 20879-20886.

38. Baskaran, S.; Roach, P. J.; DePaoli-Roach, A. A.; Hurley, T. D., Structural basis for glucose-6-phosphate activation of glycogen synthase. *Proceedings of the National Academy of Sciences of the United States of America* **2010,** *107* (41), 17563-17568.

39. Zeqiraj, E.; Tang, X.; Hunter, R. W.; Garcia-Rocha, M.; Judd, A.; Deak, M.; von Wilamowitz-Moellendorff, A.; Kurinov, I.; Guinovart, J. J.; Tyers, M.; Sakamoto, K.; Sicheri, F., Structural basis for the recruitment of glycogen synthase by glycogenin. *Proceedings of the National Academy of Sciences of the United States of America* **2014,** *111* (28), E2831-2840.

40. Baskaran, S.; Chikwana, V. M.; Contreras, C. J.; Davis, K. D.; Wilson, W. A.; DePaoli-Roach, A. A.; Roach, P. J.; Hurley, T. D., Multiple glycogen-binding sites in eukaryotic glycogen synthase are required for high catalytic efficiency toward glycogen. *The Journal of biological chemistry* **2011,** *286* (39), 33999-34006.

41. Chikwana, V. M.; Khanna, M.; Baskaran, S.; Tagliabracci, V. S.; Contreras, C. J.; DePaoli-Roach, A.; Roach, P. J.; Hurley, T. D., Structural basis for 2'-phosphate

incorporation into glycogen by glycogen synthase. *Proceedings of the National Academy of Sciences of the United States of America* **2013,** *110* (52), 20976-20981.

42. Skurat, A. V.; Dietrich, A. D.; Roach, P. J., Interaction between glycogenin and glycogen synthase. *Archives of biochemistry and biophysics* **2006,** *456* (1), 93-97.

43. Mahalingan, K. K.; Baskaran, S.; DePaoli-Roach, A. A.; Roach, P. J.; Hurley, T. D., Redox switch for the inhibited state of yeast glycogen synthase mimics regulation by phosphorylation. *Biochemistry* **2017,** *56* (1), 179-188.

44. Pederson, B. A.; Cheng, C.; Wilson, W. A.; Roach, P. J., Regulation of glycogen synthase. Identification of residues involved in regulation by the allosteric ligand glucose-6-P and by phosphorylation. *The Journal of biological chemistry* **2000,** *275* (36), 27753-27761.

45. Roach, R. J.; Larner, J., Covalent phosphorylation in the regulation glycogen synthase activity. *Molecular and cellular biochemistry* **1977,** *15* (3), 179-200.

46. DePaoli-Roach, A. A.; Vilardo, P. G.; Kim, J. H.; Mavila, N.; Vemuri, B.; Roach, P. J., Determination of mammalian glycogen synthase phosphatase activity. *Methods in enzymology* **2003,** *366*, 17-34.

47. Hardy, T. A.; Roach, P. J., Control of yeast glycogen synthase-2 by COOH-terminal phosphorylation. *The Journal of biological chemistry* **1993,** *268* (32), 23799-23805.

48. Mahalingan, K. K., *Structural Basis for Regulated Inhibition and Substrate Selection in Yeast Glycogen Synthase*. Doctoral dissertation, Indiana University. **2016**.

49. Cid, E.; Gomis, R. R.; Geremia, R. A.; Guinovart, J. J.; Ferrer, J. C., Identification of two essential glutamic acid residues in glycogen synthase. *The Journal of biological chemistry* **2000,** *275* (43), 33614-33621.

50. Hurley, T. D.; Stout, S.; Miner, E.; Zhou, J.; Roach, P. J., Requirements for catalysis in mammalian glycogenin. *The Journal of biological chemistry* **2005,** *280* (25), 23892-23899.

51. Chaikuad, A.; Froese, D. S.; Berridge, G.; von Delft, F.; Oppermann, U.; Yue, W. W., Conformational plasticity of glycogenin and its maltosaccharide substrate during glycogen biogenesis. *Proceedings of the National Academy of Sciences of the United States of America* **2011,** *108* (52), 21028-21033.

52. Hicks, J.; Wartchow, E.; Mierau, G., Glycogen storage diseases: a brief review and update on clinical features, genetic abnormalities, pathologic features, and treatment. *Ultrastructural pathology* **2011,** *35* (5), 183-196.

53. Vilchez, D.; Ros, S.; Cifuentes, D.; Pujadas, L.; Valles, J.; Garcia-Fojeda, B.; Criado-Garcia, O.; Fernandez-Sanchez, E.; Medrano-Fernandez, I.; Dominguez, J.; Garcia-Rocha, M.; Soriano, E.; Rodriguez de Cordoba, S.; Guinovart, J. J., Mechanism suppressing glycogen synthesis in neurons and its demise in progressive myoclonus epilepsy. *Nature neuroscience* **2007,** *10* (11), 1407-1413.

54. Singh, P. K.; Singh, S.; Ganesh, S., The laforin-malin complex negatively regulates glycogen synthesis by modulating cellular glucose uptake via glucose transporters. *Molecular and cellular biology* **2012,** *32* (3), 652-663.

55. Kishnani, P. S.; Steiner, R. D.; Bali, D.; Berger, K.; Byrne, B. J.; Case, L. E.; Crowley, J. F.; Downs, S.; Howell, R. R.; Kravitz, R. M., Pompe disease diagnosis and management guideline. *Genetics in Medicine* **2006,** *8* (5), 267-288.

56. Sentner, C. P.; Hoogeveen, I. J.; Weinstein, D. A.; Santer, R.; Murphy, E.; McKiernan, P. J.; Steuerwald, U.; Beauchamp, N. J.; Taybert, J.; Laforet, P.; Petit, F. M.;

Hubert, A.; Labrune, P.; Smit, G. P. A.; Derks, T. G. J., Glycogen storage disease type III: diagnosis, genotype, management, clinical course and outcome. *Journal of inherited metabolic disease* **2016,** *39* (5), 697-704.

57. Ferguson, I. T.; Mahon, M.; Cumming, W. J., An adult case of Andersen's disease--Type IV glycogenosis. A clinical, histochemical, ultrastructural and biochemical study. *Journal of the neurological sciences* **1983,** *60* (3), 337-351.

58. Ortolano, S.; Vieitez, I.; Agis-Balboa, R. C.; Spuch, C., Loss of GABAergic cortical neurons underlies the neuropathology of Lafora disease. *Molecular brain* **2014,** *7*, 7.

59. Gentry, M. S.; Guinovart, J. J.; Minassian, B. A.; Roach, P. J.; Serratosa, J. M., Lafora disease offers a unique window into neuronal glycogen metabolism. *The Journal of biological chemistry* **2018,** *293* (19), 7117-7125.

60. Ganesh, S.; Puri, R.; Singh, S.; Mittal, S.; Dubey, D., Recent advances in the molecular basis of Lafora's progressive myoclonus epilepsy. *Journal of human genetics* **2006,** *51* (1), 1-8.

61. Roach, P. J., Glycogen phosphorylation and Lafora disease. *Molecular aspects of medicine* **2015,** *46*, 78-84.

62. Brereton, M. F.; Rohm, M.; Shimomura, K.; Holland, C.; Tornovsky-Babeay, S.; Dadon, D.; Iberl, M.; Chibalina, M. V.; Lee, S.; Glaser, B.; Dor, Y.; Rorsman, P.; Clark, A.; Ashcroft, F. M., Hyperglycaemia induces metabolic dysfunction and glycogen accumulation in pancreatic beta-cells. *Nature communications* **2016,** *7*, 13496.

63. Duran, J.; Gruart, A.; Garcia-Rocha, M.; Delgado-Garcia, J. M.; Guinovart, J. J., Glycogen accumulation underlies neurodegeneration and autophagy impairment in Lafora disease. *Human molecular genetics* **2014,** *23* (12), 3147-3156.

64. Kharroubi, A. T.; Darwish, H. M., Diabetes mellitus: The epidemic of the century. *World journal of diabetes* **2015,** *6* (6), 850-867.

65. Bischof, M. G.; Krssak, M.; Krebs, M.; Bernroider, E.; Stingl, H.; Waldhausl, W.; Roden, M., Effects of short-term improvement of insulin treatment and glycemia on hepatic glycogen metabolism in type 1 diabetes. *Diabetes* **2001,** *50* (2), 392-398.

66. Bischof, M. G.; Bernroider, E.; Krssak, M.; Krebs, M.; Stingl, H.; Nowotny, P.; Yu, C.; Shulman, G. I.; Waldhausl, W.; Roden, M., Hepatic glycogen metabolism in type 1 diabetes after long-term near normoglycemia. *Diabetes* **2002,** *51* (1), 49-54.

67. Krssak, M.; Brehm, A.; Bernroider, E.; Anderwald, C.; Nowotny, P.; Dalla Man, C.; Cobelli, C.; Cline, G. W.; Shulman, G. I.; Waldhausl, W.; Roden, M., Alterations in postprandial hepatic glycogen metabolism in type 2 diabetes. *Diabetes* **2004,** *53* (12), 3048-3056.

68. Cohn, A.; Ohri, A., Diabetes mellitus in a patient with glycogen storage disease type Ia: a case report. *Journal of medical case reports* **2017,** *11* (1), 319.

69. Oki, Y.; Okubo, M.; Tanaka, S.; Nakanishi, K.; Kobayashi, T.; Murase, T., Diabetes mellitus secondary to glycogen storage disease type III. *Diabetic medicine : a journal of the British Diabetic Association* **2000,** *17* (11), 810-812.

70. Ashcroft, F. M.; Rohm, M.; Clark, A.; Brereton, M. F., Is type 2 diabetes a glycogen storage disease of pancreatic beta cells? *Cell metabolism* **2017,** *26* (1), 17-23.

71. Pelletier, J.; Bellot, G.; Gounon, P.; Lacas-Gervais, S.; Pouyssegur, J.; Mazure, N. M., Glycogen synthesis is induced in hypoxia by the hypoxia-inducible factor and promotes cancer cell survival. *Frontiers in oncology* **2012,** *2*, 18.

72. Zois, C. E.; Favaro, E.; Harris, A. L., Glycogen metabolism in cancer. *Biochemical pharmacology* **2014,** *92* (1), 3-11.

73. Dauer, P.; Lengyel, E., New roles for glycogen in tumor progression. *Trends in cancer* **2019,** *5* (7), 396-399.

74. Zois, C. E.; Harris, A. L., Glycogen metabolism has a key role in the cancer microenvironment and provides new targets for cancer therapy. *Journal of molecular medicine* **2016,** *94* (2), 137-154.

75. Shen, G. M.; Zhang, F. L.; Liu, X. L.; Zhang, J. W., Hypoxia-inducible factor 1-mediated regulation of PPP1R3C promotes glycogen accumulation in human MCF-7 cells under hypoxia. *FEBS letters* **2010,** *584* (20), 4366-4372.

76. Pescador, N.; Villar, D.; Cifuentes, D.; Garcia-Rocha, M.; Ortiz-Barahona, A.; Vazquez, S.; Ordonez, A.; Cuevas, Y.; Saez-Morales, D.; Garcia-Bermejo, M. L.; Landazuri, M. O.; Guinovart, J.; del Peso, L., Hypoxia promotes glycogen accumulation through hypoxia inducible factor (HIF)-mediated induction of glycogen synthase 1. *PloS one* **2010,** *5* (3), e9644.

77. Iida, Y.; Aoki, K.; Asakura, T.; Ueda, K.; Yanaihara, N.; Takakura, S.; Yamada, K.; Okamoto, A.; Tanaka, T.; Ohkawa, K., Hypoxia promotes glycogen synthesis and accumulation in human ovarian clear cell carcinoma. *International journal of oncology* **2012,** *40* (6), 2122-2130.

78. Cheng, K. W.; Agarwal, R.; Mitra, S.; Lee, J. S.; Carey, M.; Gray, J. W.; Mills, G. B., Rab25 increases cellular ATP and glycogen stores protecting cancer cells from bioenergetic stress. *EMBO molecular medicine* **2012,** *4* (2), 125-141.

79. Favaro, E.; Bensaad, K.; Chong, M. G.; Tennant, D. A.; Ferguson, D. J.; Snell, C.; Steers, G.; Turley, H.; Li, J. L.; Gunther, U. L.; Buffa, F. M.; McIntyre, A.; Harris, A. L., Glucose utilization via glycogen phosphorylase sustains proliferation and prevents premature senescence in cancer cells. *Cell metabolism* **2012,** *16* (6), 751-764.

80. Guin, S.; Pollard, C.; Ru, Y.; Ritterson Lew, C.; Duex, J. E.; Dancik, G.; Owens, C.; Spencer, A.; Knight, S.; Holemon, H.; Gupta, S.; Hansel, D.; Hellerstein, M.; Lorkiewicz, P.; Lane, A. N.; Fan, T. W.; Theodorescu, D., Role in tumor growth of a glycogen debranching enzyme lost in glycogen storage disease. *Journal of the National Cancer Institute* **2014,** *106* (5).

81. Schnier, J. B.; Nishi, K.; Monks, A.; Gorin, F. A.; Bradbury, E. M., Inhibition of glycogen phosphorylase (GP) by CP-91,149 induces growth inhibition correlating with brain GP expression. *Biochemical and biophysical research communications* **2003,** *309* (1), 126-134.

82. Lee, W. N.; Guo, P.; Lim, S.; Bassilian, S.; Lee, S. T.; Boren, J.; Cascante, M.; Go, V. L.; Boros, L. G., Metabolic sensitivity of pancreatic tumour cell apoptosis to glycogen phosphorylase inhibitor treatment. *British journal of cancer* **2004,** *91* (12), 2094-2100.

83. Luo, J., Glycogen synthase kinase 3beta (GSK3beta) in tumorigenesis and cancer chemotherapy. *Cancer letters* **2009,** *273* (2), 194-200.

84. Turnbull, J.; DePaoli-Roach, A. A.; Zhao, X.; Cortez, M. A.; Pencea, N.; Tiberia, E.; Piliguian, M.; Roach, P. J.; Wang, P.; Ackerley, C. A.; Minassian, B. A., PTG depletion

removes Lafora bodies and rescues the fatal epilepsy of Lafora disease. *PLoS genetics* **2011,** *7* (4), e1002037.

85. Pederson, B. A.; Turnbull, J.; Epp, J. R.; Weaver, S. A.; Zhao, X.; Pencea, N.; Roach, P. J.; Frankland, P. W.; Ackerley, C. A.; Minassian, B. A., Inhibiting glycogen synthesis prevents Lafora disease in a mouse model. *Annals of neurology* **2013,** *74* (2), 297-300.

86. Turnbull, J.; Epp, J. R.; Goldsmith, D.; Zhao, X.; Pencea, N.; Wang, P.; Frankland, P. W.; Ackerley, C. A.; Minassian, B. A., PTG protein depletion rescues malin-deficient Lafora disease in mouse. *Annals of neurology* **2014,** *75* (3), 442-446.

87. Ashe, K. M.; Taylor, K. M.; Chu, Q.; Meyers, E.; Ellis, A.; Jingozyan, V.; Klinger, K.; Finn, P. F.; Cooper, C. G.; Chuang, W. L.; Marshall, J.; McPherson, J. M.; Mattaliano, R. J.; Cheng, S. H.; Scheule, R. K.; Moreland, R. J., Inhibition of glycogen biosynthesis via mTORC1 suppression as an adjunct therapy for Pompe disease. *Molecular genetics and metabolism* **2010,** *100* (4), 309-315.

88. Pursell, N.; Gierut, J.; Zhou, W.; Dills, M.; Diwanji, R.; Gjorgjieva, M.; Saxena, U.; Yang, J. S.; Shah, A.; Venkat, N.; Storr, R.; Kim, B.; Wang, W.; Abrams, M.; Raffin, M.; Mithieux, G.; Rajas, F.; Dudek, H.; Brown, B. D.; Lai, C., Inhibition of glycogen synthase II with RNAi prevents liver injury in mouse models of glycogen storage diseases. *Molecular therapy : the journal of the American Society of Gene Therapy* **2018,** *26* (7), 1771-1782.

89. Thomas, J. A.; Schlender, K. K.; Larner, J., A rapid filter paper assay for UDPglucose-glycogen glucosyltransferase, including an improved biosynthesis of UDP-14C-glucose. *Analytical biochemistry* **1968,** *25* (1), 486-499.

90. Tang, B.; Frasinyuk, M. S.; Chikwana, V. M.; Mahalingan, K. K.; Morgan, C. A.; Segvich, D. M.; Bondarenko, S. P.; Mrug, G. P.; Wyrebek, P.; Watt, D. S.; DePaoli-Roach, A. A.; Roach, P. J.; Hurley, T. D., Discovery and development of small-molecule inhibitors of glycogen synthase. *Journal of medicinal chemistry* **2020,** *63* (7), 3538-3551.

91. Otsalyuk, V. M.; Tkachuk, T. M.; Bondarenko, S. P.; Chkhalo, V. V.; Khilya, V. P., Synthetic analogs of xanthocercin. *Chemistry of natural compounds.* **1998,** *34* (3), 284-288.

92. Wahala, K.; Hase, T. A., Expedient synthesis of polyhydroxyisoflavones. *Journal of the Chemical Society, Perkin Transactions 1* **1991,** (12), 3005-3008.

93. Khanna, M.; Imasaki, T.; Chikwana, V. M.; Perez-Miller, S.; Hunter, G. O.; Mosley, A.; Takagi, Y.; Hurley, T. D., Expression and purification of functional human glycogen synthase-1 (hGYS1) in insect cells. *Protein expression and purification* **2013,** *90* (2), 78-83.

94. Minor, W.; Cymborowski, M.; Otwinowski, Z.; Chruszcz, M., HKL-3000: the integration of data reduction and structure solution--from diffraction images to an initial model in minutes. *Acta crystallographica. Section D, Biological crystallography* **2006,** *62* (Pt 8), 859-866.

95. Bunkoczi, G.; Echols, N.; McCoy, A. J.; Oeffner, R. D.; Adams, P. D.; Read, R. J., Phaser.MRage: automated molecular replacement. *Acta crystallographica. Section D, Biological crystallography* **2013,** *69* (Pt 11), 2276-2286.

96. Collaborative Computational Project, N., The CCP4 suite: programs for protein crystallography. *Acta crystallographica. Section D, Biological crystallography* **1994,** *50* (Pt 5), 760-763.

97. Murshudov, G. N.; Skubak, P.; Lebedev, A. A.; Pannu, N. S.; Steiner, R. A.; Nicholls, R. A.; Winn, M. D.; Long, F.; Vagin, A. A., REFMAC5 for the refinement of macromolecular crystal structures. *Acta crystallographica. Section D, Biological crystallography* **2011,** *67* (Pt 4), 355-367.

98. Emsley, P.; Cowtan, K., Coot: model-building tools for molecular graphics. *Acta crystallographica. Section D, Biological crystallography* **2004,** *60* (Pt 12 Pt 1), 2126-2132.

99. Graham, F. L.; Smiley, J.; Russell, W. C.; Nairn, R., Characteristics of a human cell line transformed by DNA from human adenovirus type 5. *The Journal of general virology* **1977,** *36* (1), 59-74.

100. Contreras, C. J.; Segvich, D. M.; Mahalingan, K.; Chikwana, V. M.; Kirley, T. L.; Hurley, T. D.; DePaoli-Roach, A. A.; Roach, P. J., Incorporation of phosphate into glycogen by glycogen synthase. *Archives of biochemistry and biophysics* **2016,** *597*, 21-29.

101. Lea, W. A.; Simeonov, A., Fluorescence polarization assays in small molecule screening. *Expert opinion on drug discovery* **2011,** *6* (1), 17-32.

102. Brady, M. J.; Kartha, P. M.; Aysola, A. A.; Saltiel, A. R., The role of glucose metabolites in the activation and translocation of glycogen synthase by insulin in 3T3-L1 adipocytes. *The Journal of biological chemistry* **1999,** *274* (39), 27497-27504.

103. Zhang, J. H.; Chung, T. D. Y.; Oldenburg, K. R., A simple statistical parameter for use in evaluation and validation of high throughput screening assays. *Journal of biomolecular screening* **1999,** *4* (2), 67-73.

104. Berman, H. K.; O'Doherty, R. M.; Anderson, P.; Newgard, C. B., Overexpression of protein targeting to glycogen (PTG) in rat hepatocytes causes profound activation of

glycogen synthesis independent of normal hormone- and substrate-mediated regulatory mechanisms. *The Journal of biological chemistry* **1998,** *273* (41), 26421-26425.

105. Greenberg, C. C.; Meredith, K. N.; Yan, L.; Brady, M. J., Protein targeting to glycogen overexpression results in the specific enhancement of glycogen storage in 3T3-L1 adipocytes. *The Journal of biological chemistry* **2003,** *278* (33), 30835-30842.

106. Crook, E. D.; Daniels, M. C.; Smith, T. M.; McClain, D. A., Regulation of insulin-stimulated glycogen synthase activity by overexpression of glutamine: fructose-6-phosphate amidotransferase in rat-1 fibroblasts. *Diabetes* **1993,** *42* (9), 1289-1296.

107. Skurat, A. V.; Dietrich, A. D.; Roach, P. J., Glycogen synthase sensitivity to insulin and glucose-6-phosphate is mediated by both NH2- and COOH-terminal phosphorylation sites. *Diabetes* **2000,** *49* (7), 1096-1100.

108. Otto, M.; Breinholt, J.; Westergaard, N., Metformin inhibits glycogen synthesis and gluconeogenesis in cultured rat hepatocytes. *Diabetes, obesity & metabolism* **2003,** *5* (3), 189-194.

109. Wollen, N.; Bailey, C. J., Inhibition of hepatic gluconeogenesis by metformin. Synergism with insulin. *Biochemical pharmacology* **1988,** *37* (22), 4353-4358.

110. Fulgencio, J. P.; Kohl, C.; Girard, J.; Pegorier, J. P., Effect of metformin on fatty acid and glucose metabolism in freshly isolated hepatocytes and on specific gene expression in cultured hepatocytes. *Biochemical pharmacology* **2001,** *62* (4), 439-446.

111. Berthier, A.; Paya, M.; Garcia-Cabrero, A. M.; Ballester, M. I.; Heredia, M.; Serratosa, J. M.; Sanchez, M. P.; Sanz, P., Pharmacological interventions to ameliorate neuropathological symptoms in a mouse model of Lafora disease. *Molecular neurobiology* **2016,** *53* (2), 1296-1309.

112. Berridge, M. V.; Herst, P. M.; Tan, A. S., Tetrazolium dyes as tools in cell biology: new insights into their cellular reduction. *Biotechnology annual review* **2005,** *11*, 127-152.

113. Douillard-Guilloux, G.; Raben, N.; Takikita, S.; Ferry, A.; Vignaud, A.; Guillet-Deniau, I.; Favier, M.; Thurberg, B. L.; Roach, P. J.; Caillaud, C.; Richard, E., Restoration of muscle functionality by genetic suppression of glycogen synthesis in a murine model of Pompe disease. *Human molecular genetics* **2010,** *19* (4), 684-696.

114. Roach, P. J.; Takeda, Y.; Larner, J., Rabbit skeletal muscle glycogen synthase. I. Relationship between phosphorylation state and kinetic properties. *The Journal of biological chemistry* **1976,** *251* (7), 1913-1919.

115. Baell, J. B.; Holloway, G. A., New substructure filters for removal of pan assay interference compounds (PAINS) from screening libraries and for their exclusion in bioassays. *Journal of medicinal chemistry* **2010,** *53* (7), 2719-2740.

116. Breckenridge, B. M., and Crawford, E. J. , Glycogen synthesis from uridine diphosphate glucose in brain. *The Journal of biological chemistry* **1960,** *235*, 3054-3057.

117. Candy, D. J.; Kilby, B. A., The biosynthesis of trehalose in the locust fat body. *The Biochemical journal* **1961,** *78*, 531-536.

118. Kornberg, A., The metabolism of phosphorus-containing coenzymes. *Phosphorus metabolism* **1951,** *392*.

119. Lowry, O. H., Micromethods for the assay of enzymes. *Methods Enzymol.* **1969,** *4*, 366.

120. Murphy, D. M.; Ivanenkov, V. V.; Kirley, T. L., Bacterial expression and characterization of a novel, soluble, calcium-binding, and calcium-activated human nucleotidase. *Biochemistry* **2003,** *42* (8), 2412-2421.

121. Smith, T. M.; Hicks-Berger, C. A.; Kim, S.; Kirley, T. L., Cloning, expression, and characterization of a soluble calcium-activated nucleotidase, a human enzyme belonging to a new family of extracellular nucleotidases. *Archives of biochemistry and biophysics* **2002,** *406* (1), 105-115.

122. Kuhn, B.; Mohr, P.; Stahl, M., Intramolecular hydrogen bonding in medicinal chemistry. *Journal of medicinal chemistry* **2010,** *53* (6), 2601-2611.

123. Hunter, C. A.; Sanders, J. K., The nature of. pi.-. pi. interactions. *Journal of the American Chemical Society* **1990,** *112* (14), 5525-5534.

124. Baell, J. B., Feeling Nature's PAINS: Natural Products, Natural Product Drugs, and Pan Assay Interference Compounds (PAINS). *Journal of natural products* **2016,** *79* (3), 616-628.

125. Bisson, J.; McAlpine, J. B.; Friesen, J. B.; Chen, S. N.; Graham, J.; Pauli, G. F., Can invalid bioactives undermine natural product-based drug discovery? *Journal of medicinal chemistry* **2016,** *59* (5), 1671-1690.

126. Ouertatani-Sakouhi, H.; El-Turk, F.; Fauvet, B.; Cho, M. K.; Pinar Karpinar, D.; Le Roy, D.; Dewor, M.; Roger, T.; Bernhagen, J.; Calandra, T.; Zweckstetter, M.; Lashuel, H. A., Identification and characterization of novel classes of macrophage migration inhibitory factor (MIF) inhibitors with distinct mechanisms of action. *The Journal of biological chemistry* **2010,** *285* (34), 26581-26598.

127. Kleinboelting, S.; Ramos-Espiritu, L.; Buck, H.; Colis, L.; van den Heuvel, J.; Glickman, J. F.; Levin, L. R.; Buck, J.; Steegborn, C., Bithionol potently inhibits human soluble adenylyl cyclase through binding to the allosteric activator site. *The Journal of biological chemistry* **2016,** *291* (18), 9776-9784.

128. Ambrose, A. J.; Zerio, C. J.; Sivinski, J.; Schmidlin, C. J.; Shi, T.; Ross, A. B.; Widrick, K. J.; Johnson, S. M.; Zhang, D. D.; Chapman, E., A high throughput substrate binding assay reveals hexachlorophene as an inhibitor of the ER-resident HSP70 chaperone GRP78. *Bioorganic & medicinal chemistry letters* **2019,** *29* (14), 1689-1693.

129. Leonardi, W.; Zilbermintz, L.; Cheng, L. W.; Zozaya, J.; Tran, S. H.; Elliott, J. H.; Polukhina, K.; Manasherob, R.; Li, A.; Chi, X.; Gharaibeh, D.; Kenny, T.; Zamani, R.; Soloveva, V.; Haddow, A. D.; Nasar, F.; Bavari, S.; Bassik, M. C.; Cohen, S. N.; Levitin, A.; Martchenko, M., Bithionol blocks pathogenicity of bacterial toxins, ricin, and Zika virus. *Scientific reports* **2016,** *6*, 34475.

130. Park, S.; Gwak, J.; Cho, M.; Song, T.; Won, J.; Kim, D. E.; Shin, J. G.; Oh, S., Hexachlorophene inhibits Wnt/beta-catenin pathway by promoting Siah-mediated beta-catenin degradation. *Molecular pharmacology* **2006,** *70* (3), 960-966.

131. Saunders, L. P.; Ouellette, A.; Bandle, R.; Chang, W. C.; Zhou, H.; Misra, R. N.; De La Cruz, E. M.; Braddock, D. T., Identification of small-molecule inhibitors of autotaxin that inhibit melanoma cell migration and invasion. *Molecular cancer therapeutics* **2008,** *7* (10), 3352-3362.

132. Ayyagari, V. N.; Brard, L., Bithionol inhibits ovarian cancer cell growth in vitro - studies on mechanism(s) of action. *BMC cancer* **2014,** *14*, 61.

133. Powell, H.; Swarner, O.; Gluck, L.; Lampert, P., Hexachlorophene myelinopathy in premature infants. *The Journal of pediatrics* **1973,** *82* (6), 976-981.

134. Powell, H. C.; Lampert, P. W., Bithionol: a possible substitute for hexachlorophene. *Pediatrics* **1973,** *52* (6), 859-861.

135. Bacq, Y.; Besnier, J. M.; Duong, T. H.; Pavie, G.; Metman, E. H.; Choutet, P., Successful treatment of acute fascioliasis with bithionol. *Hepatology* **1991,** *14* (6), 1066-1069.

136. Brewer, M. K.; Uittenbogaard, A.; Austin, G. L.; Segvich, D. M.; DePaoli-Roach, A.; Roach, P. J.; McCarthy, J. J.; Simmons, Z. R.; Brandon, J. A.; Zhou, Z.; Zeller, J.; Young, L. E. A.; Sun, R. C.; Pauly, J. R.; Aziz, N. M.; Hodges, B. L.; McKnight, T. R.; Armstrong, D. D.; Gentry, M. S., Targeting pathogenic Lafora bodies in Lafora disease using an antibody-enzyme fusion. *Cell metabolism* **2019,** *30* (4), 689-705 e6.

137. Kollberg, G.; Tulinius, M.; Gilljam, T.; Ostman-Smith, I.; Forsander, G.; Jotorp, P.; Oldfors, A.; Holme, E., Cardiomyopathy and exercise intolerance in muscle glycogen storage disease 0. *The New England journal of medicine* **2007,** *357* (15), 1507-1514.

138. Orho, M.; Bosshard, N. U.; Buist, N. R.; Gitzelmann, R.; Aynsley-Green, A.; Blumel, P.; Gannon, M. C.; Nuttall, F. Q.; Groop, L. C., Mutations in the liver glycogen synthase gene in children with hypoglycemia due to glycogen storage disease type 0. *The Journal of clinical investigation* **1998,** *102* (3), 507-515.

139. Pederson, B. A.; Chen, H.; Schroeder, J. M.; Shou, W.; DePaoli-Roach, A. A.; Roach, P. J., Abnormal cardiac development in the absence of heart glycogen. *Molecular and cellular biology* **2004,** *24* (16), 7179-7187.

140. Irimia, J. M.; Meyer, C. M.; Peper, C. L.; Zhai, L.; Bock, C. B.; Previs, S. F.; McGuinness, O. P.; DePaoli-Roach, A.; Roach, P. J., Impaired glucose tolerance and predisposition to the fasted state in liver glycogen synthase knock-out mice. *The Journal of biological chemistry* **2010,** *285* (17), 12851-12861.

Curriculum Vitae

Buyun Tang

Education

- Indiana University, Indianapolis, Indiana, United States 2015-2020

  Ph.D.: Biochemistry and Molecular Biology (Minor: Diabetes)

- Iowa State University, Ames, Iowa, United States 2012-2015

  Master of Science: Plant Biology

- Huazhong Agricultural University, Wuhan, Hubei, China 2008-2012

  Bachelor of Science: Agronomy

Research Experience

- Graduate Research Assistant 2016-2020

  Laboratory of Thomas D. Hurley, Indiana University School of Medicine

  Project: High-throughput screening, kinetic, structural, and cellular characterization of small molecule inhibitors of glycogen synthase for the treatment of glycogen storage diseases.

- Graduate Research Assistant 2013-2015

  Laboratory of Yanhai Yin, Iowa State University

  Project: Molecular mechanisms of plant hormone brassinosteroid-regulated growth and drought stress response.

Presentations

- Discovery and Development of Small-molecule Inhibitors of Glycogen Synthase. Poster presentation. 5th Annual CDMD Symposium 2019. Indianapolis, IN.
- Structural, Biochemical and Biological Evaluation of Hexachlorophene and

Bithionol as Glycogen Synthase Inhibitors. Poster presentation. High Throughput Chemistry and Chemical Biology, Gordon Research Conference 2019. New London, NH.

- Small-molecule Inhibitors of Glycogen Synthase as Therapeutics for the Treatment of Lafora Disease. Poster presentation. The 38th Midwest Enzyme Chemistry Conference 2018. Evanston, IL.
- Characterization of Small-molecule Inhibitors of Glycogen Synthase. 4th International Lafora Workshop 2018. Poster presentation. La Jolla, CA.
- Small-molecule Inhibitors of Glycogen Synthase. 4th Annual CDMD Symposium 2018. Poster presentation. Indianapolis, IN.
- Structural and Kinetic Characterization of a Small-molecule Inhibitor of Glycogen Synthase. Oral presentation. Biochemistry Research Day 2017. Indianapolis, IN.
- Characterization of a Small-molecule Inhibitor of Glycogen Synthase. Poster presentation. 3rd Annual CDMD Symposium 2017. Indianapolis, IN.

Publications

- **Tang B***, Morgan C*, Mahalingan K, Contreras C, Johnson S, Kirley T, Hurley T, Roach P, DePaoli-Roach A. Development of a non-radioactive high throughput screen assay to identify modulators of human glycogen synthase. *In preparation*. *Contributed equally
- **Tang B**, Frasinyuk M, Chikwana V, Mahalingan K, Morgan C, Segwich D, Bondarenko S, Mrug G, Wyrebek P, Watt D, DePaoli-Roach A, Roach P, Hurley T. Discovery and development of small-molecule inhibitors of glycogen synthase. Journal of Medicinal Chemistry. 2020, 63, 7, 3538-3551.

- Jiang H*, **Tang B***, Xie Z, Nolan T, Ye H, Song GY, Walley J, Yin Y. GSK3□like kinase BIN2 phosphorylates RD26 to potentiate drought signaling in Arabidopsis. The Plant Journal. 2019, 100, 5, 923-937. *Contributed equally
  (Outstanding Original Research Article Prize Winner)
- Xie Z, Nolan T, Jiang H, **Tang B**, Zhang M, Li Z, Yin, Y. The AP2/ERF transcription factor TINY modulates Brassinosteroid-regulated plant growth and drought responses in Arabidopsis. The Plant Cell. 2019, 31, 8, 1788-1806.
- Basavarajappa HD, Sulaiman RS, Qi X, Shetty T, Babu SS, Sishtla KL, Lee B, Quigley J, Alkhairy S, Briggs CM, Gupta K, **Tang B**, Shadmand M, Grant MB, Boulton ME, Seo SY, Corson TW. Ferrochelatase is a therapeutic target for ocular neovascularization. EMBO molecular medicine. 2017, 9, 6, 786-801.
- Ye H, Liu S, **Tang B**, Chen J, Xie Z, Nolan TM, Jiang H, Guo H, Lin HY, Li L, Wang Y, Tong H, Zhang M, Chu C, Li Z, Aluru M, Aluru S, Schnable PS, Yin Y. RD26 mediates crosstalk between drought and brassinosteroid signalling pathways. Nature communications. 2017, 8, 14573.
- Li L, Zheng W, Zhu Y, Ye H, **Tang B**, Arendsee ZW, Jones D, Li R, Ortiz D, Zhao X, Du C, Nettleton D, Scott PM, Salas-Fernandez MG, Yin Y, Wurtele ES. QQS orphan gene regulates carbon and nitrogen partitioning across species via NF-YC interactions. Proceedings of the National Academy of Sciences. 2015, 112, 47, 14734-14739.

Awards

- Best Poster Award 2017
  3rd Annual CDMD Symposium

- DeVault Fellowship, Diabetes and Obesity Research Training Program 2016
  Indiana University School of Medicine